USING THE GPS TO COLLECT TRAJECTORY DATA FOR EJECTION SEAT DESIGN, VALIDATION, AND TESTING

THESIS

Brian Reece Tredway, Captain, USAF

AFIT/GE/ENG/02M-27

DEPARTMENT OF THE AIR FORCE
AIR UNIVERSITY

AIR FORCE INSTITUTE OF TECHNOLOGY

Wright-Patterson Air Force Base, Ohio

Report Documentation Page

Report Date	**Report Type**	**Dates Covered (from... to)**
11 Mar 02	Final	Aug 01 - Mar 02

Title and Subtitle Using the GPS to Collect Trajectory Data for Ejection Seat Design, Validation, and Testing	**Contract Number**
	Grant Number
	Program Element Number
Author(s) Capt Brian Reece Tredway, USAF	**Project Number**
	Task Number
	Work Unit Number
Performing Organization Name(s) and Address(es) Air Force Institute of Technology Graduate School of Engineering and Management (AFIT/EN) 2950 P Street, Bldg 640 WPAFB, OH 45433-7765	**Performing Organization Report Number** AFIT/GE/ENG/02M-27
Sponsoring/Monitoring Agency Name(s) and Address(es) AFRL/HEPA ATT: Mr. John Plaga Q. Street, Bldg 824 WPAFB OH 45433	**Sponsor/Monitor's Acronym(s)**
	Sponsor/Monitor's Report Number(s)
Distribution/Availability Statement Approved for public release, distribution unlimited	
Supplementary Notes The original document contains color images.	

Abstract
The dynamic characteristics of an aircraft ejection seat are a crucial concern when evaluating aircraft ejection systems and their ability to separate aircrew members safely from disabled aircraft. Every ejection seat model undergoes real-time dynamic tests to determine potential injury to aircrew members during ejection. Ejection seat tests are conducted at high-speed test tracks. The test track facilities provide the required telemetry and high-speed photography to monitor and validate the aircraft escape system performance. Ejection seat test and evaluation requires very accurate position and velocity determination during each test run to determine the relative positions between the aircraft, ejection seat, manikin, and the ground. Current test and evaluation systems rely on expensive video camera systems to determine the position and velocity profiles. This research presents the design and test results from a new GPS-based system capable of monitoring all major ejection-test components. Small, low-power, lightweight GPS receivers, capable of handling high accelerations, are mounted on the manikin and/or ejection seat to obtain the position and velocity during the ejection sequence. The research goal is to augment the camera system with a differential GPS-based measurement system capable of providing accuracy that meets or exceeds the current video systems accuracy.

Subject Terms
Global Positioning System, GPS, Ejection Seats, Differential GPS, DGPS, Navigation, Theodolite

Report Classification	**Classification of this page**
unclassified	unclassified
Classification of Abstract	**Limitation of Abstract**
unclassified	UU

Number of Pages
170

Disclaimer

The views expressed in this thesis are those of the author and do not reflect the official policy or position of the United States Air Force, Department of Defense, or the U. S. Government.

AFIT/GE/ENG/02M-27

USING THE GPS TO COLLECT TRAJECTORY DATA FOR EJECTION SEAT DESIGN, VALIDATION, AND TESTING

THESIS

Presented to the Faculty

Department of Electrical and Computer Engineering

Graduate School of Engineering and Management

Air Force Institute of Technology

Air University

Air Education and Training Command

In Partial Fulfillment of the Requirements for the

Degree of Master of Science in Electrical Engineering

Brian Reece Tredway, BSEE

Captain, USAF

March 2002

AFIT/GE/ENG/02M-27

USING THE GPS TO COLLECT TRAJECTORY DATA FOR EJECTION SEAT DESIGN, VALIDATION, AND TESTING

Brian Reece Tredway, BSEE
Captain, USAF

Approved:

Lt Col Mikel M. Miller (Chairman)	7 March 2002 date
Dr. Peter S. Maybeck (Member)	7 March 2002 date
Maj John F. Raquet (Member)	7 MAR 2002 date

Acknowledgments

I would like to start by thanking Mr. John Plaga from the Air Force Research Lab, Human Effectiveness division, for his contributions as my thesis sponsor. Without John's support this research would never have left the ground. I would also like to express my appreciation to Mr. Doug Coppess for his help and hard work during the hardware configuration. Doug brought a lifetime of experience to this research and more than once put up with my battery of questions about manikins, testing, electronics, and how to tune a blues guitar.

My thesis advisor, Lt Col Mikel Miller, deserves special thanks for all the work he did behind the scenes. On more than on occasion when the project looked like it was dead, he somehow found the funds to keep it alive. I consider myself very fortunate to have had an advisor who shared my enthusiasm for this project. I would also like to thank my committee members, especially Major John Raquet, the undisputed Matlab master, for their help during the research. I was constantly amazed by Major Racquet's knowledge level for even the smallest Global Positioning System detail.

I also want to thank Mr. Dick Higgins at Hurricane Mesa Test Track in Hurricane Utah. Considering this project didn't contribute a dime to his site, Dick and his crew were great. I appreciate the genuine interest they expressed in the success of my GPS research.

Finally, I would like to thank my wife. I would not have been able to finish this research without her support and understanding.

Brian Reece Tredway

Table of Contents

Page

Page

List of Figures

Page

Page

Page

Page

List of Tables

List of Acronyms

AFB ..... Air Force Base
DoD ..... Department of Defense
CORS ..... Continuously Operating Reference Stations
DGPS ..... Differential Global Positioning System
DIVEPACS .... DGPS Independent Velocity, Position, and Altitude Collection System
DLL ..... Delay Lock Loop
FLL ..... Frequency Lock Loop
GDOP ..... Geometric Dilution of Precision
GLONASS ..... Global Navigation Satellite System
GPS ..... Global Positioning System
HDOP ..... Horizontal Dilution of Precision
HMTT ..... Hurricane Mesa Test Track
HSTT ..... High-Speed Test Track
ION ..... Institute of Navigation
IRIG ..... Inter-Range Instrumentation Group
JPATS ..... Joint Primary Aircraft Training System
KEAS ..... Knots Equivalent Air Speed
MEO ..... Medium Earth Orbit
NCO ..... Numerically Controlled Oscillator
NGS ..... National Geodetic Survey
NMEA ..... National Marine Electronics Association
OCXO ..... Original Equipment Manufacture
OEM ..... Oven Controlled Crystal Oscillator
OPUS ..... On-line Positioning User Service
PDOP ..... Position Dilution of Precision
PLL ..... Phase Lock Loop
PPM ..... Parts Per Million
PRN ..... Pseudo-Random Noise
RMS ..... Root Mean Square
SV ..... Space Vehicle
TCXO ..... Temperature Compensated Crystal Oscillator
XO ..... Crystal Oscillator
UERE ..... User Equivalent Range Error
VHS ..... Video Home System

AFIT/GE/ENG/02M-27

Abstract

The dynamic characteristics of an aircraft ejection seat are a crucial concern when evaluating aircraft ejection systems and their ability to separate aircrew members safely from disabled aircraft. Every ejection seat model undergoes real-time dynamic tests to determine potential injury to aircrew members during ejection. Ejection seat tests are conducted at high-speed test tracks. The test track facilities provide the required telemetry and high-speed photography to monitor and validate the aircraft escape system performance. Ejection seat test and evaluation requires very accurate position and velocity determination during each test run to determine the relative positions between the aircraft, ejection seat, manikin, and the ground. Current test and evaluation systems rely on expensive video camera systems to determine the position and velocity profiles.

This research presents the design and test results from a new GPS-based system capable of monitoring all major ejection-test components. Small, low-power, lightweight GPS receivers, capable of handling high accelerations, are mounted on the manikin and/or ejection seat to obtain the position and velocity during the ejection sequence. The research goal is to augment the camera system with a differential GPS-based measurement system capable of providing accuracy that meets or exceeds the current video systems accuracy.

USING THE GLOBAL POSITIONING SYSTEM TO COLLECT TRAJECTORY DATA FOR EJECTION SEAT DESIGN, VALIDATION, AND TESTING

I. Introduction

Background

Since their inception ejection seats have been tested at ejection seat proving grounds. The different test facilities consist of long sled tracks with the required telemetry and high-speed photography equipment to monitor and validate each aircraft escape system performance.

This section briefly describes the ejection seat testing program and presents the design and performance results from a new differential Global Positioning System (GPS) based system capable of measuring the position and velocity of all the major ejection system components during ejection sled tests, as well as actual in-air ejection tests.

Ejection Seat Test and Evaluation

This section briefly outlines the ejection seat test and evaluation process. Chapter 3 details the specific ejection seat tests performed during this research.

Located at Holloman AFB, N.M., the 846th Test Squadron maintains and operates one of the Air Force's largest ejection seat proving grounds. Test tracks, like the one at Holloman, are designed to simulate selected portions of the flight environment under

highly controlled conditions. These test facilities give system designers the capability to fill the gap between laboratory investigations and full-scale flight tests.

The ejection seat is placed into an aircraft fuselage mounted to a rocket sled as shown in Figure 1. This configuration allows the ejection seat designers to test the ejection seat's performance as it enters the air stream at different orientations, simulating real world ejection events. The sled speed can be varied from zero to well over the speed of sound. The average test speed is 400 knots equivalent air speed (KEAS) [2].

Figure 1. Manikin and Rocket Sled

Manikins are used to simulate an aircrew member during the ejection tests. The manikin is designed to resemble the human body with the same range of motion and associated degrees of freedom. The manikin is outfitted with standard aircrew gear to simulate actual flight weight and center of gravity accurately for a pilot under mission

conditions. A manikin dressed in aircrew gear for ejection testing is shown below in Figure 2.

Figure 2. Manikin Dressed for Ejection

The manikin, ejection seat, and rocket sled are instrumented to provide data that is used to analyze the ejection seat performance characteristics, and manikin physiological data. To avoid the possibility of telemetry data dropout, the data collected by the manikin sensors is stored inside the manikin in a data logger for post-processing. The data logger and its battery are located in the manikin chest cavity to provide it physical protection during the test.

During the ejection trials, the major system components, such as the ejection seat and manikin, position are tracked by a combination of 16mm and 70mm high-speed film and

Video Home System (VHS) theodolite video cameras. The theodolite cameras collect the manikin or ejection seat component trajectory data. The theodolite system is designed to obtain a trajectory for either the manikin or ejection seat during the test. The theodolite's accuracy can be a few inches or a few feet, depending on the type of test conducted and the measuring equipment utilized. The cameras are strategically located along the track to provide the best coverage available for the planned speed and trajectory. A typical ejection test uses 15 high-speed film and 5 VHS theodolite cameras to monitor the ejection sequence [6].

Problem Definition

The goal of this research is to develop a new system, called the Differential GPS, Independent VElocity, Position, and Altitude Collection System (DIVEPACS), to augment the current video based trajectory determination system. DIVEPACS should meet or exceed the current video system's sub-meter accuracy [2]. DIVEPACS supplies its own power, data logger, and control interface, making it totally independent from the monitored platform and existing video based systems.

Scope

The goal of this research is to develop a system to measure the ejection component's position and velocity with an accuracy that meets or exceeds the current theodolite VHS video system. The system was designed to augment, not replace, the current high-speed

film cameras and reduce the number of theodolite cameras necessary during ejection seat test and evaluation.

The research equipment budget covered two Ashtech G12 receivers, two data loggers, multiple antennas, and two trials at a high-speed test track. During this research, the benefits of different antenna locations and receiver configurations, different differential GPS position algorithms, and the DIVEPACS's operational limits were investigated.

A number of different flight profiles and receivers configurations were investigated. The tests began with static data collection in both stand-alone and differential GPS (DGPS) mode to establish a baseline for receiver accuracy. The different flight profile dynamics progressively increased from walking to freefall and finally to full-scale 600-knot rocket sled tests. The GPS simulator was utilized to test ejection flight profiles that could not be investigated during the high-speed test track trials.

Overview

This thesis is divided into five chapters and four appendices. Chapter 2 describes the history of ejection seat test and evaluation, the GPS, and the factors affecting its accuracy. A number of differential position algorithms are also described as they apply to this research. Chapter 3 details the different test phases for the DIVEPACS as well as the different hardware configurations. Chapter 3 also describes in detail the ejection seat test and evaluation program at Hurricane Mesa High-Speed Test Track (HMTT). Chapter 4 describes the different simulations, data collections, and ejection test results. Chapter 5 summarizes the results and also describes some possible areas for future research. Appendix A contains the technical information about the different manikins

used in the research and the type of data collected. Appendix B lists the different NMEA messages used in the research. Appendix C contains the complete wiring diagrams for the custom cables necessary to configure the hardware. Appendix D lists the specification sheets provided by the manufacture for different GPS receivers, data loggers, and antennas. The final section, Appendix E is the preliminary paper on this research published in the September 2001 *Proceedings Of The International Technical Meeting Of The Satellite Division of The Institute of Navigation (ION).*

II. Theory

This chapter presents the theory used in this research. The chapter outlines ejection seat test and evaluation, the Global Positioning System (GPS), the factors affecting GPS receiver accuracy, and GPS receiver performance in highly dynamic environments as they apply to this research.

Ejection Seat Test and Evaluation

Overview

The first known ejection system was tested in 1912. The system used a parachute extracted by a small cannon to pull a weighted dummy from an aircraft. Parachute escape systems were installed in aircraft and balloons during WWI. By WWII the Germans had improved the parachute, which led to the ejection seat becoming the standard for emergency crew extraction. The first successful ejection occurred in January 1942 from a German Heinkel He-280 jet fighter. These early systems are credited with over 60 successful ejections during WWII [20].

The Americans studied the early Heinkel seat designs in the early 1940's, but it wasn't until 1946 that the Republic F-84 Thunderjet became the first production American jet fighter to be equipped with an ejection seat. During the Korean conflict almost 2000 US Air crews experienced combat ejections. Unfortunately, only 77% of the aircrew ejected safely without injury. With refinements in the automatic release restraint systems, parachute deployment systems, and aerodynamic deployment stabilization, the

survival rates went up in the 1954-1958 period to 81%, where they remained into the mid 80's. Today Martin-Baker, a leading ejection seat manufacture, boasts over 6000 lives saved in successful ejections. Today's ejections seats can safely extract crewmembers from zero airspeed through 600 knots at all altitudes up to 50,000 feet [20].

Today, escape system test programs are more comprehensive than ever. The NACES, the Navy's newest ejection seat by Martin-Baker, is reported to have undergone over 120 ejections over a wide range of conditions before it was delivered. Modern ejection seat test facilities are separated into static and dynamic testing and include human engineering evaluation. The static tests ensure the specifications are met for flight qualification and certification. The dynamic tests demonstrate the seats operation under actual ejection conditions. The escape systems are tested at extreme speeds and altitudes at high-speed test tracks and flight vehicle test facilities. The human engineering tests evaluate the aircrew-to-seat interface, flight clothing compatibility, and life support system integration [19].

This research focused on the dynamic ejection seat test and evaluations conducted at the high-speed test tracks and flight vehicle test faculties. Ejection seat test and evaluation requires very accurate position and velocity determination during each test run to determine the relative positions between the aircraft, ejection seat, manikin, and the ground. Two different data types are collected during ejection seat test and evaluation: the physiological data such as neck loading and spinal compression, and the ejection seat and manikin (after the manikin/seat separation) position and velocity profiles. Although humans and animals have been used in the past, today the majority of the physiological data is collected by extremely accurate and robust sensors built into manikins designed

specifically for escape system testing. This research investigates a new GPS-based system for determining the position and velocity profiles.

Global Positioning System (GPS)

GPS System Overview

This section is as an introduction to the GPS. For additional information, please refer to the text by Misra and Enge [8].

GPS is a satellite-based radio navigation system developed and operated by the U.S. Department of Defense. The first GPS satellite was launched in the late 1970's. Although used for many years earlier, the system was not declared fully operational until 1995 [8]. The GPS is designed to give precise position, velocity, and time information to anyone with a GPS receiver. Figure 3 is an artist rendering of a GPS satellite in orbit around the earth.

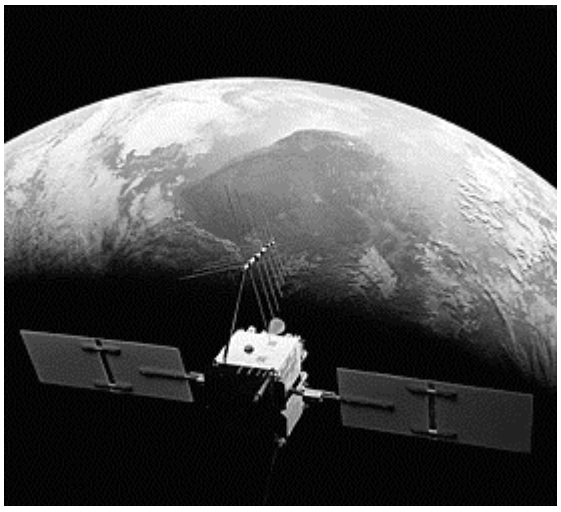

Figure 3. GPS Satellite [10]

System Architecture. The Global Positioning System's three main parts are the space, user, and the control segment as shown in Figure 4.

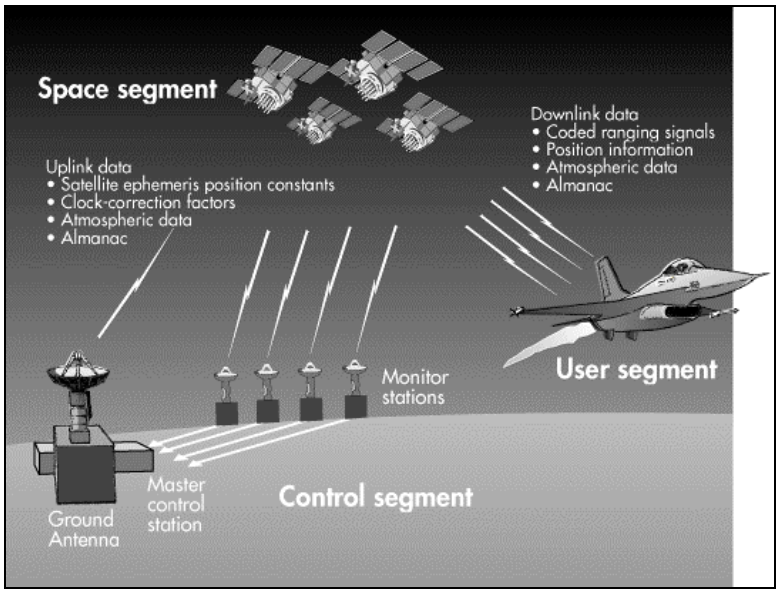

Figure 4. GPS Segments [10]

Space Segment. The space segment is made up of the GPS satellites. As of 24 January 2002, the GPS constellation consisted of 29 operational satellites [9]. The satellites is located in one of six orbital planes set at 55 degrees inclination. The satellites are in a medium earth orbit (MEO) at an altitude of 22,200 km. Each GPS satellite has an orbital period of 11 hours and 56 minutes and remains in view above the horizon for approximately 5 hours on average [8]. With the current 29-satellite constellation, a typical user can expect to have 6-8 satellites in view.

Control Segment. The Control Segment consists of a master control station (MCS) and five tracking stations located around the world. The MCS, located at Schriever AFB in Colorado Springs, is responsible for the system command and control, and continually

monitoring each satellite's orbit and health. In addition to the MCS, the five remote tracking stations are located on the islands of Hawaii, Kwajalein, Ascension, Diego Garcia, and at Cape Canaveral. These unmanned stations are controlled by the MCS. The tracking station locations are shown in Figure 5.

Figure 5. GPS Control Network [12]

The remote monitoring stations communicate with the satellites through dedicated ground antennas and with the MCS via ground and satellite links.

User Segment. The user segment is comprised of all the GPS receivers. Anyone with a GPS receiver can convert the satellite signals to precise position, velocity and time estimates. Today there are hundreds of models available on the market, ranging in price from less than one hundred dollars to tens of thousands of dollars. Normally with increased cost comes increased accuracy and capability.

GPS Signal

GPS satellites transmit on two separate frequencies referred to as the L1 (1575.42 MHz) and the L2 frequency (1227.60 MHz). Two separate signals are broadcast on the L1 frequency, one for civilian users and one for Department of Defense (DoD) users. The signal broadcast on the L2 frequency is designed for DoD-authorized users only. Each signal consists of the L1 and L2 carrier, ranging code, and navigation data.

The ranging code is a specific sequence of zeros and ones called a pseudo-random noise (PRN) code and is unique to each satellite. The algorithm creates a sequence of "chips" similar to those shown in Figure 6. GPS satellites transmit two different ranging codes, the coarse/acquisition (C/A) code, and the precision P(Y) code. The C/A code is a sequence of 1023 chips and is intended for civilian and DoD authorized users. The C/A ranging code modulates the L1 carrier. The second ranging code is the precision P(Y) code. The P code is encrypted into a Y-code and is intended for DoD-authorized users only and modulates both the L1 and L2 carriers. The P(Y) code is much longer than the C/A code, consisting of approximately 10^{14} chips. The chipping rate for the C/A code is 1.023 MHz. The chipping rate for the P(Y) code is 10 times faster, shortening the chip wavelength to 30 meters. The complete 1024 chip C/A code is repeated each millisecond. The P-code requires a full week to send.

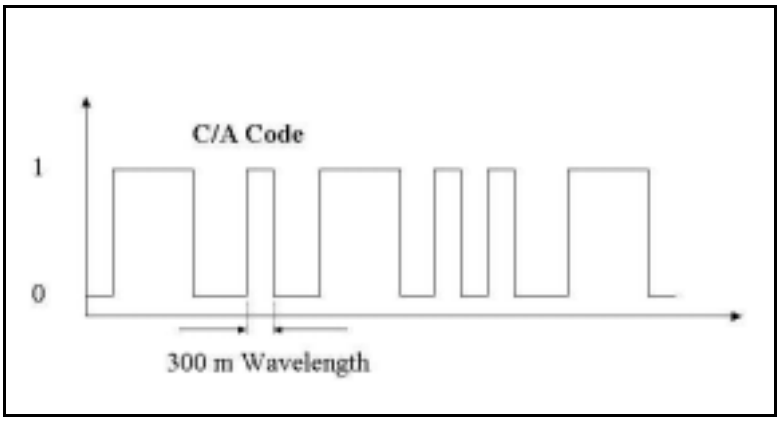

Figure 6. C/A Code

The navigation data are transmitted in a 50 bits-per-second stream. The information contained in the navigation data includes the satellite ephemeris, satellite clock errors, satellite almanac, time transfer information, ionospheric models, and an index of satellite signal and data accuracy. The complete navigation message is sent over a 12.5-minute period. The three GPS signal components are shown in Figure 7.

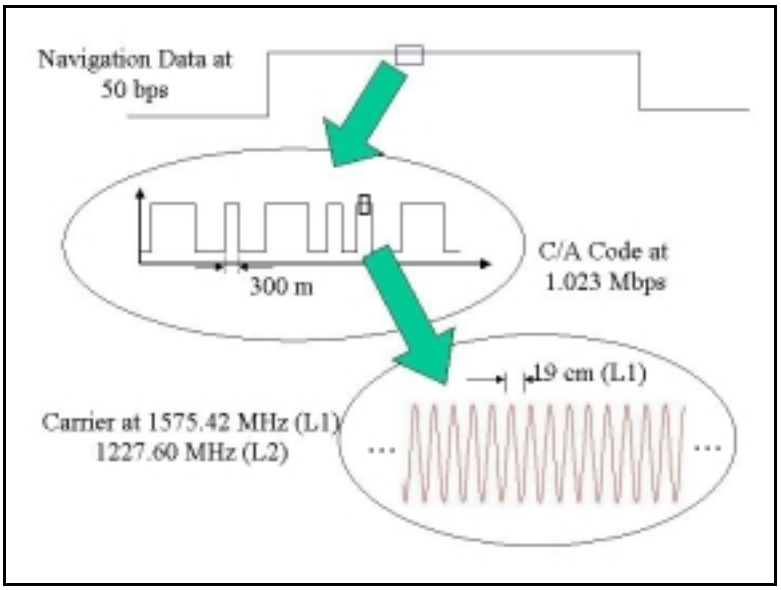

Figure 7. GPS Signal Components

The GPS signal time domain representation is shown in Equation (1):

$$s_{L1}(t) = \sqrt{2P_c}\ D(t)\,x(t)\cos(2\pi f_{L1}t + \theta_{L1}) + \sqrt{2P_{Y1}}\ D(t)\,y(t)\sin(2\pi f_{L1}t + \theta_{L1})$$
$$s_{L2}(t) = \sqrt{2P_{Y2}}\ D(t)\,y(t)\sin(2\pi f_{L2}t + \theta_{L2}) \qquad (1)$$

where

$\sqrt{2P_c}$	=	Signal Amplitude for Signal Carrying C/A Code on L1
$\sqrt{2P_{Y1}}$	=	Signal Amplitude for Signal Carrying P(Y) Code on L1 and L2
$D(t)$	=	Navigation data
$x(t)$	=	P(Y) and C/A Code Sequences
$\cos(2\pi f_{L1}t + \theta_{L1})$	=	Carrier L1 or L2
θ_{L1}	=	Phase Offsets on L1 and L2

Both the C/A and P codes are a special type called a Gold code. Gold codes were chosen because they have unique auto-correlation and cross-correlation properties that enable all the satellites in the GPS constellation to transmit at the same time and at the same frequency. The auto-correlation function only takes on a limited number of values and the main peaks are very steep and easily distinguished from the sidelobes. The distinctive peak and sidelobes are shown in Figure 8.

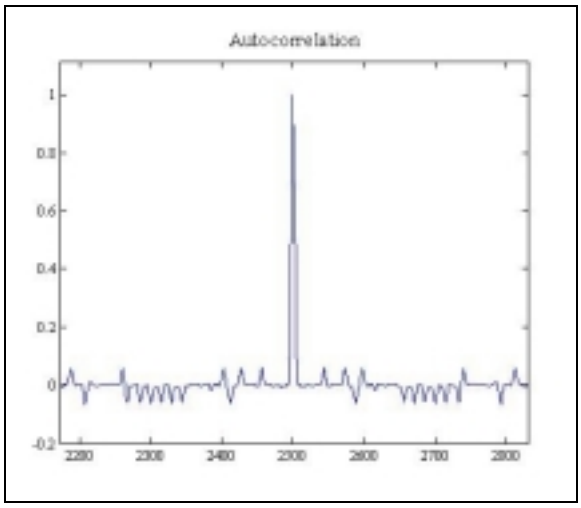

Figure 8. Sample C/A Code Autocorrelation

It is these properties that enable the receivers to track the different satellite signals precisely. Both the navigation message and the ranging code use binary phase shift keying to modulate the signal.

GPS Measurement Models

GPS receivers calculate position by measuring the distance from the receiver to at least four different GPS satellites. The distance, called a *pseudorange*, is calculated by measuring the time difference from the time the GPS satellite sent the signal to the time the GPS receiver collected the signal, and multiplying by the signal propagation velocity. Equation (2) is a representation of a pseudorange measurement from a receiver to the j^{th} satellite.

$$\rho_j = r + c(\delta t_u - \delta t_{SV} + \delta t_D) \qquad (2)$$

where

$$\begin{aligned}
\rho_j &= \textit{Pseudorange measurement from satellite } j \ (m) \\
r &= \textit{True range to receiver} \ (m) \\
c &= \textit{Speed of light} \ (m/s) \\
\delta t_u &= \text{Re}\textit{ceiver clock error} \ (s) \\
\delta t_{SV} &= \textit{Satellite clock error} \ (s) \\
\delta t_D &= \textit{Additional error effects} \ (s) \\
T_S &= \textit{True signal transmit time} \\
T_u &= \textit{Time signal received if there were no errors}
\end{aligned}$$

The relationship between true range and pseudorange is shown in Figure 9. These symbols will be used for the remainder of this thesis. The next section details the other errors in the pseudorange measurement modeled in Equation (2) as additional error effects.

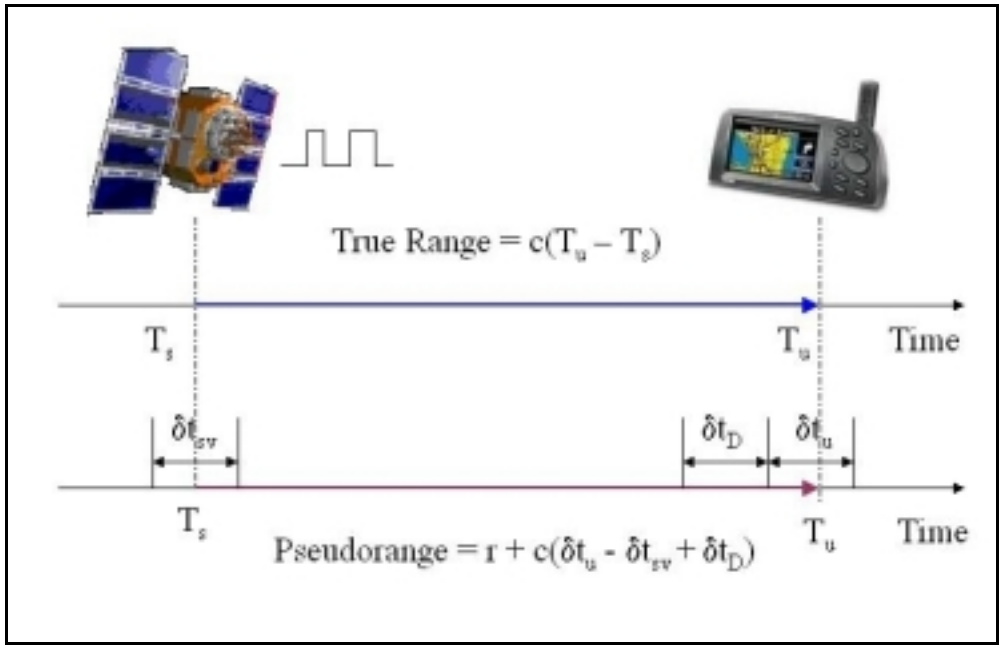

Figure 9. True Range vs. Pseudorange

Factors Affecting GPS Accuracy

In the previous section the assumption was made that the receiver clock error was the only measurement error. A better model for GPS measurements include satellite clock error, receiver clock error, atmospheric errors, ephemeris errors, measurement noise, and multipath. Equation (3) is the full pseudorange equation, showing each of the different factors that affect measurement accuracy. Each of the different error sources is described in the following sections.

$$\rho_j = r + c(\delta t_u - \delta t_{sv} + \delta t_{trop} + \delta t_{ion} + \delta t_{noise} + \delta t_{mp} + \delta t_{hw} + \delta t_{SA}) \qquad (3)$$

where

ρ_j = *Pseudorange measurement from satellite* j
δt_u = *Receiver clock error* (s)
δt_{sv} = *Satellite clock error* (s)
δt_{trop} = *Delay due to troposphere* (s)
δt_{ion} = *Delay due to ionosphere* (s)
δt_{noise} = *Delay due to GPS receiver noise and resolution noise* (s)
δt_{mult} = *Delay due to multipath* (s)
δt_{hw} = *Delay due to hardware errors* (s)
δt_{SA} = *Delay due to selective availability* (s)
r = *True range to receiver* (m)
c = *Speed of light* (m/s)

The hardware noise is often neglected, and currently selective availability is turned off. Selective availability was a DoD attempt to control the accuracy of GPS to non-DoD users. Intentional dithering the time and ephemeredes data provided in the navigation

message degraded the GPS signal for non-authorized users. Selective Availability was discontinued in May of 2000.

Each nanosecond of satellite clock error adds approximately 1 foot of error to the position solution. For this reason, the satellites are equipped with very accurate Cesium or Rubidium atomic clocks. Even these very accurate clocks accumulate an error of one nanosecond every three hours [11]. To resolve the satellite clock drifts, they are continuously monitored by ground stations and compared with the master control clock system, which is a combination of more than 10 atomic clocks [11]. The satellite clock error adds approximately 1.5 meters rms error to the position solution.

As is for the satellite clock, any error in the receiver clock causes inaccuracies in distance measurements. It is not practical from a physical or financial viewpoint to equip GPS receivers with highly accurate atomic clocks. To overcome the receiver clock limitations, the error in the receiver clock is typically treated as a "fourth unknown". By simultaneously measuring four satellites, you can determine the receiver's three-dimensional position and accurately measure the receiver clock error.

Atmospheric errors result from signal propagation through the earth’s atmosphere. Atmospheric refraction lengthens the signal path, making the satellite’s position appear further away. The atmosphere’s upper layer, called the ionosphere, contains charged particles that lower the code frequency (chipping rate), while increasing the carrier frequency. The effect on the signal path length is frequency dependent. The higher the frequency, the less it is affected by the ionosphere. The ionosphere effect can be estimated by measuring the difference in the L1 and L2 signal arrival time in dual frequency receivers or using an ionospheric model in single frequency receivers. The

G12 receiver used in this research incorporates the ionospheric model defined in ICD-GPS-200 to mitigate ionospheric effects [13]. Figure 10 is a plot of the delay caused by the ionosphere for a single satellite. This data was collected on 6 May 2001 at Duck, North Carolina using a stationary GPS receiver. The delay increases during the afternoon hours and is also as the satellite elevation approaches the horizon. The ionospheric errors are the largest single source of error in a single frequency receiver and can add as much as 5 – 7 meters (rms) of error to the position solution (or much higher during times of high ionospheric activity).

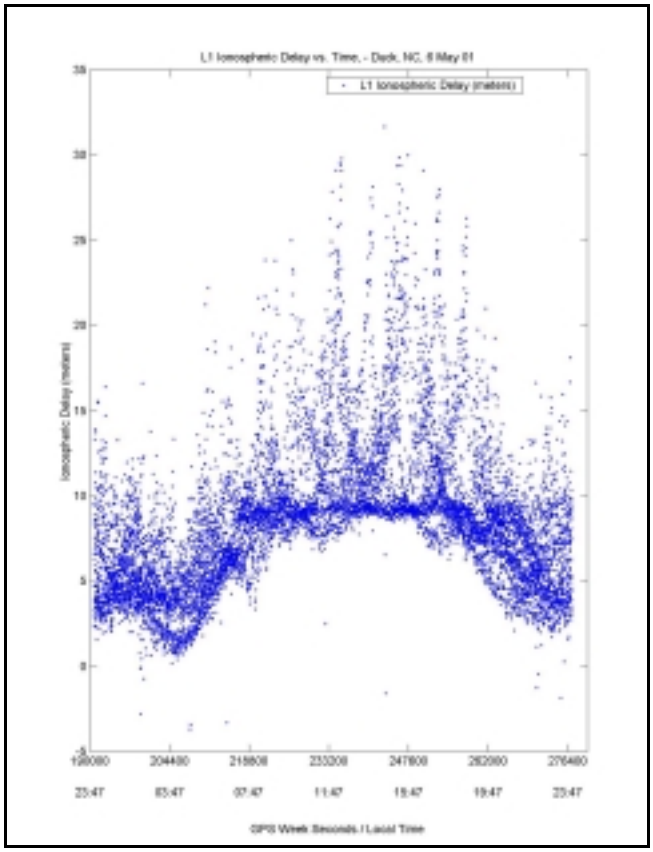

Figure 10. L1 Ionospheric Delay vs. Time

The troposphere is the lower region of the atmosphere composed of dry gases and water vapor. It has the effect of slowing down both the code and carrier frequencies. Unfortunately, unlike the ionospheric effects, tropospheric effects cannot be removed using dual frequency systems. Many models are available to estimate the errors based on user location, temperature, and humidity. If not modeled, the troposphere typically adds 1-2 meters (rms) of error to the position solution. When modeled the error (rms) drops to 5 – 20 cm [8].

Ephemeris errors represent how well the satellite position is known. One of the main functions of the control network is to monitor the GPS constellation and to update the predicted orbits of the satellites. In addition to the control segment predicted ephemeredes, which are broadcast in real time by each satellite, the National Geodetic Survey computes precise ephemeris data for post-processing, which may be obtained from the NGS Orbits Web Page or from the U.S Coast Guard's Navigation Center. Historically, the control segment provides ephemeris data with accuracy on the order of a few meters [9].

Receiver measurement errors result from the random noise in the RF band at L1 and L2 frequencies. The antenna collects both the noise and the signal and feeds them into the receiver for processing. Receiver noise contributes only a small amount of error to the position solution, typically on the order of a few centimeters [13].

Multipath errors are caused by signals reflected from the ground and other objects that reach the antenna and interfere with the direct signal, as shown in Figure 11. The lower the satellite elevation, the larger the multipath contribution. The error magnitude depends on the delay between the direct signal and reflected signal. Locating the

receiver's antenna away from reflective objects or using special antennas can significantly reduce the error. Multipath typically contributes 1-5 meters (rms) of error to the position solution [8].

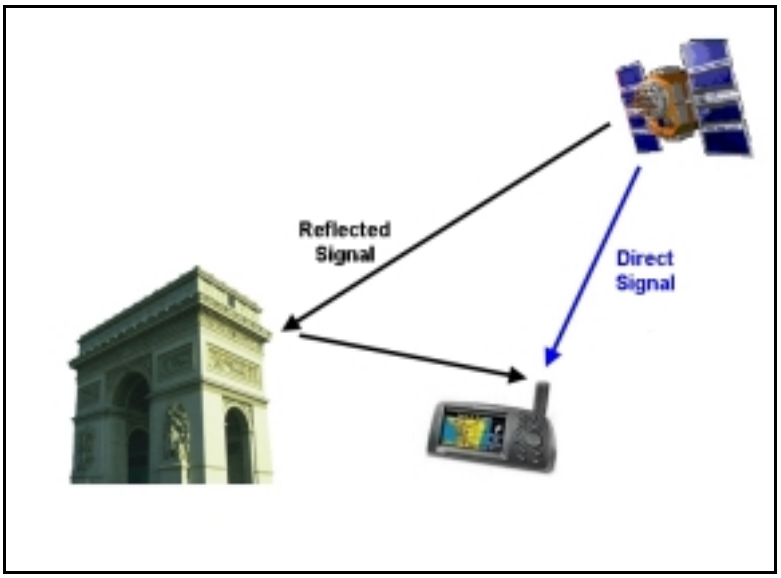

Figure 11. Multipath

Dilution of Precision (DOP)

Now that the different errors sources have been described, Dilution of Precision (DOP) can be introduced. The errors described in the previous section such as multipath and ionospheric errors can be combined and described by a single error statistic called the user range error (URE). The URE, as described in Equation (4), is the root-sum-square of the standard deviations for the clock, ephemeris, tropospheric, ionospheric, multipath, and receiver noise. URE provides a single, convenient measure of pseudorange estimation accuracy and is expressed in units of length.

$$\sigma_{URE} = \sqrt{\sigma_{sv}^2 + \sigma_{eph}^2 + \sigma_{trop}^2 + \sigma_{ion}^2 + \sigma_{mp}^2 + \sigma_{noise}^2} \quad (4)$$

where

$$\sigma_{URE} = User\ range\ error$$
$$\sigma_{sv}^2 = Variance\ of\ the\ satellite\ clock\ error$$
$$\sigma_{eph}^2 = Variance\ of\ the\ satellite\ ephemeris\ error$$
$$\sigma_{trop}^2 = Variance\ of\ the\ tropospheric\ error$$
$$\sigma_{ion}^2 = Variance\ of\ the\ ionospheric\ error$$
$$\sigma_{ion}^2 = Variance\ of\ the\ multipath\ error$$
$$\sigma_{noise}^2 = Variance\ of\ the\ receiver\ error$$

The GPS end-user is often more interested in position estimation accuracy. When describing the final position measurement errors, it is often easier to convert the latitude, longitude, and altitude GPS measurements into a local east-north-up (ENU) coordinate frame. The origin for the frame is the user's initial position. The user movement is then measured as a relative position change from the initial starting point. The RMS 3-D error can now be described as shown in Equation (5) in terms of the variance in the east, north, and up directions.

$$RMS\ 3\text{–}D\ Error \cong \sqrt{\sigma_E^2 + \sigma_N^2 + \sigma_U^2} \quad (5)$$

where

$$\sigma_E^2 = Variance\ of\ the\ east\ component$$
$$\sigma_N^2 = Variance\ of\ the\ north\ component$$
$$\sigma_U^2 = Variance\ of\ the\ up\ (vertical)\ component$$

The position estimate variances depend on the URE and a satellite geometry measure called Dilution of Precision (DOP). The DOP characterizes the user-satellite geometry. The lower the DOP value, the better the satellite geometry. The best satellite geometry is when the satellites are located at wide angles to each other. The best way to understand DOP is to visualize it as inversely proportional to the volume enclosed by a tetrahedron created by four satellites. If the four satellites are spread across the users field-of-view, they define a large volume. If the satellites are grouped close together in a line or tightly grouped in one region in the user's field-of-view, they define a small volume. This relationship between DOP and satellite geometry is shown in Figure 12.

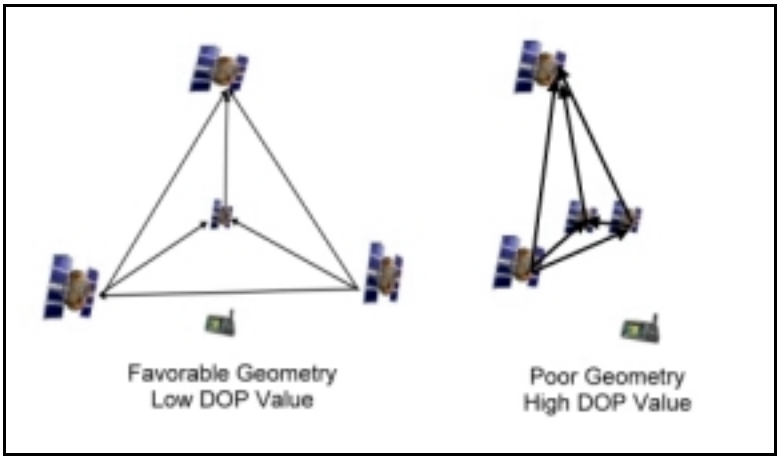

Figure 12. DOP and User-Satellite Geometry

The relationship between RMS 3-D errors, URE, and DOP is described in Equation (6).

$$RMS\ 3\text{–}D\ Error = \sqrt{\sigma_E^2 + \sigma_N^2 + \sigma_U^2} = \sigma_{URE} \cdot PDOP \qquad (6)$$

where

$$\sigma_{URE} = S\tan dard\ deviation\ of\ the\ user\ range\ error$$
$$\sigma_N^2 = Variance\ of\ the\ north\ component$$
$$\sigma_E^2 = Variance\ of\ the\ east\ component$$
$$\sigma_U^2 = Variance\ of\ the\ up\ (vertical)\ component$$

Position dilution of precision (PDOP) describes the 3-D position error. Other common measures are the Horizontal DOP (HDOP), Vertical DOP (VDOP), and Time DOP (TDOP). For additional information on DOP, the reader should reference the text by Misra and Enge [8].

GPS Receivers

Today's GPS receivers offer extraordinary accuracy and flexibility. Many manufactures offer high-end Original Equipment Manufacture (OEM) receivers capable of sub-meter positioning accuracy. Often the modules are designed not only to receive GPS signals, but also the Russian Global Navigation Satellite System (GLONAS) signals or signals from land-based and satellite-based GPS pseudolite augmentation systems. This section describes modern GPS receiver's features and limitations. Appendix D contains the specification sheets for the Ashtech® G12, Ashtech® Z-Surveyor, and the H.O. Data data logger, and the antennas used in the different phases of this research.

Regardless of the receiver type, the basic task is the same, to collect the GPS signals and provide the user with the precise position, velocity, and time data. Normally, the data is passed to the user in the form of structured messages or raw data that can be used by the end user to calculate position and velocity. The next sections contain a detailed description of the data output by the receiver, a discussion of some receiver limitations,

factors affecting accuracy, and receiver requirements for operation in highly dynamic environments.

NMEA and Raw Measurements

The National Marine Electronics Association (NMEA) standard defines an electrical interface and data protocol for communications between marine instrumentation. In a NMEA message, the data from the GPS receiver is transmitted in the form of "sentences." The NMEA messages used in this research are detailed in Appendix B. A sample NMEA message is shown in Table 1.

Table 1. Example NMEA Message Format

$PASHR,POS,0,06,172437.00,3714.389682,N,11313.256039,W,01564.848,R,000.0,000.0,000.0,02.5,01.7,01.9,01.4,UE00*3A	
Field	**Description**
0	Position fix type
06	Number of satellites used in position computation
172437.00	Current UTC Time hhmmss
3714.389682	Latitude
N	Latitude sector
11313.256039	Longitude
W	Longitude sector
01564.848	Altitude above mean sea level (m)
R	Reserved
000.0	True track/true course over ground (deg)
000.0	Vertical velocity (m/s)
02.5	PDOP
01.7	HDOP
01.9	VDOP
01.4	TDOP
1.2	Firmware version
UE00*3A	Checksum

Each sentence contains a header to identify the type of message, followed by a number of data fields separated by commas, and terminated by an optional checksum, and a carriage return/line feed. The checksum is used to verify that the data transmitted by the receiver is a complete and valid sentence. There are over 20 different NMEA messages that provide data such as user position, velocity, and the number of satellites in view. Many receivers also offer the option of outputting proprietary messages that differ from the NMEA messages.

In addition to the NMEA-formatted messages, many receivers can output raw data measurements. The raw measurements include such information as receiver channel number, satellite PRN number, pseudorange measurement, signal-to-noise ratio, GPS time, and carrier phase measurements. This information is necessary when a user wants more control over the position calculations, or the ability to filter the data before calculating position or velocity.

Receiver Tracking Under High Dynamics

The main goal of this research was to design a GPS-based system to track the ejection seat component's position and velocity during an ejection test and evaluation trial. One of the biggest initial challenges was to identify a GPS receiver capable of operating reliably in that type of environment. In this section the design characteristics that affect a typical GPS receiver's dynamic performance are introduced. This section also describes the fundamentals of quartz oscillators, and the design trade-offs involved with code and carrier tracking loops.

The three main types of quartz oscillators are the crystal oscillator (XO), the temperature compensated crystal oscillator (TCXO), and the oven controlled crystal oscillator (OCXO). The characteristics of interest are the different crystal oscillator's accuracy, drift, and frequency instability. In addition to the crystal oscillators, GPS satellites use atomic oscillators. The three main types of atomic oscillators are rubidium, cesium, and hydrogen master. The important environmental factors that affect the performance of a XO in a GPS receiver are temperature, aging, vibration, shock, and accelerations.

Ambient temperature change can be the principal reason for frequency instability in a XO. The effect of temperature changes on most crystal oscillators is parabolic, with the inflection point near room temperature, so both extreme cold (-50° c) and extreme heat (70° c) can cause the frequency to drop [14].

Aging, or long-term drift, is the change in the oscillator output frequency over time. The change is due to mechanical breakdown of the XO packaging or internal connections. The effect of aging is a gradual increase in output frequency. Typical values are 1-2 ppm/year [14].

Acceleration changes a crystal oscillator's frequency. The acceleration can be a steady-state acceleration, vibration, shock, or a simple change in attitude. The frequency varies regardless of which axis is aligned with the axis of acceleration. The amount of frequency change depends on the acceleration magnitude and direction, and on the oscillator's acceleration sensitivity. Typical XO sensitivity values are in the range of 10^{-9}/g to 10^{-10}/g [14].

Vibration can also increase the sensitivity of a crystal oscillator to acceleration. A vibration in the range of 450 Hz can increase the acceleration sensitivity by as much as 17-fold [14]. In ejection seat test and evaluation, the receiver can undergo accelerations as high as 18 Gs and vibration in the 500 – 2000 Hz range [2]. As was discussed, vibrations and accelerations can have a significant effect on how well a GPS receiver can track signals under high dynamics. The GPS receiver cannot distinguish between the dynamic stress from the platform dynamics and the apparent dynamics from clock errors. For further information on the fundamentals of quartz oscillators, see the text by Blair [14].

GPS Receiver Tracking Loops

Figure 13 shows the two tracking loops in a GPS receiver. The inner loop, through the coder, is the code-tracking loop. The code-tracking loop is called a delay lock loop (DLL). The outer loop, through the carrier NCO, is either a phase lock loop (PLL), or frequency lock loop (FLL), or a possible combination of the two.

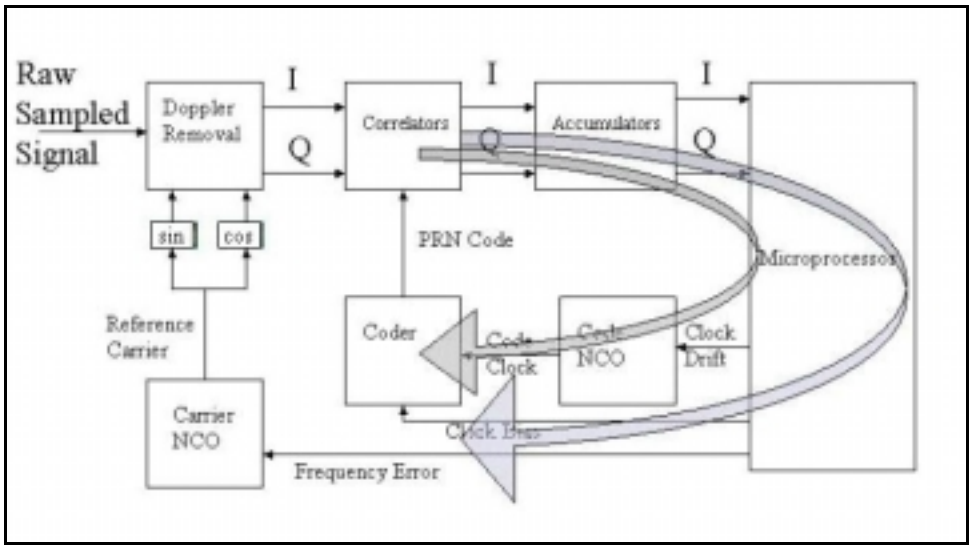

Figure 13. GPS Receiver Signal Processing Section

Carrier Tracking Loops. The outer loop in Figure 13 is the carrier-tracking loop. The carrier-tracking loop is the weak link in terms of the receiver's dynamic tracking performance [14]. The three main parts of a carrier-tracking loop are the carrier predetection integrators, discriminators, and loop filters. These three components determine the tracking loop performance for thermal noise error and maximum line-of-sight dynamics stress threshold. If a receiver is designed to operate under high dynamics, the predetection integration should be short, the discriminator should be a FLL, and the carrier loop filter bandwidths should be wide. A short predetection integration time decreases the Doppler phase measurement accuracy. A FLL is not as accurate as a PLL or a Costas loop, but it is less sensitive to dynamic stress. A Costas loop is a type of PLL that is insensitive to data bit sign changes. The receiver-tracking loop must be able to track the sign changes in the ranging code chips even when the possibility of a navigation data bit sign change exists. The loop filter is designed to reduce as much noise as possible in order to produce an estimate of the original signal. A receiver designed to

operate under high acceleration dynamics may incorporate a third-order loop because it is the least sensitive to dynamic stress. To reduce the receiver's insensitivity to jerk stress further, the loop bandwidth should be kept as wide as possible. As and example, Topcon, a GPS manufacturer, incorporates a third order tracking loop filter with a 20Hz noise bandwidth for its high-dynamics GPS receiver [17]. The user can set the G12 GPS receiver noise bandwidth. The three options available are 10, 20, and 50 Hz. The 50 Hz setting is recommended for highly dynamic, medium phase noise conditions.

Code Tracking Loops. The inner loop in Figure 13 is the code-tracking loop. The three main parts of a code tracking loop are the code predetection integrators, discriminators, and loop filters. Similar to the carrier-tracking loop, these three components determine the loop performance for thermal noise error and maximum line-of-sight dynamics stress threshold [14]. The code tracking loops use delay lock loops (DLL) in the loop discriminators. The user can set the G12 GPS code loop parameter. The three options available are 1.0, 0.5, and 0.1 Hz. The 1.0 Hz setting is recommended for fast range availability (5 seconds), medium range noise conditions.

Phase Lock Loop Tracking Errors

The rule-of-thumb for receiver design is that the phase tracking error, σ_{PLL}, must stay within 15° for the PLL to remain locked onto the carrier signal. This relationship is shown in Equation (7) [15].

$$\sigma_{PLL} = \sqrt{\sigma_t^2 + \sigma_v^2 + \theta_A^2} + \frac{\theta_e}{3} \leq 15^\circ \qquad (7)$$

where

σ_{PLL} = Phase tracking error
σ_t^2 = Thermal noise
θ_e = Dynamic stress error
σ_v^2 = Vibration induced jitter
θ_A^2 = Allan variance-induced oscillator jitter

Of the three noises sources inside the square root of Equation (7), the thermal noise is the dominant term over the vibration and Allan variance. The vibration and Allan variance may often be neglected [15]. As described above, the thermal noise is a function of the carrier loop noise bandwidth, predetection integration time (PIT), and carrier to noise power. The vibration-induced errors are a function of the carrier frequency, oscillator vibration sensitivity, and the random vibration frequency. The Allan Variance is a function of the PLL noise bandwidth and the oscillator's vibration sensitivity. The Allan Variance is inversely proportional to the noise bandwidth. The 1-sigma jitter decreases as the PLL noise bandwidth increases.

The remaining term in Equation (7) is the dynamic stress error term θ_e. The dynamic stress error is a function of the tracking loop order and the PLL noise bandwidth. It is also a function of the relative motion between the satellite and receiver and the satellite clock drift. The tracking loops cannot distinguish between relative motion and clock drift. As the PLL noise bandwidth increases, the dynamic stress error increases, which increases the 1-sigma PLL tracking error. The end result is that the PLL cannot tell the difference between the dynamic stress on the platform and the errors due to clock errors,

dynamic stress on the oscillators, or thermal noises. All these factors fall under the 15° rule of thumb for PLL tracking.

This section on GPS receivers and their performance under high dynamics is only a brief introduction to the subject. For further reading please refer to Kaplan [14]

Differential GPS

Up to this point, the topics have focused on the accuracy and performance of a stand-alone GPS receiver. The goal of this research is to design a GPS-based system that can match the existing high-speed film system accuracy. To achieve the greatest possible accuracy from the GPS sensors, differential techniques must be used to remove the dominant error sources. A common real-time DGPS system is shown in **Figure 14**.

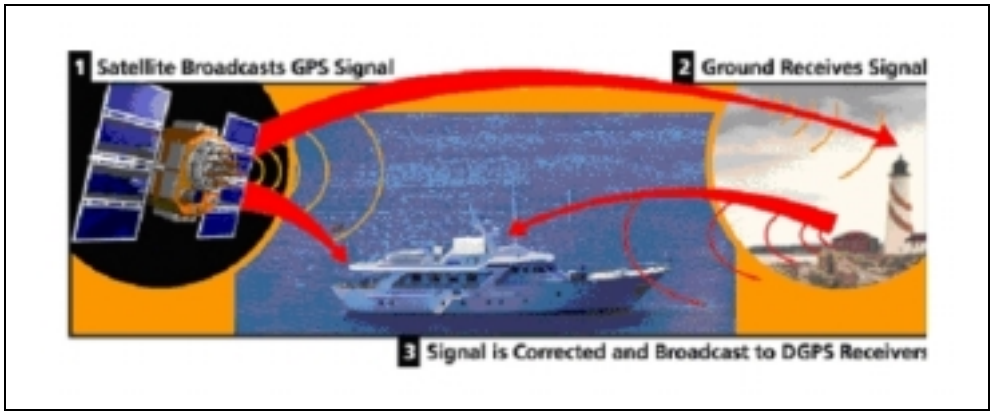

Figure 14. DGPS [9]

The difference between DGPS and a GPS receiver operating as a stand-alone unit is the addition of a second independent GPS receiver operating as a reference station. The differences between the measured distances and the calculated distances to the satellites

are continuously determined by the reference receiver, and these differences are then transmitted as corrections to the mobile GPS receiver, or stored for post-processing. Post-processing is often easier to implement, because it doesn't require the additional hardware such as hard-wire data links or transmitters. Post-processing also eliminates data latency because the corrections can be applied to the same time epoch for each measurement. The advantage of real-time corrections depends on the application. Some precise navigation applications may require real-time corrections.

The increased accuracy of DGPS is based on the fact that errors such as satellite ephemeris and ionospheric delay are similar for receivers separated by distances as large as hundreds of kilometers. Theses errors, in addition to being spatially correlated, tend to vary slowly over time. The reference station estimates the errors for each satellite and provides them to the mobile receiver with some delay called *latency*. The further the mobile user is from the reference station, or the longer the latency, the less benefit derived from the differential correction. Table 2 gives a summary of these errors and their reduction in DGPS mode. This table is from the Kaplan text [14] dated before S/A was turned off. The important errors that are removed by DGPS are the user segment and the satellite position errors. The error estimates in Table 2 are calculated with the user collocated with the reference station.

Table 2. Estimated GPS C/A-Code Pseudorange Error Budget

Segment Source	Error Source	GPS 1-sigma Error (m)	Local Area DGPS 1-sigma Error (m)
Space	Satellite Clock Stability	3.0	0
	Satellite perturbations	1.0	0
	Selective Availability	32.3	0
	Other (Thermal radiation, etc.)	0.5	0
Control	Ephemeris prediction error	4.2	0
	Other (Thurster performance, etc.	0.9	0
User	Ionospheric Delay	5.0	0
	Tropospheric Delay	4.5	0
	Receiver noise and resolution	4.5	2.1
	Multipath	2.5	2.5
	Other (interchannel bias, etc.)	0.5	0.5
System UERE	Total (rms)	33.3	3.3

The local area DGPS (LADGPS) reference station in Table 2 refers to a reference station that is close to the mobile receiver. The type of measurements and correction algorithms for DGPS fall into three main categories, code measurements only, carrier-phase measurements, and carrier-smoothed code measurements. Each implementation has its strengths and weaknesses, depending on the type of application and environment.

Code-Only DGPS

Code-based DGPS is the simplest form of differential error correction. It entails the reference station sending out to the users the difference between its surveyed position and the GPS-derived position. The user's can then apply the corrections to their GPS-computed latitude, longitude, and geodetic height. In code-based DGPS, the reference stations usually fall into two categories, local area DGPS (LADGPS), and wide area

DGPS (WADGPS). In LADGPS one reference station is used for GPS receivers close to the station. A WADGPS uses a network of reference stations to calculate and update the error information for an entire region.

This Code-based technique requires the user and reference station to compute the GPS position based on the same group of satellites. This is often impractical to implement even when the separation between the reference station and mobile receiver is small. An alternate method is for the reference station to calculate pseudorange corrections for each satellite in view. The mobile receiver can then incorporate the pseudorange corrections for the common satellites. The corrections are only valid for a short period of time. Thus, the receiver must apply each correction at a time corresponding to its own pseudorange measurement. It is important to note that the common errors between the reference station and the mobile receiver become increasingly decorrelated as the separation distance increases. To implement code-based DGPS, the user's receiver must be able to output raw pseudorange data for each satellite in view. Code-only DGPS can provide accuracy in the 2-3 meter (rms) range [8].

Carrier Phase DGPS

Carrier phase is the next type of DGPS measurement algorithm. The carrier frequency for L1 is 1575.42 MHz and has a wavelength is 19cm. By tracking and measuring the carrier phase, position accuracy as small as a few millimeters is possible. The carrier phase can be measured to tenths of a cycle or better. Carrier phase is not without drawbacks. The carrier signals, even though they are modulated with navigation and ranging codes, carry no time-tags that distinguish one cycle from another. GPS

receivers can accurately measure the carrier cycle, but not "which" cycle. This limitation is known as integer ambiguity. Many algorithms have been proposed to solve for the integer ambiguity. Most are fairly complex to implement and limit the separation between the mobile receiver and reference station to tens of kilometers [8]. Often the code measurements can be used to aid the ambiguity resolution problem. The most serious drawback to carrier phase DGPS is the time it takes to form a position solution and the possibility of the carrier-lock loss, but if the ambiguity can be accurately determined, the payoff is unmatched accuracy. For additional information on carrier phase tracking, the reader should reference [8].

Carrier Smoothed

The last type of DGPS measurement is carrier smoothed. Carrier smoothed measurements combine the absolute, but less precise, measurements of code based techniques with the precision of the ambiguous carrier phase techniques. Carrier-smoothed code is easier to implement than pure carrier phase measurements and improves the accuracy of DGPS to the 0.5 m range. For additional information on carrier smoothed tracking, see [8].

DGPS Differencing Techniques

To eliminate some of the nuisance parameters further, such as satellite clock errors or receiver clock errors, measurements between the reference and mobile receiver and multiple satellites can be "differenced" at each measurement epoch. The two common

difference techniques are single difference and double difference. Figure 15 shows the configuration for single differencing. Single differencing is often used to increase the accuracy of code-based DGPS further.

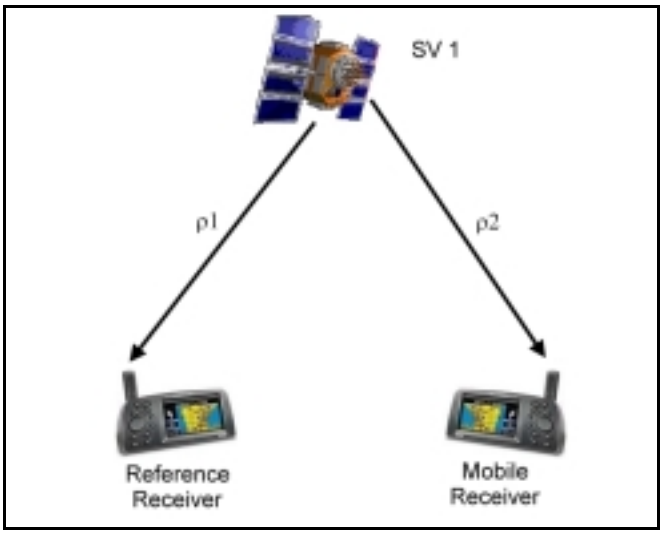

Figure 15. DGPS - Single Differencing

In single differencing, difference measurements between one satellite and two receivers are collected. Equation (8) is the standard representation of a pseudorange measurement. The hardware noise is often neglected, and currently selective availability is turned off.

$$\rho_j = r + c(\delta t_u - \delta t_{sv} + \delta t_{trop} + \delta t_{ion} + \delta t_{noise} + \delta t_{mp} + \delta t_{hw} + \delta t_{SA}) \qquad (8)$$

where

ρ_j = *Pseudorange measurement from satellite* j

δt_u = *Receiver clock error* (s)

δt_{sv} = *Satellite clock error* (s)

δt_{trop} = *Delay due to troposphere* (s)

δt_{ion} = *Delay due to ionosphere* (s)

δt_{noise} = *Delay due to GPS receiver noise and resolution noise* (s)

δt_{mult} = *Delay due to multipath* (s)

δt_{hw} = *Delay due to hardware errors* (s)

δt_{SA} = *Delay due to selective availability* (s)

r = *True range to receiver* (m)

c = *Speed of light* (m/s)

Single Differencing. Single differencing is calculated by subtracting the pseudorange measurement between the reference receiver to a satellite and the mobile receiver and the same satellite as shown in Equation (9):

$$\Delta\rho_{12}^{j} = \Delta\rho_{1}^{j} - \Delta\rho_{2}^{j} \tag{9}$$

$$\Delta\rho_{12}^{j} = r_{12}^{j} + c(\delta t_{u12}^{j} + \delta t_{trop12}^{j} + \delta t_{ion12}^{j} + \delta t_{noise12}^{j} + \delta t_{mp12}^{j})$$

where

Δ = *Single Difference DGPS*

$\Delta\rho_{12}^{j}$ = *Single Difference between receivers* 1 *and* 2 *and the* j^{th} *satellite*

r = *True range to satellite*

c = *Speed of light* (m/s)

δt_{u12}^{j} = *Receiver clock error* (s)

δt_{trop12}^{j} = *Tropospheric error* (s)

δt_{ion12}^{j} = *Ionospheric error* (s)

$\delta t_{noise12}^{j}$ = *Receiver noise error* (s)

δt_{mp12}^{j} = *Multipath error* (s)

The advantage of single differencing is that the SV clock error is cancelled and the tropospheric and ionospheric errors are reduced. The drawback to single differencing is that the multipath and noise is amplified by a factor of $\sqrt{2}$ [14].

Double Differencing. The second type of differencing technique is double differencing. Double differencing uses single difference measurements between two satellites and the reference and mobile receivers and is shown in Figure 16.

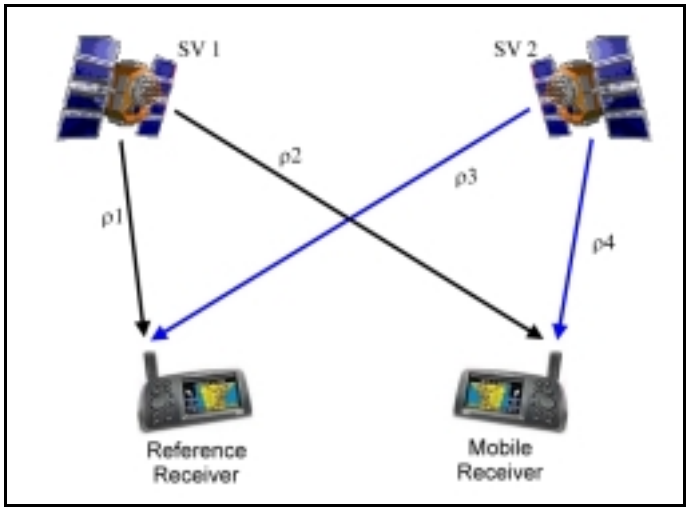

Figure 16. DGPS Double Differencing

To implement double differencing, the single difference between the reference and mobile receivers and one satellite are differenced from the single difference of the mobile and reference receiver and another satellite, as shown in Equation (10):

$$\nabla\Delta\rho_{12}^{SV1SV2} = \Delta\rho_{12}^{SV1} - \Delta\rho_{12}^{SV2} \tag{10}$$

$$\nabla\Delta\rho_{12}^{SV1SV2} = \nabla\Delta r_{12}^{SV1SV2} + c(\nabla\Delta\delta t_{trop12}^{SV1SV2} + \nabla\Delta\delta t_{ion12}^{SV1SV2} + \nabla\Delta\delta t_{noise12}^{SV1SV2} + \nabla\Delta\delta t_{mp12}^{SV1SV2})$$

where

$$\begin{aligned}
\Delta\nabla &= \textit{Double Difference DGPS} \\
\Delta\rho_{12}^{SV1SV2} &= \textit{Double Difference between receivers } 1 \textit{ and } 2 \textit{ and satellites } 1 \textit{ and } 2 \\
\nabla\Delta r_{12}^{SV1SV2} &= \textit{True range to satellite } (m) \\
c &= \textit{Speed of light } (m/s) \\
\nabla\Delta\delta t_{trop12}^{SV1SV2} &= \textit{Tropospheric error } (s) \\
\nabla\Delta\delta t_{ion12}^{SV1SV2} &= \textit{Tonospheric error } (s) \\
\nabla\Delta\delta t_{noise12}^{SV1SV2} &= \text{Re}\textit{ceiver noise error } (s) \\
\nabla\Delta\delta t_{mp12}^{SV1SV2} &= \textit{Rultipath error } (s)
\end{aligned}$$

By differencing two single difference measurements, the satellite clock error and receiver clock error are both cancelled. Like single differencing, the tropospheric and ionospheric errors are reduced. The drawback is similar to single differencing in that both the multipath and noise are amplified, in this case by a factor of 2.

DGPS Errors

The strength of DGPS is its ability to remove the receiver and satellite clock errors. Even with single or double differencing techniques, some errors still remain. The errors can be grouped into two categories, correlated and uncorrelated errors. The uncorrelated errors included are multipath and measurement noise. Neither increases as the distance

from the mobile receiver to the reference station increases. For code-only DGPS, multipath and receiver noise will typically add 1 – 3 meters of error [14].

Correlated errors are spatially related and include ephemeris, ionospheric, and tropospheric errors. The position errors are related to the satellite ephemeris. If the broadcast ephemeris is incorrect, the calculated satellite position will differ from the true satellite position. The error can often be calculated by comparing the broadcast ephemeris with the precise ephemeris. The ephemeris in DGPS applications typically adds a few centimeters of error for baselines under a few hundred kilometers. The ionospheric errors are spatially correlated, because for short baselines, the GPS signal passes through approximately the same atmosphere. Differential ionospheric errors typically add only a few centimeters of error [14]. The last correlated error is due to the signal passing through the troposphere. Tropospheric errors should always be modeled out in the DGPS calculations due to their dependence on receiver altitude. If the mobile receiver and reference receiver are at significantly different altitudes, such as in in-flight ejection seat testing, the errors introduced can be in the order of a few meters. When properly modeled, the errors due to the troposphere remain small, normally on the order of a few centimeters [14].

Summary

The chapter has described the general theory behind the GPS. It introduced the different factors that affect its accuracy as well as the concept of DOP, a factor that relates ranging error to position error. The next section introduced GPS receivers and some design features that affect how well they perform in a highly dynamic environment.

The last section described DGPS and the Code, Carrier Phase, and Carrier Smoothed DGPS algorithms. Chapter 3 will describe how the GPS, with all the limitations described in this chapter, was used to collect data for the ejection seat design and test community.

III. Methodology

Overview

While Chapter 2 focused on the general theory relevant to this research, Chapter 3 begins with the DIVEPACS design criteria and progresses through each phase of the research methodology. In addition, Chapter 3 details the research data collection and analysis process associated with each different test phase.

Design Criteria

Table 3 summarizes the initial design criteria for the system. The initial criteria were based on data collected during the Russian K-36 ejection seat design, validation, and testing [2].

Table 3. Initial System Design Criteria

Criteria	Specification
Position Accuracy	Meets or exceeds the current high-speed film system accuracy of 18 inches rms [2].
Size and Weight	Comparable to the two-pound survival radio carried by aircrew member in the SRU-21/P survival vest.
Power On/Off	Capable of remotely applying or disconnecting power to the internal battery source due to the safety concerns when the unit is operated near ejection sled rockets.
Acceleration	18 g's

Criteria	Specification
Jerk	400 g/s
Vibration	0.1G2/Hz (10 – 2000 Hz)
Antenna Size	Small enough to fit inside aircrew helmet, or if placed on outside of shell must have a low profile so the unit does not add additional neck loading from wind drag.
Type of data collected	3-dimensional position and velocity. Raw pseudorange and satellite data for DGPS post processing.
Data latency	Post process position data. Matlab® software used to calculate DGPS position and velocity solution.
Sampling Rate	20 Hz
Data Collection Duration	2 Hours

Assumptions and System Description

Assumptions

When the project was first conceived, several assumptions were made about how the unit would be employed. The first assumption was that the tests would always be conducted in a location where the antenna would have a clear view of the sky. Secondly, the tests must be within the operating range of a commercially available GPS receiver. GPS receivers have export restrictions that limit their ability to collect data above 1000 knots maximum speed, and 60,000-foot maximum altitude. The monitored platform should provide some measure of protection from shock and vibration for the DIVEPACS and the antenna. The plastic case is designed to protect the equipment, but the unit must be mounted securely to the platform. DIVEPACS was designed to collect position data for post-processing. It is however capable of outputting data in real time through an RS-

232 serial port. The last assumption is that the end user for the equipment has access to, and a basic working knowledge of, Matlab®. Both the single point positioning algorithm and the differential GPS algorithm were implemented using Matlab® software.

System Description

DIVEPACS was originally designed for ejection testing. The main system components are the GPS receiver, data logger, antenna, and power supply. All the components, with the exception of the antenna, must be small enough to fit into the aircrew survival vest worn by the manikin. This configuration keeps the DIVEPACS located close to the manikin's center of mass. It is important that any bulky items placed on the manikin are positioned symmetrically around the manikin center, so that the equipment doesn't cause the manikin to become unstable in flight and tumble when it enters the airstreams. When used for other applications, the only limitation is to place the antenna so it has an unobstructed view of the sky. Figure 17 shows the final DIVEPCS configuration for ejection seat testing.

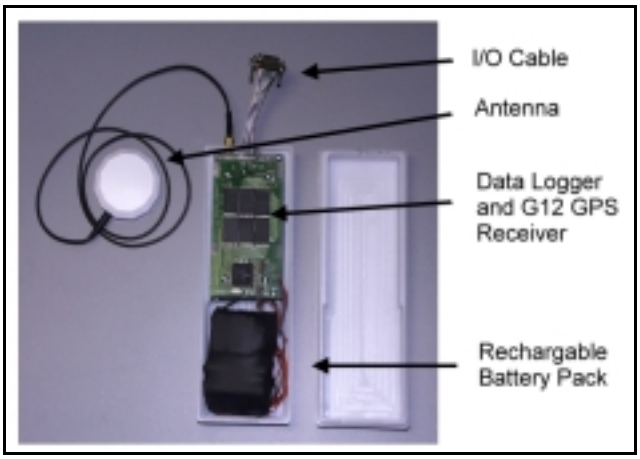

Figure 17. DIVEPACS Configured for Ejection Testing

GPS Receiver. In a typical ejection sequence the ejection components experience accelerations as high as 20g [2]. The DIVEPACS incorporates an Ashtech® G12 Original Equipment Manufacture (OEM) GPS Receiver. The G12 is the top circuit card in Figure 18.

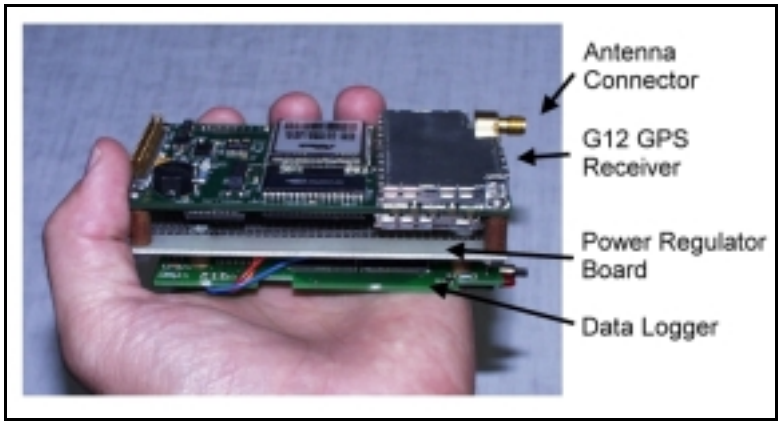

Figure 18. G12 Receiver, Data Logger, and Voltage Regulator

The G12 is an original equipment manufactured (OEM), 12-channel, single frequency (L1), coarse acquisition (C/A) code, and carrier receiver. The manufacturer's

specifications state that the receiver offers consistent and reliable tracking with peak acceleration rates greater than 23 g's, over 450 g/s of jerk, and vibration levels of 0.1G2/Hz [3]. The G12 can collect data up to 1000 knots maximum velocity at a maximum altitude of 60,000 feet.

The re-acquisition time is 2 seconds, and the hot start time to first fix is 11 seconds. Re-acquisition time is the amount of time it takes a GPS receiver to reacquire a position solution after a momentary signal loss. Hot start time refers to the time it takes the receiver to acquire a position solution initially when it has the current satellite almanac in memory. G12 can output NEMA messages, Ashtech® proprietary messages, and raw measurements.

One design constraint on the overall system, to include the GPS receiver, data logger, and power supply, is that it be small enough to fit into the survival vest's pockets. The size of the G12 is 108mm x 58.4mm.

The G12 is limited to a 20 Hz sampling rate. Based on the test data from previous ejections, a 20 Hz sample rate should be adequate to determine the manikin's position and velocity [2]. When the G12 sample rate is set sample at either 10 or 20 Hz, only ten satellites are used to calculate a position solution. The specification sheet for the G12 is included in Appendix D.

Antenna. The antenna is manufactured by Antenna Technology Inc. and is specifically designed for GPS signals. The unit is 2.1 inches in diameter and 0.75 inches tall including the mounting base. It is an active antenna providing a 26 dB gain

improvement. The antenna weighs 2.8 ounces and has a 1 Watt power consumption. The specification sheet for the antenna is included in Appendix D.

Figure 19. GPS Antenna and Aircrew Helmet

Data Logger. All the data collected from the DIVEPACS GPS receiver is stored in an H.O. Data Compu-Log RS-12DD data logger for post-processing. The data logger is designed to collect and store the output from any RS-232 source at up to 115,000 bps. The data is placed into non-volatile memory so it is protected in the event of power loss. Figure 20 shows the RS-12DD in the original container. Due to the shock and vibration expected in an actual ejection, the original container, I/O connections, and power supply were replaced. The R2-12DD is the bottom of the three circuit boards in Figure 18.

Figure 20. HO DATA Data Logger

Power Supply. The black package below the G12 and data logger in Figure 17 is a rechargeable battery pack. Eight 1.25-volt AA nickel metal hydride batteries power both the G12 and data logger. The battery package also contains the power isolation relay used to separate battery power from the G12 and data logger. The batteries are charged in the case through the GPS Ejection Module Internal cable shown in Appendix C, Figure 78.

Phase I – Bench Testing

Static Data Collection

The first testing phase used static data collections. The initial configuration for the equipment consisted of a G12 OEM receiver in an Ashtech sensor case, an HO DATA data logger in the original factory container, and a rechargeable battery pack. The antenna was mounted on a standard skydiving helmet along with a combination barometric altimeter and data logger. The antenna was mounted on the helmet in preparation for the next phase of testing. The separate components are shown in Figure 21 on an aircrew survival vest.

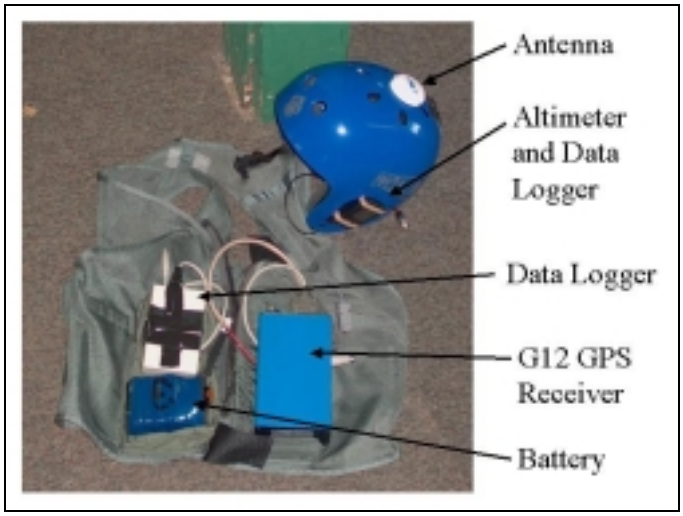

Figure 21. Equipment on Survival Vest

Before testing could begin a custom GPS to Logger Cable had to be fabricated to connect the G12 sensor to the battery pack and data logger. The schematic for the GPS to Logger Cable is shown in Figure 76, Appendix C. The GPS to Logger Cable also connects the G12 sensor to a PC through the serial port for data downloading and GPS receiver configuration. This first testing phase focused on configuring the DIVEPACS hardware so the data from the G12 could be stored in the data logger, and writing the Matlab® code necessary to analyze the data. Several static data collections were accomplished to test the hardware and software and to determine a baseline for the receiver accuracy and the length of time data could be collected before exceeding the data logger's memory capacity.

GPS Simulator

A GPS simulator was used to simulate the flight profiles that could not be tested at a high-speed test track or during freefall testing. The GPS simulator was the ST2760 by Spirent Communications. The simulator test configuration is shown below.

Figure 22. GPS Simulator

The user can create simulation scenarios and control both the receiver flight profile and GPS constellation configuration. The simulator can vary GPS constellation variables such as signal strength and nuisance parameters such as ionospheric and satellite clock errors. The flight scenarios can include several of different maneuvers to test the receiver's ability to track under different velocity, acceleration, and jerk profiles.

Phase II – Freefall Testing

Overview

The second phase of testing was freefall flight. The primary goal of Phase II testing was to ensure the DIVEPACS could reliably track enough satellites to determine a 3-dimensional position and velocity if the manikin began tumbling in flight. The other goal was to test the equipment configuration. It was important to determine how well the equipment would handle the shock and vibration of freefall and parachute deployment prior to testing the unit in an actual ejection. Freefall was the natural choice for testing equipment designed to monitor ejection profiles. The manikin rotations can be closely duplicated in freefall to test the GPS receiver's ability to remain locked onto the satellites as the antenna's pointing direction changes. The other benefit to freefall testing that made it so advantageous was the low cost and availability. As many as five tests were accomplished in a single test session for a fraction of the single trial cost at a high-speed test track. The short turn around time between trials enabled equipment modifications to be immediately tested and verified.

DIVEPACS Configured for Freefall Testing

Figure 23 shows the DIVEPACS as it was configured for freefall testing. One difference between the freefall configuration and the ejection configuration is the modification of the survival vest pockets to fit around the parachute harness. The other difference is the use of the lightweight skydiving helmet. Neither of these modifications changed the GPS receiver’s and data logger’s operating characteristics.

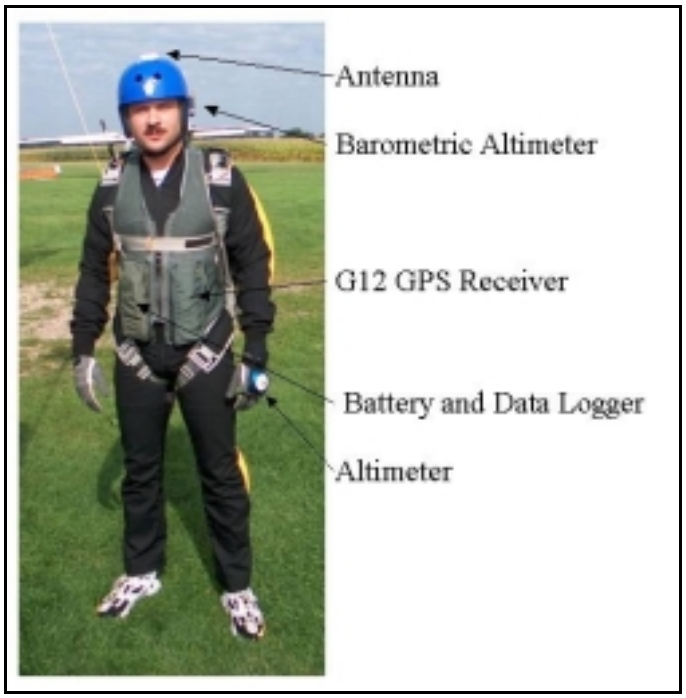

Figure 23. Phase II Configuration

Although the maximum velocity during freefall is approximately 140 mph, compared to the 600+ mph ejection velocity, the freefall environment is similar to an actual ejection. In both cases the equipment must be located close to the bodies center of mass with the weight evenly distributed so that the equipment does not cause the manikin to become unstable as it enters the air stream. The accelerations from the parachute opening are two or three g's for both freefall testing and ejection testing. The main difference between the two, that can not be duplicated, is the initial 15 to 18 g accelerations experienced by the manikin from the rocket sled accelerating down the track and the acceleration from the ejection seat leaving the cockpit. Once the parachute is deployed this phase of testing and the ejection environment are identical.

The GPS receiver, data logger, and battery are packed into the aircrew survival vest's two large pockets. The GPS antenna was placed on top of the helmet. The antenna was

placed slightly toward the rear of the helmet because the most stable freefall position is with the front of the body toward the ground with the head tilted back toward the horizon. This position keeps the back of the head and the antenna oriented toward the sky.

The maximum aircraft exit altitude for freefall testing is 13,500 feet with parachute deployment no later than 2,500 feet. The maximum freefall time is approximately 60 seconds. The freefall velocity is on average 125 mph. Depending of the type of canopy, the relative speed over ground can be as fast as 40 mph.

Phase III – Ejection Seat Test and Evaluation

Overview

This section provides the details of how data is collected during ejection test and evaluation at a high-speed test track. Each of the major test components is described, along with a brief concept of operations. Finally, the details of how the DIVEPACS was incorporated into the testing are described.

Hurricane Mesa High Speed Test Track

Hurricane Mesa, Utah, hosts the nation's only privately-owned supersonic test track. Hurricane Mesa Test Track (HMTT) is owned and operated by Universal Propulsion Company, Inc. (UPCO). The track is built on top of Hurricane Mesa near St. George in Southern Utah. HMTT is designed to simulate selected portions of the flight environment under accurately programmed and instrumented conditions. This facility gives escape system designers the capability to fill the gap between laboratory

investigations and full-scale flight tests. The 12,000 ft. track is fully capable of handling propulsion velocities up to supersonic. The track level is at 5,100 MSL with the track terminating at a 500-foot vertical cliff. The mesa's sloping terrain provides an additional drop of 1,000 ft. to the valley floor below. Figure 24 shows an aerial view of the HMTT facility.

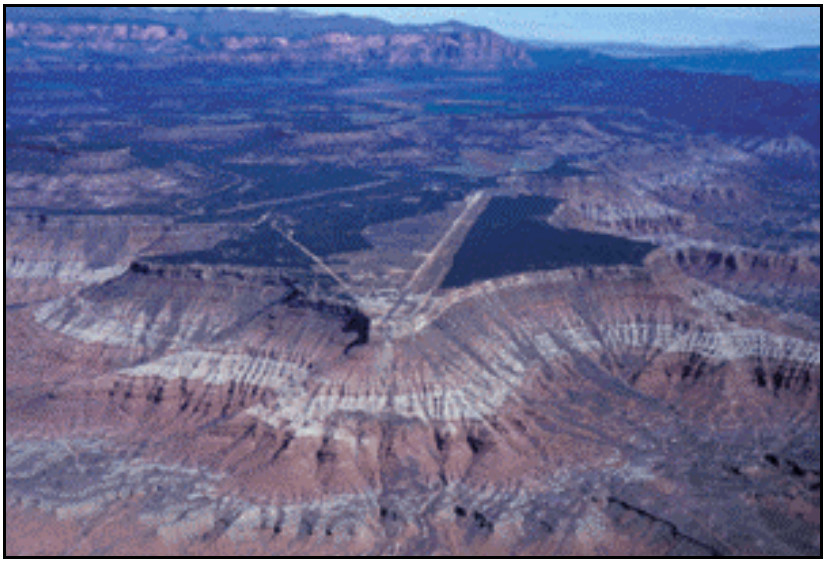

Figure 24. Hurricane Mesa Test Track

Rocket Sled. Figure 25 shows the F-15 forebody rocket sled connected to three separate rocket sleds. The furthest sled, called "Flat Boy", and the middle sled called "Box Boy", are pusher sleds that separate from the F-15 sled after their rockets burn out. The remaining rocket sled called "Red Genie", is permanently connected to the F-15 sled by the bar shown in the figure.

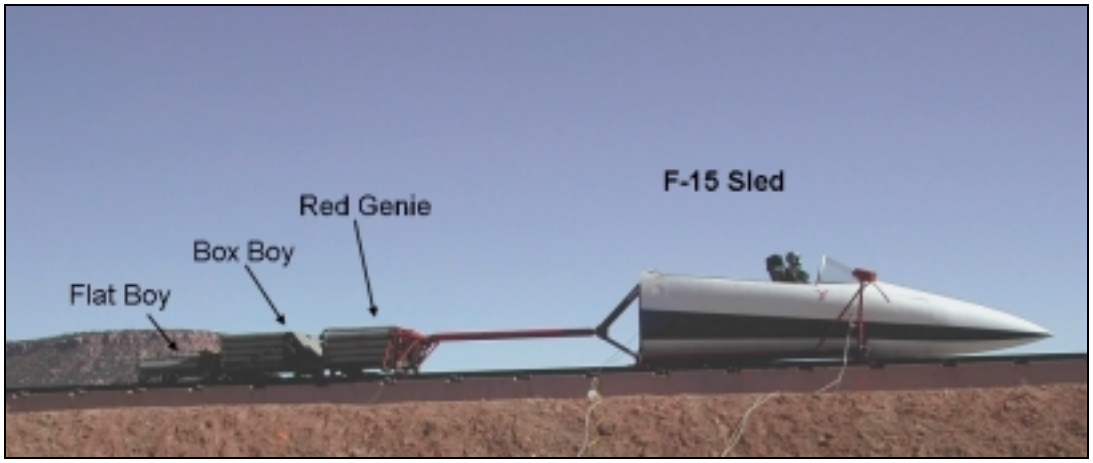

Figure 25. F-15 Rocket Sled

The F-15 sled shown is configured with six rocket stages to reach 630 knots equivalent air speed (KEAS). The speed depends on the ejection seat model and type of test. For a typical ejection seat test, the average speed is 400 KEAS [2].

Event Timing. After the initial rockets fire, all other events are trigged by a series of screen boxes located along the track. As the sled reaches each screen box an electrical contact knife mounted on the sled completes the electrical circuit and triggers the event. A typical screen box is shown below in Figure 26.

Figure 26. Screen Box

Sled Velocity Data. The sled velocity is calculated using sensors mounted on the sled slippers that pass by permanent magnets mounted along the track. The data collected by the sled-mounted sensors was used as the truth data for the DGPS speed over ground calculations. A water break stopped the sled once the ejection seat cleared the cockpit. The water break uses a scoop mounted under the sled to collect water and redirect it forward to slow the sled down. Flooding the track's center section at different levels controls the sled deceleration rate.

Manikins. Manikins are used to simulate the aircrew member. One type of manikin is the Advanced Dynamic Anthropomorphic Manikin (ADAM) as shown in Figure 27.

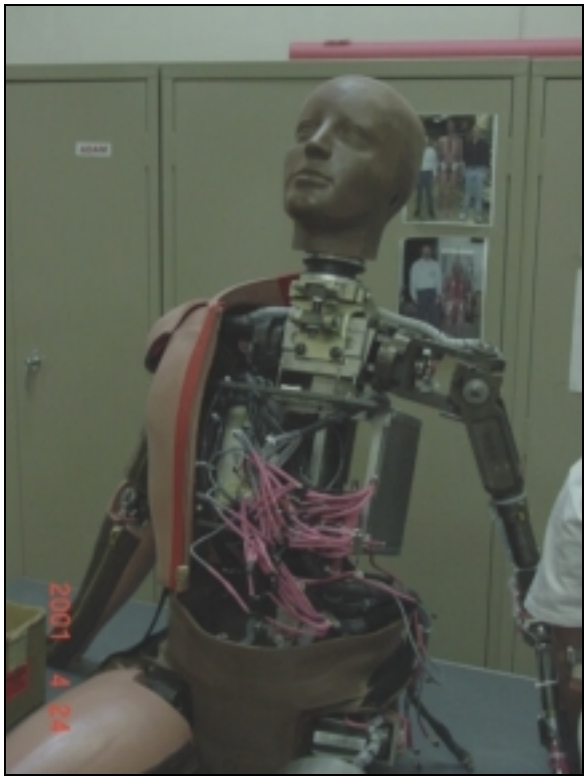

Figure 27. ADAM Manikin

The ADAM is one of the larger manikins. ADAM is 74.3 inches tall and weights 217 pounds. Over forty sensors located throughout the manikin convert mechanical movement into electrical signals. In addition to the sensors located at each joint, accelerometers and compression sensors monitor important parameters such as neck loads and spinal compression. The manikin is designed to resemble the human body with the same range of motion and associated degrees of freedom. Regardless of which manikin is used, it is outfitted with the same flight gear to simulate the actual flight weight and center of gravity locations for a pilot.

Manikin Data Logger. To avoid the possibility of telemetry data dropout, the data collected by the manikin sensors is stored inside the manikin in a data logger similar to the one shown in Figure 28 for post-processing. The data logger and its battery are located in the manikin chest cavity to provide them some level of physical protection. Each data logger can collect and store up to 64 analog channels at a sample rate of up to 20,000 Hz. The ADAM can hold two 64-channel data loggers.

Figure 28. Manikin Data Logger

Tracking Cameras. High-speed film cameras are used to track the ejection system components. 16mm and 70 mm high-speed motion picture film tracking cameras are strategically located on the rocket sled and track to provide the best coverage available for the given speed and trajectory. A typical ejection test uses 15 cameras to monitor the ejection sequence [6]. The high-speed film coverage allow the test personnel to examine an ejection sequence frame by frame to monitor different events, such as whether the ejection seat and manikin remained stable during the ejection sequence. Figure 29 shows one of the three 16mm high-speed cameras located on the F-15 sled. The camera's protective cover is open for this picture.

Figure 29. 16mm High-speed Sled Camera

Theodolite Cameras. Trajectory data during ejection seat testing is obtained by a VHS camera system called a Theodolite. The theodolite cameras obtain a true space position trajectory for the manikin or ejection seat during the test. The position is calculated by triangulation methods using multiple theodolites at precisely known locations. Inter-Range Instrumentation Group (IRIG) timing is encoded in each theodolite station and is the basis for timing correlation [7]. IRIG is standard timing used a test facilities. Figure 30 shows the computer station used to calculate the position data from the theodolite cameras. The manikin position is calculated for each time epoch by marking the manikin position on the TV monitor with a series of crosshairs. The position accuracy obtained is dependent upon how well the operator can align the crosshairs to the same point on the manikin at each time epoch and how precisely the theodolite camera positions are known.

Figure 30. Theodolite Data Conversion

The theodolites are fitted with wide-angle lenses so they can observe large portions of the track area. Figure 31 shows a typical ejection profile plotted with data from the theodolite video system. All final data were processed utilizing two smoothing passes and a 9-point fourth-order smoothing algorithm. The theodolite's position accuracy shown in this graph is 40 – 60 cm [6].

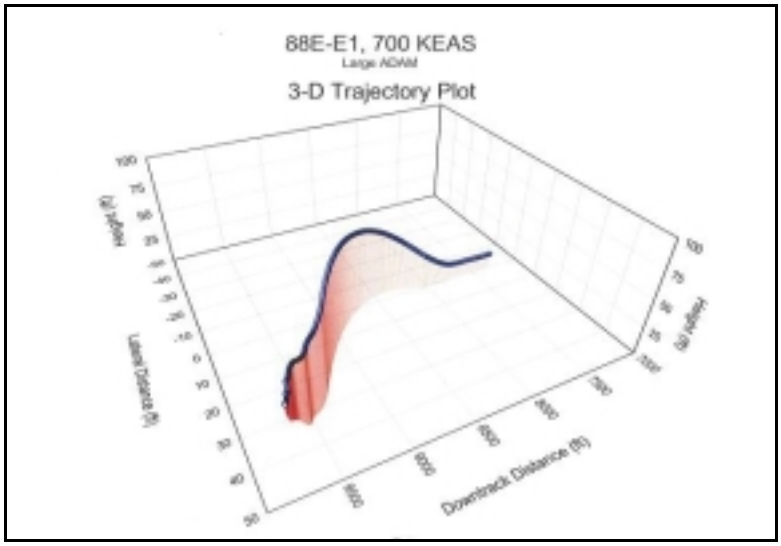

Figure 31. 3-D Trajectory Plot

The trajectory plot is for the manikin only. As shown in Figure 31, the manikin and ejection seat left the fuselage at a downtrack distance of approximately 7500 ft and rose to a height of approximately 100 ft, where the manikin separated from the ejection seat and then landed about 30 feet to the track's left.

DIVEPACS Configuration for Rocket Sled Ejection Testing

The first challenge was to assemble the components into a case that could protect the receiver and data logger during the ejection sequence. The G12 and data logger circuit boards were removed from the factory containers and placed into the specially designed container shown in Figure 32. The special container and connectors were designed to protect the system, should the manikin fall directly on the equipment as it lands under the parachute. The original battery and I/O cables were replaced with plastic connectors designed specifically to withstand the ejection forces. The data logger will retain the data even if the I/O cables are damaged and the battery disconnected.

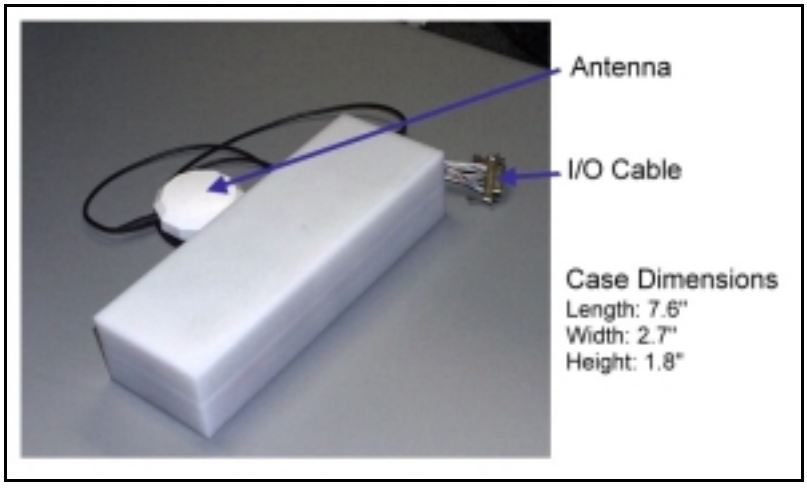

Figure 32. DIVEPACS Configured for Ejection Testing

In this configuration, the DIVEPACS has two operating constraints, the internal battery capacity, and the 12 MB of internal memory in the data logger. Table 4 lists the DIVEPACS estimated operational limits.

Table 4. DIVEPACS Battery and Memory Limitations

Battery Capacity	5.5 Hours Continuous Operation With Ashtech Marine III Antenna
Battery Capacity	6 Hours Continuous Operation With Antenna Technologies Handheld Antenna
Memory Capacity (By Number of Messages)	150,000 Messages (50,000 POS and 100,000 CT1 Messages)
Memory Capacity (By Sample Rate)	1 Hz – 41 Hours* 5 Hz – 8 Hours* 10 Hz – 4 Hours 20 Hz – 2 Hours ** Beyond Internal Battery Capacity*

The DIVEPACS was placed inside the survival vest large radio pocket. For safety reasons the DIVEPACS battery had to remain disconnected from the receiver and data logger through a relay until just prior to launching the sled down the track. At HMTT all battery power must be isolated from the ejection seat and rocket sled sensors while track personnel are arming the rocket motors. The relay was triggered remotely using the Ejection Seat Interface at Test Time connector and Ethernet cable shown in Appendix D, Figure 77. The Ethernet cable ran inside the survival vest then down the manikin's G-suit to a pull out connector inside the cockpit. Another pull out connector at the sled's rear connected a 500-foot Ethernet cable to a safe area where the DIVEPACS battery relay was triggered approximately 10 minutes prior to the sled launch. The different connectors are shown in Figure 33. The 10-minute warm-up period prior to sled launch

was to ensure the receiver had acquired enough satellites for a stable 3-dimensional position solution. This is important, since each time an additional satellite is tracked by the receiver, the position solution can have a small jump discontinuity due to the receiver logic calculating a new solution based on the new information and new satellite geometry. The extended warm-up time minimized the possibility of acquiring additional satellites during the ejection sequence.

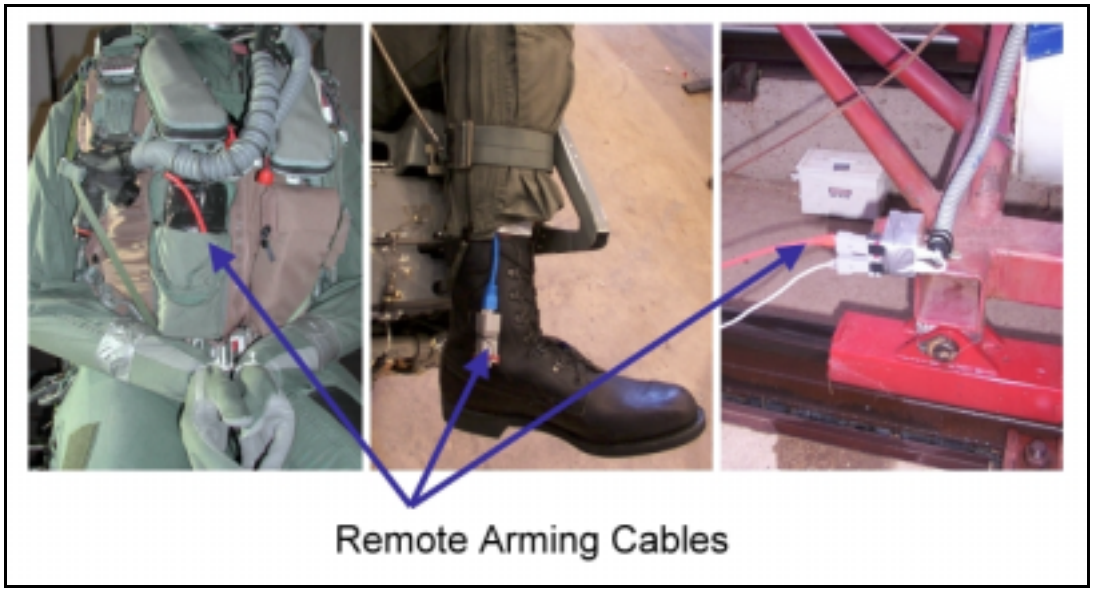

Figure 33. Remote Arming Cables

DGPS Reference Station

Determining Reference Station Location. The DIVEPACS must be operated in DGPS mode to obtain the most accurate position and velocity solution. Hurricane Mesa High-Speed Test Track does not have a GPS reference station on site. A separate GPS receiver had to set up and its location accurately determined.

One method for determining the reference station position is to average the location determined by the receiver over a period of time. For users with single frequency receivers, the collection should be in the nighttime when the ionospheric errors are the lowest.

Another method used to determine the reference station location is to send the data from the receiver to the National Geodetic Survey (NGS). The NGS oversees a network of continuously operating reference stations (CORS) that provide GPS data free of charge. The CORS sites collect carrier phase and code range measurements throughout the United States and other parts of the world. A map of the CORS network is shown below.

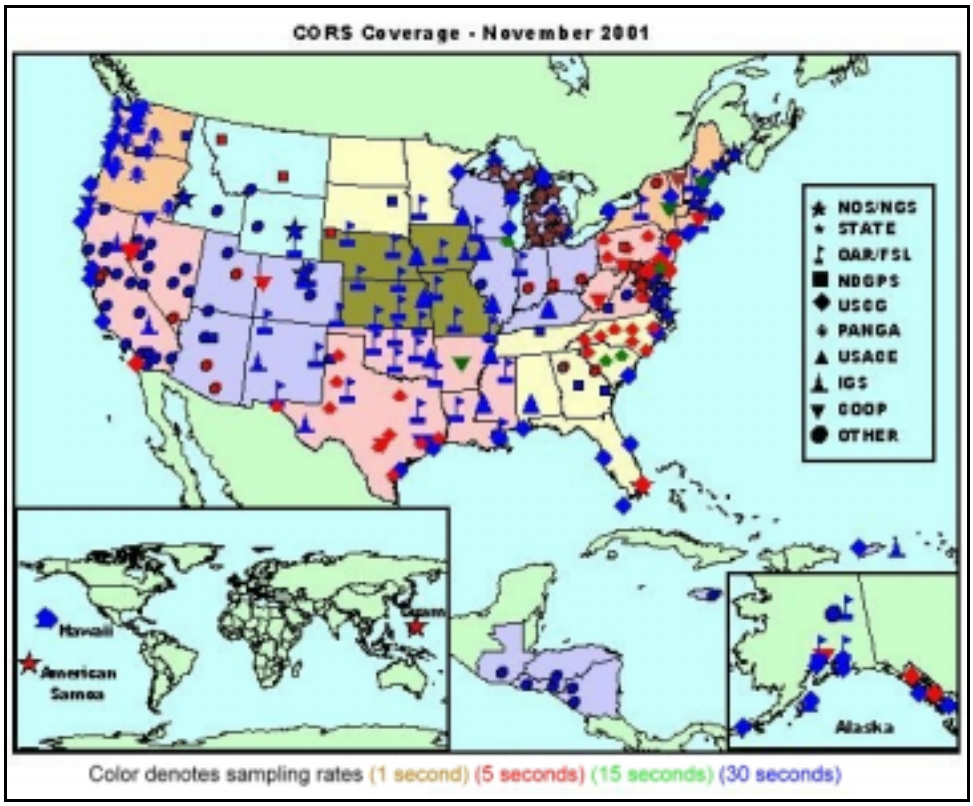

Figure 34. CORS Network [18]

The NGS maintains several utilities that can help users determine a GPS receiver position with centimeter level accuracy. Users in the field can send GPS data files to the NGS over the Internet. The data is processed to determine a position using NGS On-line Positioning User Service (OPUS) computers and software and sent back to the user by e-mail. A restriction to this service is that the uploaded data must be dual frequency carrier-phase data collected for a minimum of two hours and sampled at 5, 10, 15 or 30 seconds [18]. An analysis of the accuracy obtained from averaging the data from a single receiver compared to the CORS determined position is presented in Chapter 4, Phase I - Bench Testing and GPS Simulator.

HMTT Reference Station. A location was required for the DGPS reference station. Since both ejection trials started at the 5200-foot marker on the 12,000-foot long track, a location near this point would be ideal. The fence surrounding the water well, show in Figure 35, directly across from the sled initiation point was chosen.

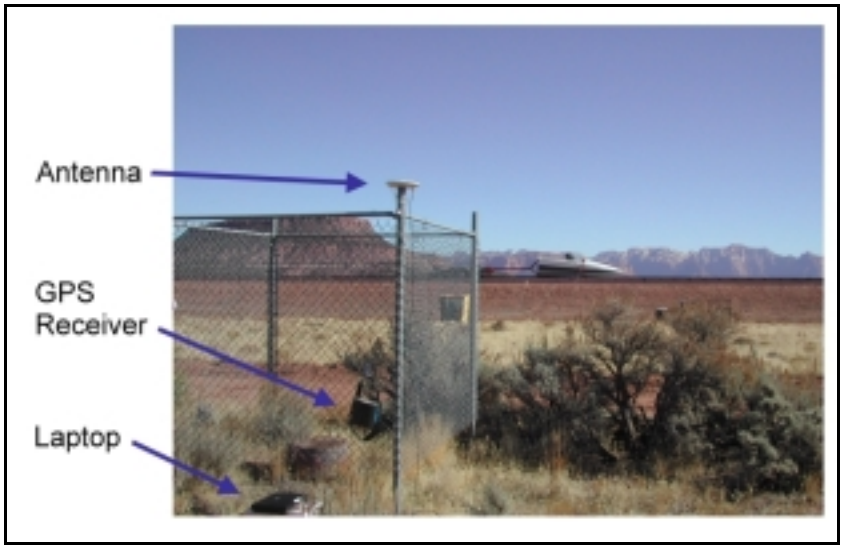

Figure 35. DGPS Reference Station

A fence surrounding the well made an ideal location to set up a DGPS reference station. The fence is a unique feature that can easily be located in future tests, and is located far enough away so that the rocket blast does not damage the equipment.

At the time of these tests, only one G12 GPS receiver was available so an Ashtech Z-Surveyor was used as the reference station GPS receiver. The technical specifications of all the GPS equipment used during the research are described in detail in Appendix D. The Z-Surveyor and antenna can be seen in Figure 35 mounted on the chain link fence and corner post. The data collected from the Z-Surveyor included the raw measurements and the NMEA GGA, GSV, and POS messages. The details of these messages are described in Appendix B. The three NMEA messages were logged directly to a laptop via the serial port. The laptop can be seen in the lower left corner of Figure 35. The raw data collected was stored on an internal PCMCIA card.

Summary

In this chapter the DIVEPACS design criteria and initial assumptions for the system were described. The testing began with simple bench top testing and evolved into full-scale ejection trials. During the equipment buildup, the software was written to convert the NMEA messages and raw pseudorange data into accurate position and velocity solutions. The next chapter details the results from the three testing phases.

IV. Results and Analysis

Overview

This chapter is divided into the three sections. It begins with the results and analysis from the Phase I bench testing, which included static collections and GPS simulator runs. The next section presents the results and analysis from the Phase II freefall experiments conducted at the Skydive Green County dropzone. The final section details the two rocket sled ejection trials at Hurricane Mesa Test Track (HMTT).

Phase I - Bench Testing and GPS Simulator

Static Data Collection- Stand-Alone Mode

The first bench tests were static data collections. The static collections provided a baseline for the G12 receiver accuracy in stand-alone mode without any differential corrections. The data was collected over a two-week period using the GPS antenna mounted on the AFIT rooftop. The duration for each sample was approximately 2 ½ hours. Figure 36 shows the results from a typical static collection. The red diamond indicates the DIVEPACS's mean position measurement. The green square is the true position as determined by the NGS OPUS in the spring of 2001. The red square is the position determined by the NGS OPUS in January of 2002.

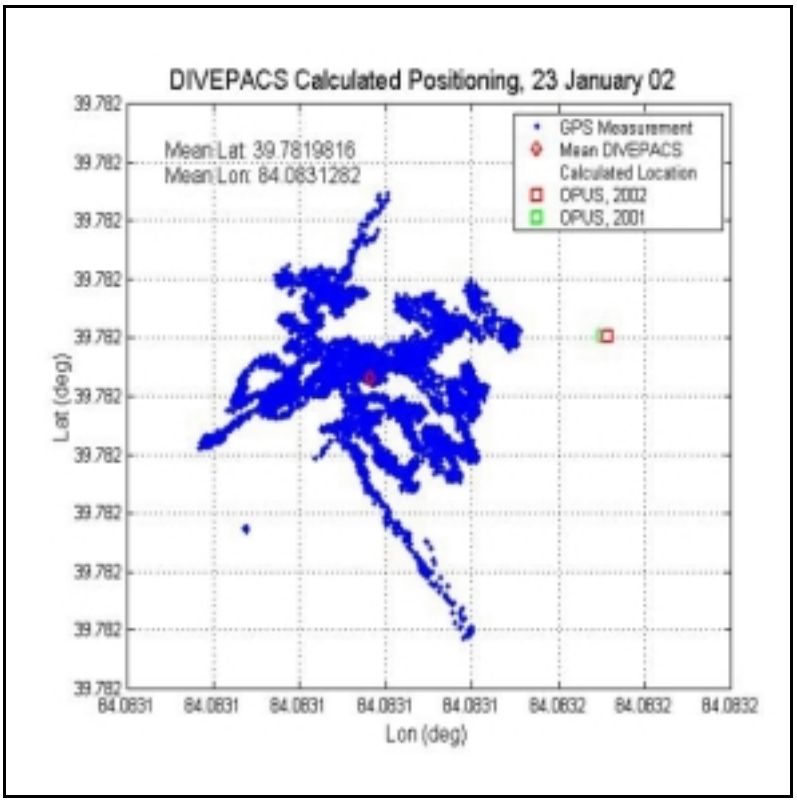

Figure 36. DIVEPACS Static Collection, 23 January 2002

The position accuracy is displayed in meters by transforming the estimated position in the latitude, longitude, and altitude frame into the local level frame as shown in Figure 37. This example indicates the typical accuracy levels recorded during this research. The data's 2DRMS accuracy was 1.5 – 2.5 meters in the horizontal direction, and 7 – 10 meters (RMS) in the vertical direction.

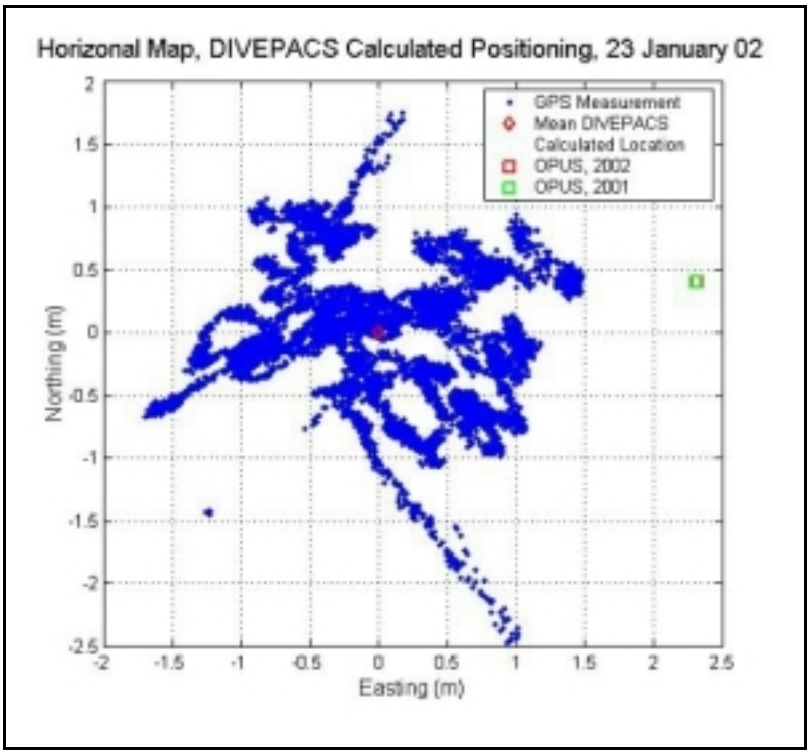

Figure 37. DIVEPACS Static Collection, Horizontal Map, 23 January 2002

The 2002 OPUS calculated position is slightly less than two centimeters to the left of the 2001 OPUS calculated position. At this resolution it is difficult to distinguish the two separate markers. In this example the data appears to have a bias in the east direction. This data was collected over a 1 ½ hour period. The errors in each direction are zero mean so in collections with longer sample periods the bias is removed. The OPUS accuracy is summarized in Table 5 [18].

Table 5. OPUS Published Accuracy

OPUS RMS Accuracy		
Latitude (m)	Longitude (m)	Altitude (m)
0.029	0.011	0.013

The DIVEPACS's stand-alone accuracy could be improved by collecting data during the evening when the errors due to the ionosphere delay are at the lowest. Careful antenna placement away form reflective surfaces would also improve the accuracy. In Figure 38, the altitude, north, and east measurements are shown over the collection period. The spikes in the position data occur each time the receiver gains or looses a satellite.

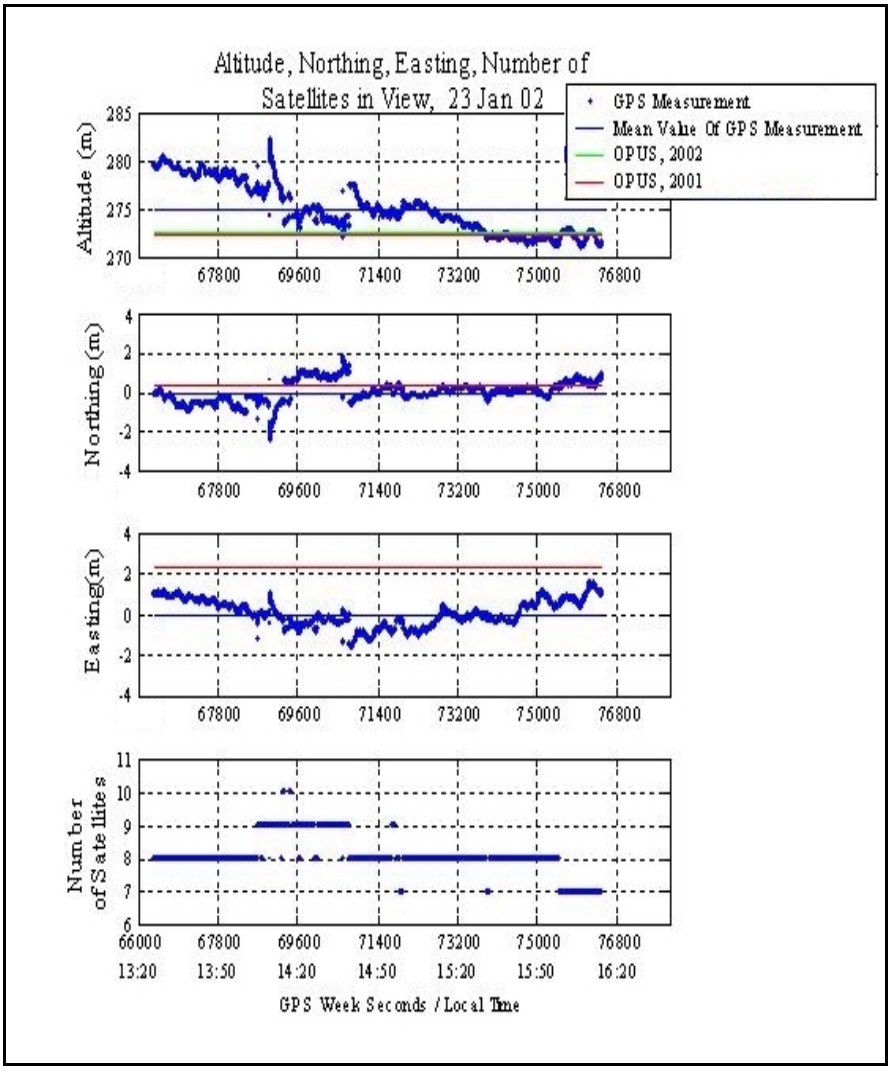

Figure 38. DIVEPACS Measurements Over Time, 23 January 2002

The green line is the 2002 OPUS altitude, northing, and easting measurement. The blue line is the DIVEPACS's mean altitude measurement. The red line is the altitude, northing, and easting measurement as determined by OPUS in the spring of 2001. The two OPUS calculations are indistinguishable at this resolution in the northing and easting directions. The largest errors in each direction correspond to the time when a new satellite first comes into view or when a satellite is dropped from view. Longer sample periods do not necessarily cause the errors to decrease. The errors will not decrease over time if the number of satellite in view continues to vary.

Figure 39 is an error magnitude histogram in the altitude and north and east directions. The errors in the three directions tend to be normally distributed, with the largest errors being in the altitude measurements. This is typical for GPS applications.

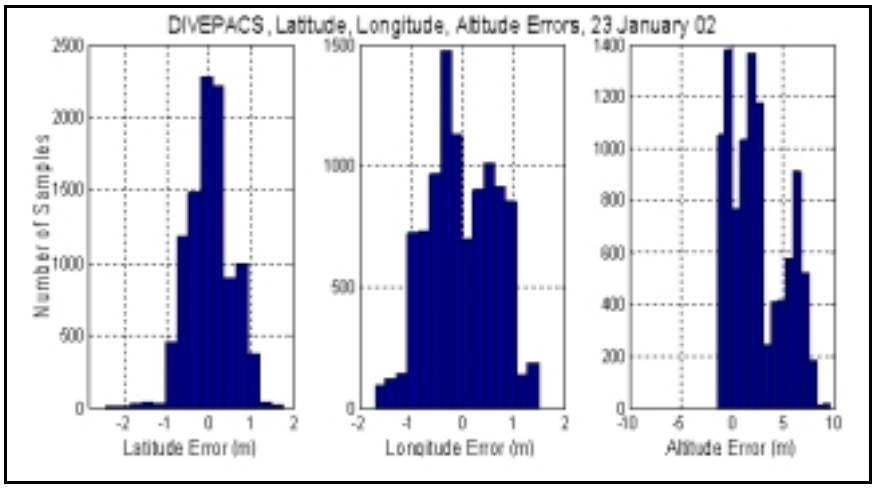

Figure 39. Latitude, Longitude, and Altitude Errors

Two static data collections were conducted in January to provide a baseline for the DIVEPACS receiver accuracy. The collection results are shown in Table 6. The results summarized are typical for the DIVEPACS in the stand-alone static mode. The bias is

due to the short collection periods (two hours on average) and is typically removed for collection periods over 5 hours.

Table 6. DIVEPACS Stand-Alone Bias and Accuracy, 23 and 24 Jan 02

	Bias			RMS Accuracy		
	Latitude (m)	Longitude (m)	Altitude (m)	Latitude (m)	Longitude (m)	Altitude (m)
23 Jan	1.47	-1.45	2.28	0.41	0.56	2.47
24 Jan	2.31	1.58	23.39	1.47	0.38	3.49

Static Data Collection - Code Based Differential Corrections

The next bench testing experiments investigated the G12's performance when applying code based differential corrections to the static data measurements. Figure 40 shows a data plot from a stationary antenna that was collected over a 5-hour period. The plot on the left is the stand-alone position in the local level frame. The plot on the right is the same data, shown at the same measurement scale, after the differential corrections were applied. The green square in each figure is the true antenna position as determined by the NGS OPUS software. The red square indicates the mean value for the latitude and longitude calculations.

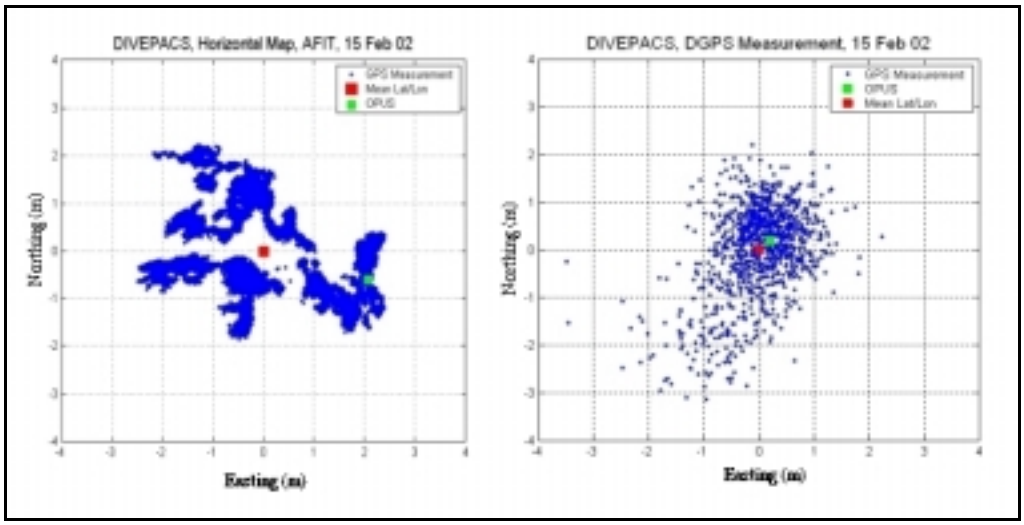

Figure 40. DIVEPACS Stand-Alone and DGPS Static Collection, Horizontal Map

The improvements in the accuracy are summarized in Table 7. These DGPS accuracy results are consistent with the manufacture specifications for the G12 receiver. The largest improvement is in the bias removal. In the stand-alone mode the receiver calculated position is within two meters of the true position. In the differential mode, the receiver calculated position is less than one meter from the true position.

Table 7. Stand-Alone and DGPS, Bias and RMS Accuracy

	Latitude (m)	Longitude (m)	Altitude (m)
Stand-Alone			
Bias	-0.62	2.06	0.10
RMS	0.81	1.6	1.1
DGPS			
Bias	-0.20	-0.20	0.55
RMS	0.73	0.48	0.55

Figure 41 plots the latitude, longitude, altitude, and number of satellites in view over the same collection period. As described, the DGPS RMS accuracy for the longitude and latitude are less than 2 meters.

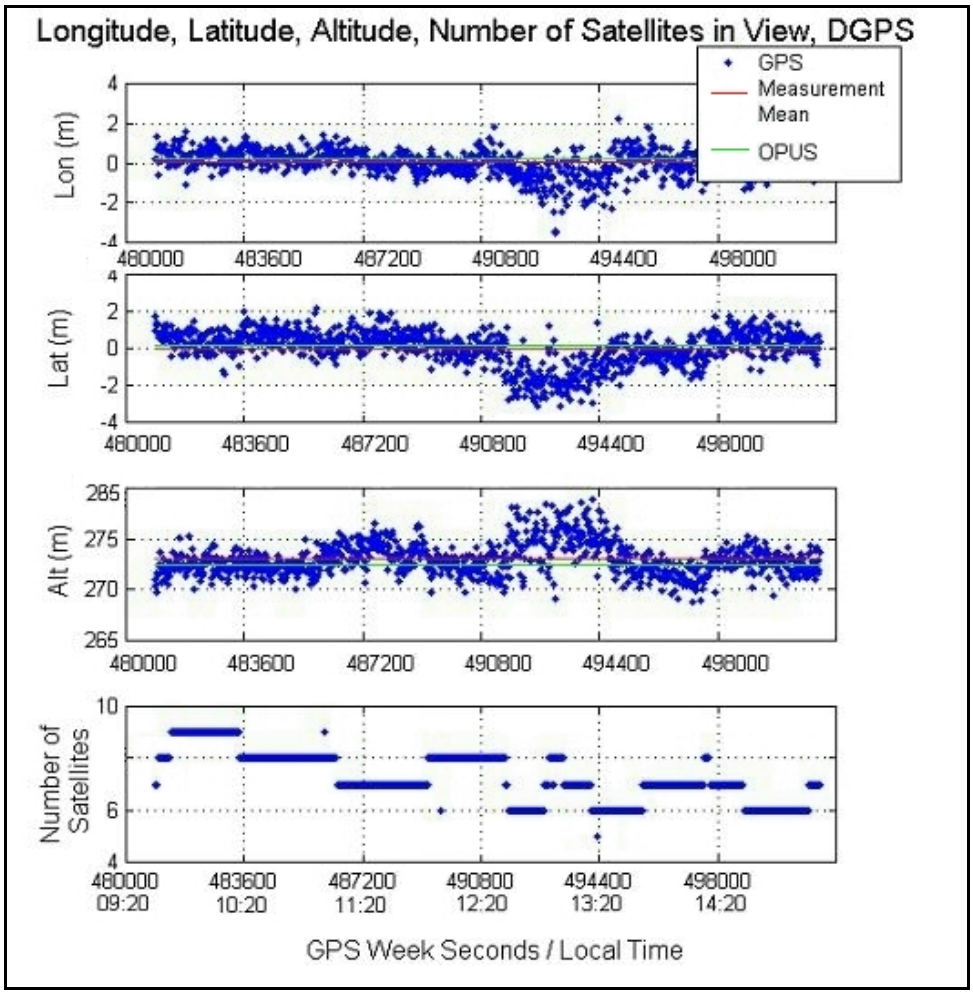

Figure 41. DIVEPACS, DGPS Measurements Over Time, 15 Feb 02

The largest errors correspond to the period when the numbers of satellites in view vary the most over time. This decrease in accuracy is evident in the time period of 12:20 – 13:20.

Figure 42 is an error magnitude histogram in the longitude, latitude, and altitude. The errors, while biased, tend to be normally distributed in the three directions. In each collection, the largest errors were in the altitude measurements, as expected given the satellite geometry.

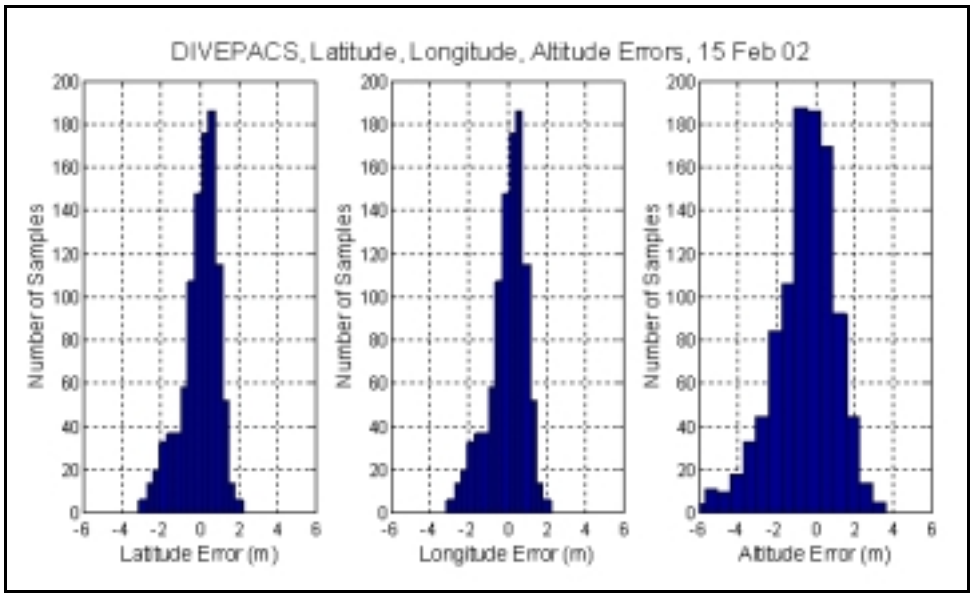

Figure 42. DGPS, Latitude, Longitude, and Altitude Errors

GPS Simulator

The next bench test evaluated the DIVEPACS's dynamic performance using the GPS simulator. The simulator was used to simulate the dynamic profiles the DIVEPACS would experience during actual rocket sled ejection testing, and to simulate flight profiles that could not be investigated at the HMTT.

The simulation scenarios were all straight-line acceleration profiles. Two seven-set simulations were evaluated. The first seven simulations were with a 10-satellite constellation, the next seven with an 8-satellite constellation. In both groups the maximum velocity was increased from 100 m/s to 400 m/s. Each simulation tested the receiver's ability to remain locked onto the satellites in an environment similar to a rocket sled profile. The details for each scenario are listed in Table 8. The details for scenario number seven are covered later in this section.

Table 8. Summary of Straight Line Acceleration Simulations

Scenario Number	Sample Rate (Hz)	Number of Satellites in Constellation	Duration of Acceleration (sec)	Acceleration (m/s)	Final Velocity (knots)	Acceleration Tracked
1	5	10	5	100	194	Yes
2	5	10	5	150	291	Yes
3	5	10	5	200	389	Yes
4	5	10	5	250	486	Yes
5	5	10	5	300	583	Yes
6	5	10	5	350	680	Yes
7	5	10	5	400	776	**No**
8	5	8	5	100	194	Yes
9	5	8	5	150	291	Yes
10	5	8	5	200	389	Yes
11	5	8	5	250	486	Yes
12	5	8	5	300	583	Yes
13	5	8	5	350	680	Yes
14	5	8	5	400	776	Yes

The results for the first scenario are shown in Figure 43. The same data was collected during each simulation. The first plot in Figure 43 is the sled velocity profile. The sled remained stationary for 600 seconds to allow the receiver time to acquire satellites. The sled then accelerated for a 5 second period to a maximum velocity of 100 m/s. The simulated profile is different from the sled profile at HMTT in that, in the simulation the sled continues at the maximum velocity for 300 seconds.

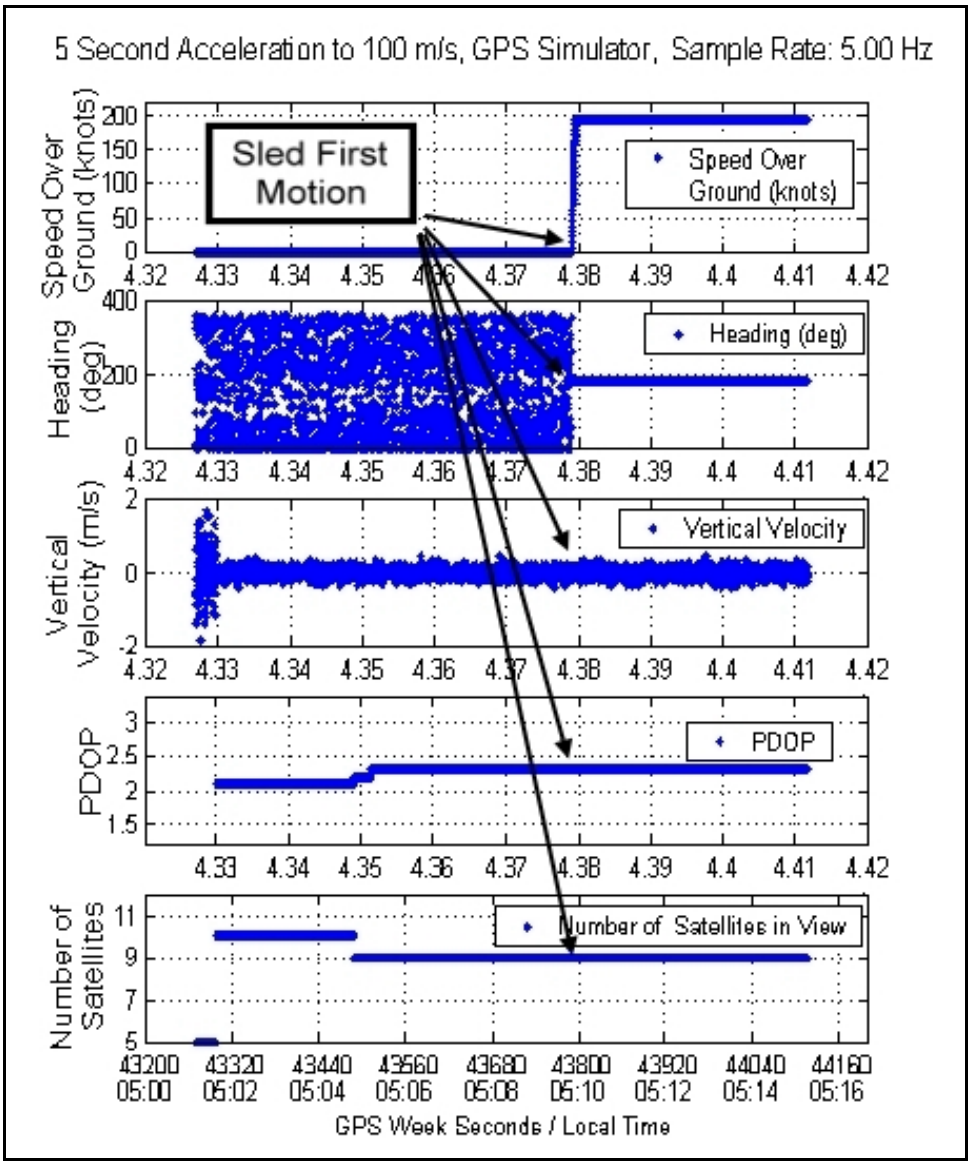

Figure 43. GPS Simulator, Straight Line Acceleration

The second plot in Figure 43 is the sled heading over time. Since the receiver is stationary during the simulation's first 600 seconds, the GPS receiver cannot determine and accurate heading, therefore, the measured heading varies from 0 to 360 degrees. The DIVEPACS was able to detect sled first motion and measure the sled heading as it accelerated to the final maximum velocity. The third plot in Figure 43 is the vertical

velocity over time. The DIVEPACS vertical velocity estimation errors were consistently under 2 m/s after the initial satellite acquisition transients.

The fourth plot in Figure 43 is the PDOP value over the simulation run. The PDOP values in the simulations vary between 2.0 and 2.5. These values are comparable to those recorded during the two sled trials at HMTT. Figure 44 shows the GPS constellation for the first 7 simulations. The satellites are shown in their initial position. There is very little change in the satellite geometry over the short simulation period. The satellite geometry was favorable, although many of the satellites were close to the 10-degree elevation mask. The elevation mask is the minimum satellite elevation for raw measurement data output. The receiver was configured to output raw measurement data for all tracked satellites with an elevation of 11 degrees or higher.

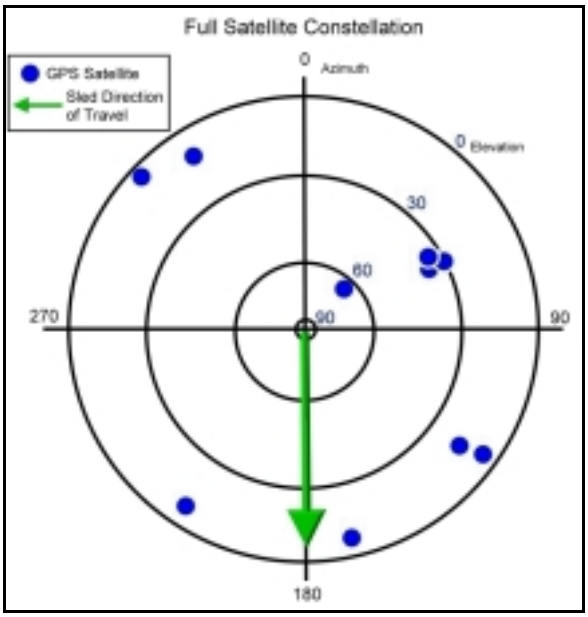

Figure 44. GPS Simulator Full Satellite Constellation

The final plot in Figure 43 is the number of satellites used in the position solution over the simulation period. This number is higher than either of the two tests at HMTT. In the second set of 7 simulations the number of available satellites was reduced from 10 to 8. The average signal-to-noise ratio for each satellite in the simulations was lower than experienced for the two trials at HMTT.

The results for the 350 m/s and 400 m/s accelerations are shown in Figure 45 and Figure 46. The DIVEPACS performed well in the first seven simulations with a full satellite constellation.

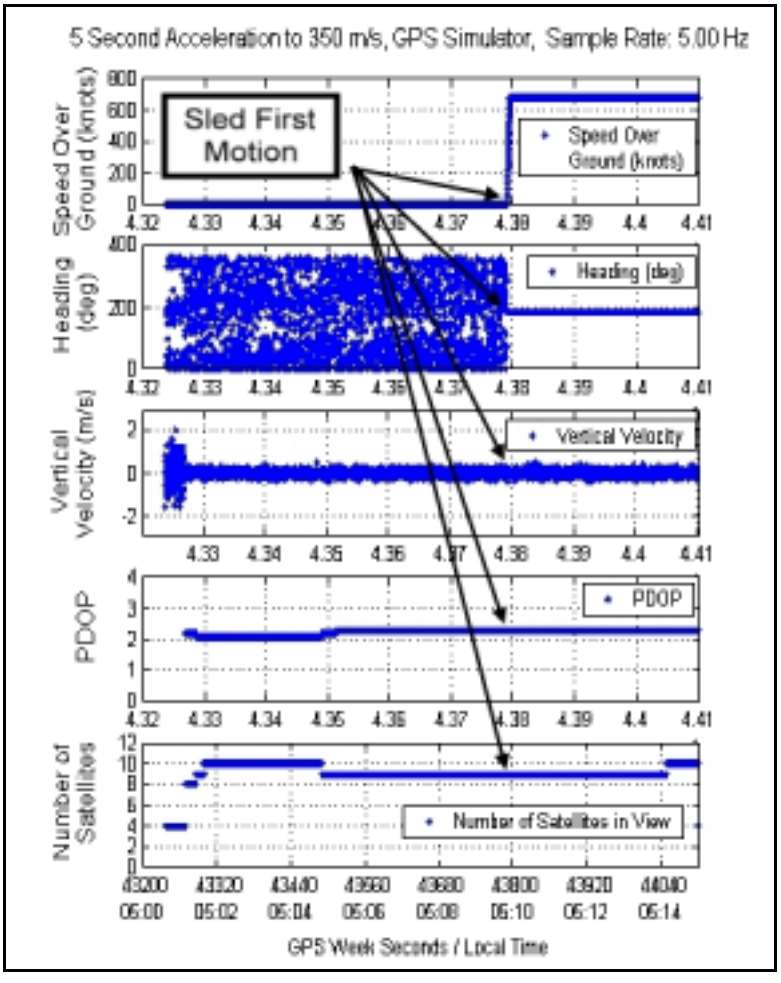

Figure 45. 5 Second Acceleration to 350 m/s, Full Constellation

The first time the receiver temporally lost lock was at the 300 m/s velocity. The receiver handled the 350 m/s acceleration without losing any satellites. It was able to estimate the true heading and speed over ground quickly.

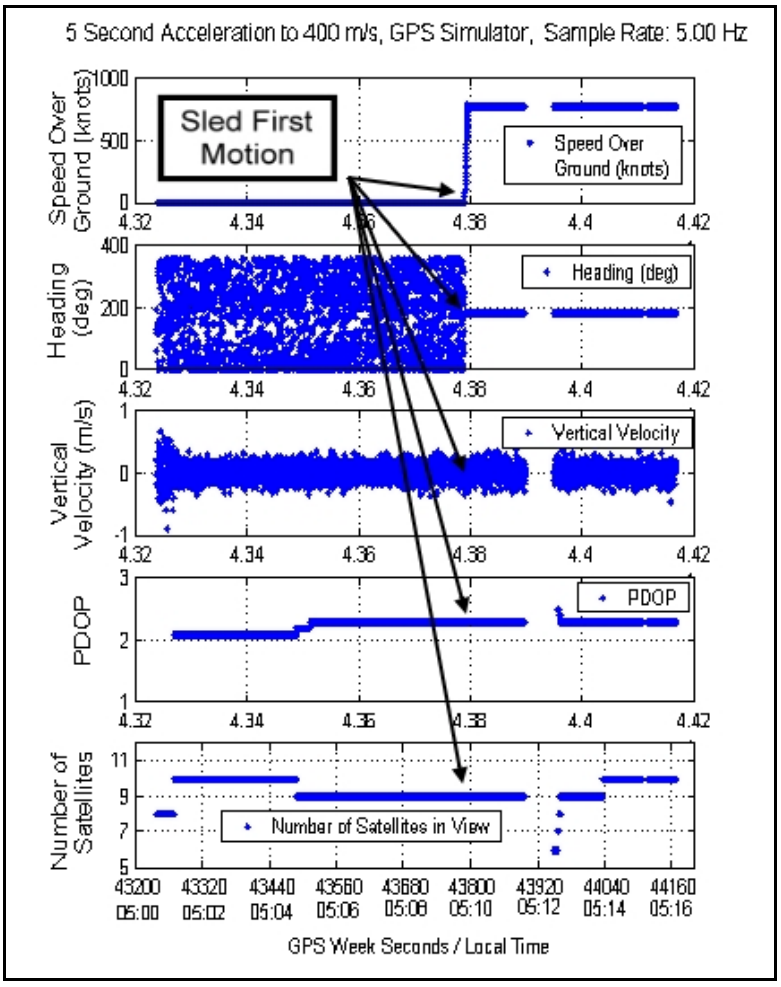

Figure 46. 5 Second Acceleration to 400 m/s, Full Constellation

The first time the receiver lost lock for an appreciable time with a satellite was during the acceleration to 400 m/s. The DIVEPACS tracked during the acceleration, then lost lock approximately 2 minutes after the velocity stabilized to 400 m/s. As shown in Fig

48, the receiver did reacquire and track all 10 visible satellites. 400 m/s is over 775 knots, which is significantly higher the 630 knots reached by the rocket sled at the two trials at HMTT.

The next simulation set dropped the number of visible satellites from 10 to 8. The average number of satellites tracked by the DIVEPACS during the two trials at HMTT was seven. The geometry for the reduced constellation is shown in Figure 47.

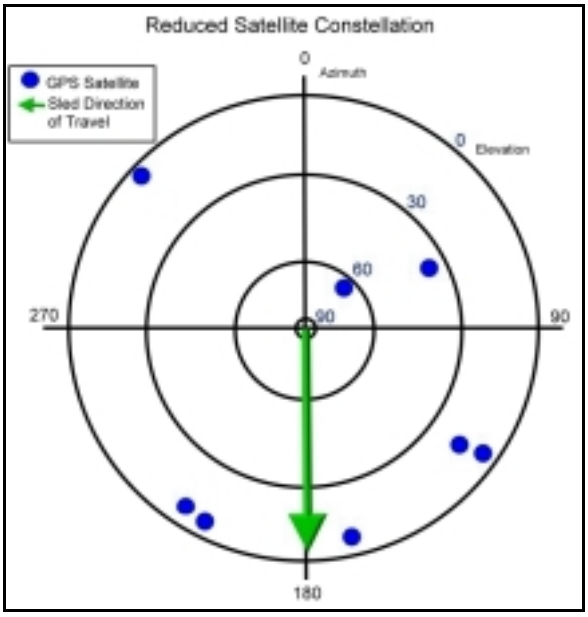

Figure 47. Reduced Satellite Constellation

The simulations were run again with the reduced constellation. The results for the 300 m/s and 400 m/s accelerations are shown in Figure 48 and Figure 49.

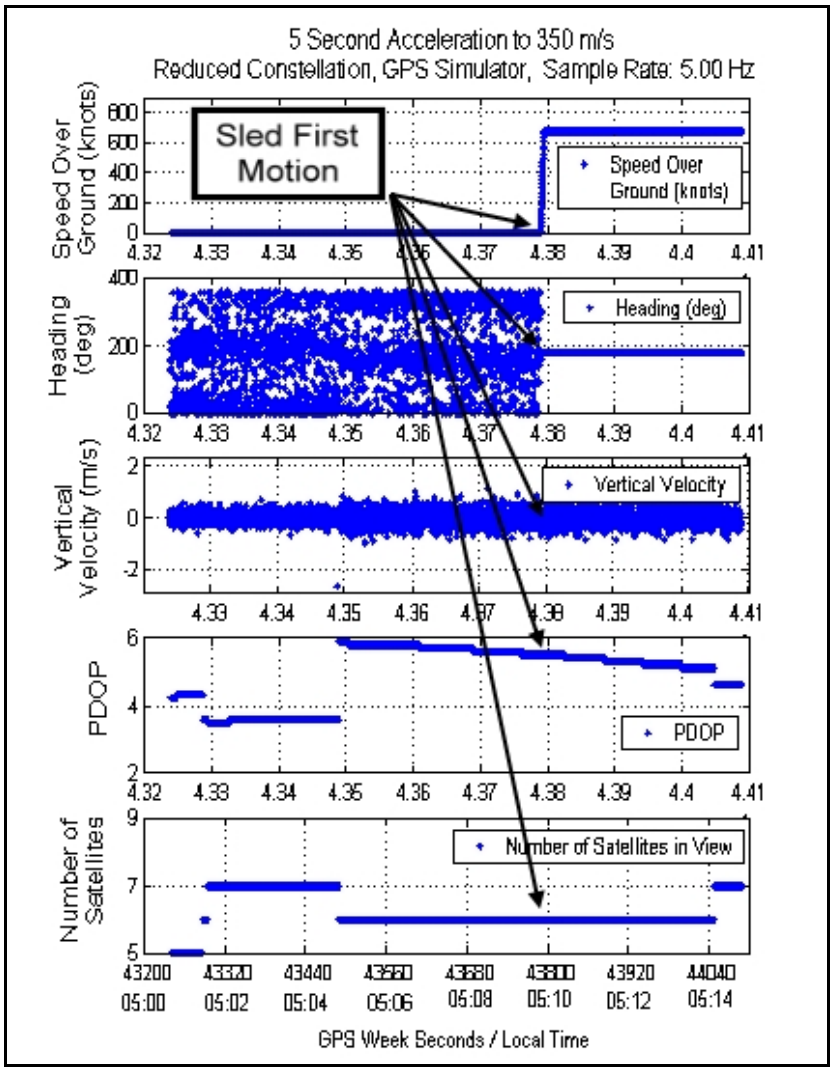

Figure 48. 5 Second Acceleration to 350 m/s, Reduced Constellation

The DIVEPACS performed well with the reduced constellation for both the 350 m/s and 400 m/s simulations. It tracked the acceleration and quickly estimated the correct heading and speed over ground.

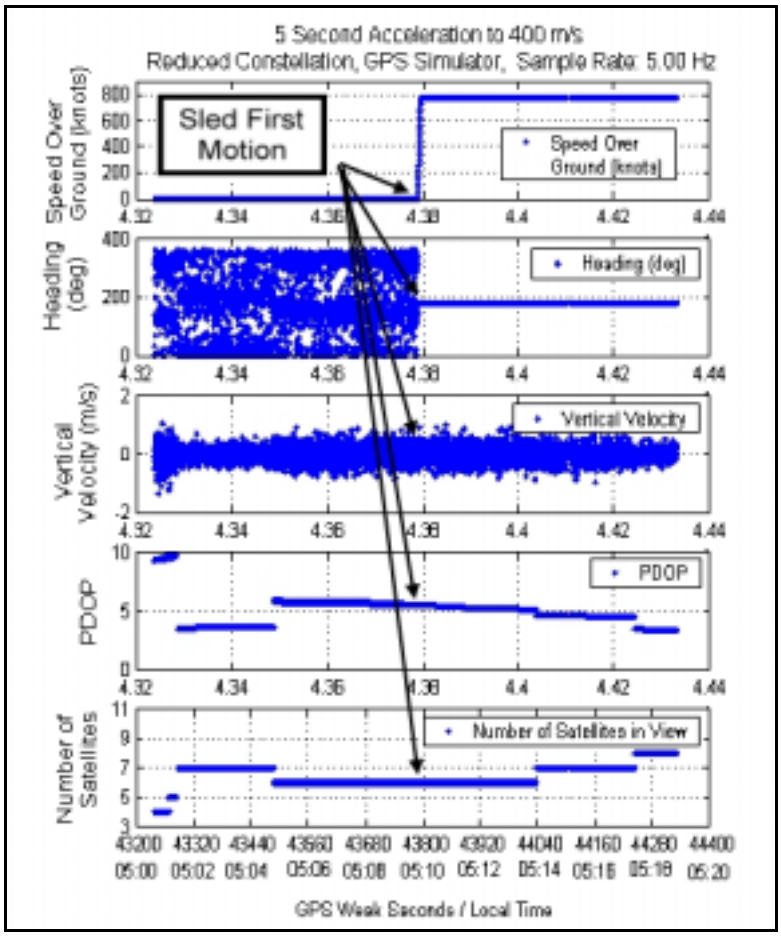

Figure 49. 5 Second Acceleration to 400 m/s, Reduced Constellation

The noticeable difference between the full constellation test results and the second reduced constellation test results was caused by the increase in the PDOP values due to removing two satellites from the constellation. The DIVEPACS tracked the straight-line accelerations in 13 of the 14 simulations. The one simulation where the DIVEPACS temporally lost lock was the 400 m/s, or 776-knots test with the full constellation, which is well above the acceleration level on the rocket sled in the Phase III trials at HMTT. The receiver is designed to track straight-and-level flight velocities up to 1000 KEAS. The temporary satellite lock loss is probably a problem with the simulator, not the GPS receiver.

Phase II – Freefall Testing

Overview

Phase II testing's primary goal was to ensure the DIVEPACS could reliably track enough satellites to determine a 3-dimensional position and velocity if the manikin began tumbling in flight. The other goal for this phase was to test the equipment configuration. It was important to determine how well the DIVEPACS would handle the shock and vibration of freefall and parachute deployment prior to the testing at Hurricane Mesa. The tests were conducted during the four-month period from July to October 2001 at Skydive Green County, Xenia Ohio, a local skydiving dropzone.

The test plan was to build up the system in parts. Each component was thoroughly tested in freefall before adding it to the configuration. The first component tested was the antenna. The antenna was mounted to the top of a standard skydiving helmet as shown in Figure 50 using screws through the plastic shell into pre-existing threaded holes in the antenna base.

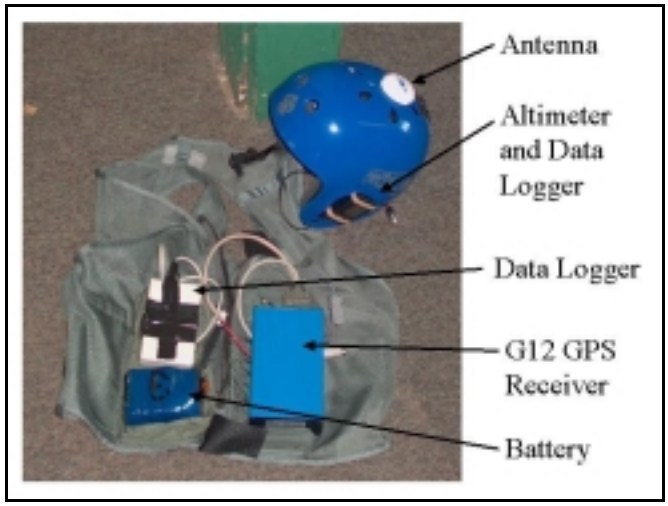

Figure 50. DIVEPACS Configured for Freefall Testing

The testing showed the antenna mount was strong enough to handle the canopy opening shock, but a means of securing the antenna lead had to be found. The antenna lead proved to be the weakest part of the system throughout the entire research.

The next item tested was the data logger. The data logger is shown in its original case in Figure 50. The data logger in the original case has an internal 9-volt battery and 9-pin I/O serial cable. The data logger is designed to collect and store the output from any RS-232 source at a rate of up to 115,000 bps. The data is placed into non-volatile memory so it is protected in the event of power loss and can only be downloaded or erased using a software program included with the data logger. The data logger performed well under the shock and vibration of canopy deployment. On average, the data logger would corrupt 20 lines of NMEA message data out of every 25,000 collected.

The remainder of the testing used the full configuration shown in Figure 50. The G12 receiver was in the Ashtech® sensor configuration with an internal power regulator and external female DB-25 connector. A 12-volt rechargeable battery pack powered the G12 through the DB-25 connector. The G12 was connected to a laptop through the serial port and configured prior to connecting it to the data logger. All the data collected from the GPS receiver was stored in an H.O. Data Compu-Log RS-12DD data logger for post-processing.

Westwind and Casa Freefall Tests

2 September 2001. The first successful freefall tests were completed on 2 September 2001. The preliminary testing goals were to determine if the equipment could be configured to fit into the survival vest pockets and not interfere with the parachute

harness or cause freefall instability, to produce a position solution in non-differential mode during stable freefall, and to determine if the system would track during high dynamics such as tumbling.

The G12 Sensor, battery, and data logger were installed into the aircrew survival vest as shown in Chapter 3, Figure 23. Figure 51 shows the flight profile for the first test. The G12 was unable to lock onto enough satellites inside the aircraft to form a position solution. In subsequent tests it was determined that the antenna had to be closer to the aircraft Plexiglas door in order to track enough satellites to measure the aircraft flight profile. Tracking inside the aircraft was a problem unique to the freefall testing and is not a requirement for the final system.

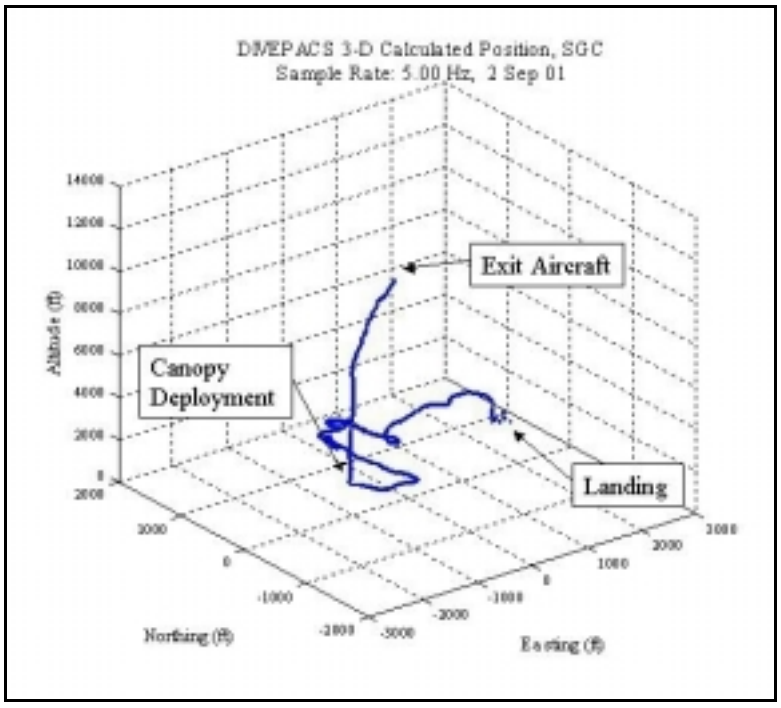

Figure 51. Freefall Flight Profile, 2 September 2001

The average freefall period was 55 seconds before the parachute was deployed. This was ample time for the G12 GPS receiver to acquire enough satellites to form a position solution. Fifty-five seconds was also enough time for the operator to complete multiple turns and rotations to test the effects that different antenna configurations had on the receiver's ability to remain locked on enough satellites to form a measurement solution.

The position solution was calculated by the GPS receiver and reported using the NEMA 3-D GGA position message. The NEMA POS message could not be used due to the 3000-meter maximum altitude limitation. The G12 sample rate was set to 5 Hz. The flight profile is consistent with a normal freefall skydive. The sharp changes in the flight direction after canopy deployment shown in Figure 51 are spiral turns flown to reduce the altitude quickly before returning to the drop zone.

The Pro-Track helmet mounted barometric altimeter recorded an exit altitude from the aircraft of 13,650 feet. The position accuracy for the barometric altimeter is approximately 50 feet. The GPS locked onto enough satellites to calculate the first position solution at 13,648 feet. Based on the data collected during other freefall tests, the actual altitude at aircraft exit was probably a little higher than the barometer altimeter measured. The total freefall time between exit and position solution was less than 1 second. This is consistent with the manufacture specifications for the G12 receiver. The receiver had been tracking before entering the aircraft so the almanac and ephemeris were less than 1 hour old.

The discontinuity shown in Figure 51 at the beginning of freefall may be due to additional satellites coming into view. The receiver went from tracking four satellites as the operator exited the aircraft to 10 during the 55-second freefall. The discontinuity

probably resulted from the additional satellites coming into view and changing the satellite geometry. The operator attempted to remain in a stable freefall position during this test. The only time the antenna was not pointed as close to zenith as possible was during the initial aircraft exit. It is possible that the initial discontinuity is due to the antenna sweeping from the horizon to a zenith direction.

Figure 52 shows a plot of the number of satellites tracked and the corresponding altitude during the test. The receiver never tracked fewer than 4 satellites during freefall, canopy deployment, or the flight time under canopy back to the drop zone. The number of satellites tracked did drop by one when the chute deployed. The drop in satellites may be due to the operator's head jerking down when the canopy opened. The reason for the change in the number of satellites tracked after landing is due to the operator looking down to adjust and remove the equipment.

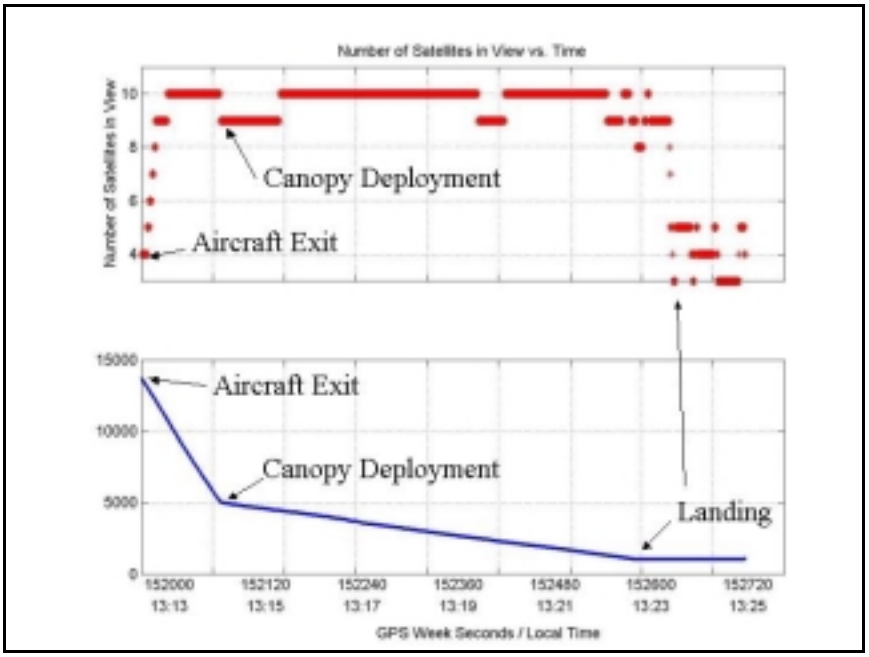

Figure 52. Number of Satellites in View, 2 September 2001

The additional component weight increased the average freefall speed (as recorded by the helmet-mounted altimeter) from 124 mph to 132 mph. The weight of the separate G12 sensor, data logger, and rechargeable battery pack was heavier than the DIVEPACS's weight in the final configuration. No difference to freefall stability was noticed with the additional equipment mounted in the survival vest.

21 September 2001. The next test shown was completed on 21 September 2001. The flight profile is shown in Figure 53. In this jump, the system was set closer to the aircraft's large Plexiglas door so the aircraft flight profile could be recorded.

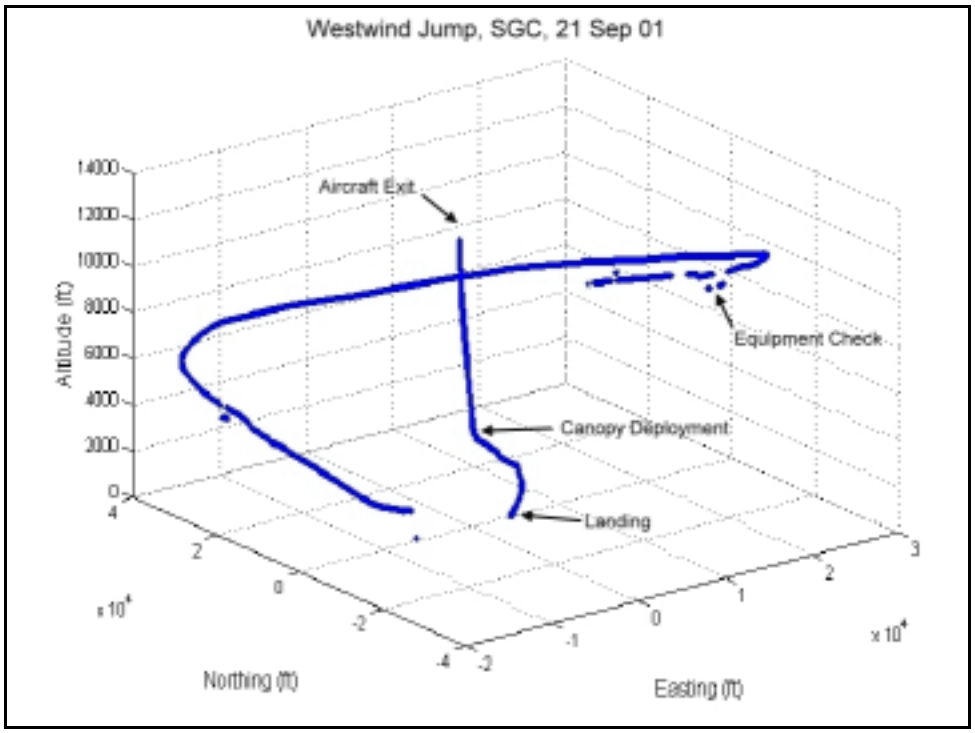

Figure 53. Westwind Jump, SGC, 21 Sep 01

The two flight profile portions not recorded are during the pre-jump equipment check when the operator adjusted the helmet and parachute harness. The other large gap in satellite coverage is when the aircraft's body shielded the antenna as the operator stood just prior to exiting the aircraft. The operator was able to stand outside the aircraft door for approximately 2 seconds before beginning freefall. The helmet-mounted altimeter recorded the exit altitude at 13,300 feet. The G12 sensor reacquired 4 satellites at 13,164 feet. This again was consistent with the manufacture specifications for a 2-second re-acquisition time.

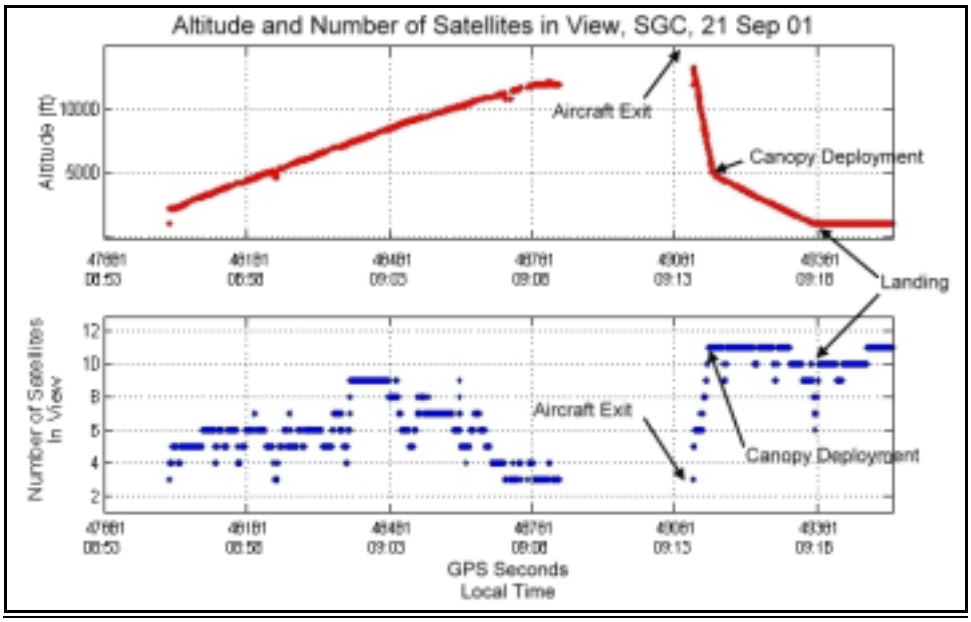

Figure 54. Altitude and Number of Satellites in View, SGC, 21 Sep 01

As shown in Figure 54, the number of satellites tracked quickly jumped from 4 to 11 during the 52-second freefall period. While in freefall the operator completed two 360-degree turns and one backwards roll. The receiver never tracked fewer than 4 satellites during freefall, canopy deployment, or the flight time under canopy back to the drop

zone. The number of satellites tracked did not drop when the chute deployed. The number did change during the flight under canopy back to the dropzone. This may be due to the operator looking up and down to check the canopy operation. The reason for the change in the number of satellites tracked after landing is due to the operator looking down to adjust and remove the equipment.

Phase II Summary

Phase II tests were very successful for testing the different equipment configurations. As many as five tests were accomplished in a single testing session, enabling equipment modifications to be immediately tested and verified. In total, over 20 freefall tests were completed with different equipment configurations. The only configuration that could not be testing during freefall was the one with DGPS corrections. An unfortunate combination of weather delays and equipment failures made it impossible to gather the data necessary to apply differential corrections.

The freefall tests showed that the G12 with the helmet-mounted antenna could acquire and remain locked on enough satellites to record the manikin's 360-degree turns and rolls expected during the rocket sled trials. However, the number of satellites tracked probably varies too quickly to apply carrier phase DGPS techniques. The data logger performed well under the shock of canopy deployment. The antenna cable connector was the only system part requiring modification. The case built for the Phase III tests is designed to protect the antenna connector on the G12 OEM board.

Phase III – Ejection Seat Test and Evaluation

Overview

The final research phase involved actual ejection seat test and evaluation trials at the Hurricane Mesa Test Track (HMTT) located near the town of Hurricane Utah. The ejection trials were conducted during the 26 October to 14 November 2001 timeframe. Two rocket sled trials were evaluated, both at a 630 KEAS sled velocity. This final section begins with the results and analysis from the DGPS reference station constructed at HMTT for the ejection trials on 31 October and 14 November 2001.

Reference Station Collection

The reference station equipment for all data collection during the trials at HMTT is described in Appendix D. Table 9 summarizes the position calculation completed on 12 November 2001.

Table 9. Reference Station Position Calculation Summary

Collection Location	Hurricane Mesa High-Speed Test Track
Date	12 Nov 01
Time (Local)	1024 - 1132
GPS Receiver	Ashtech Z-Surveyor
Antenna	Ashtech Marine III L1/L2
NGS OPUS Calculated Position	Not Available
Ashtech Z-Surveyor Calculated Position	Latitude: 37.239804 Longitude: 113.220957 Altitude: 5134.96 feet

An NGS OPUS position calculation is not available because the two hour minimum sample period was not met during the HMTT trials. The two-hour sampling requirement was not known until after the tests at HMTT were completed. The final position was

determined by averaging the GPS measurements epochs over several collection periods ranging from 1 hour to 1 hour 45 minutes. A simple collection is shown below in Figure 55 in the latitude, longitude, and altitude frame, and the ENU frame.

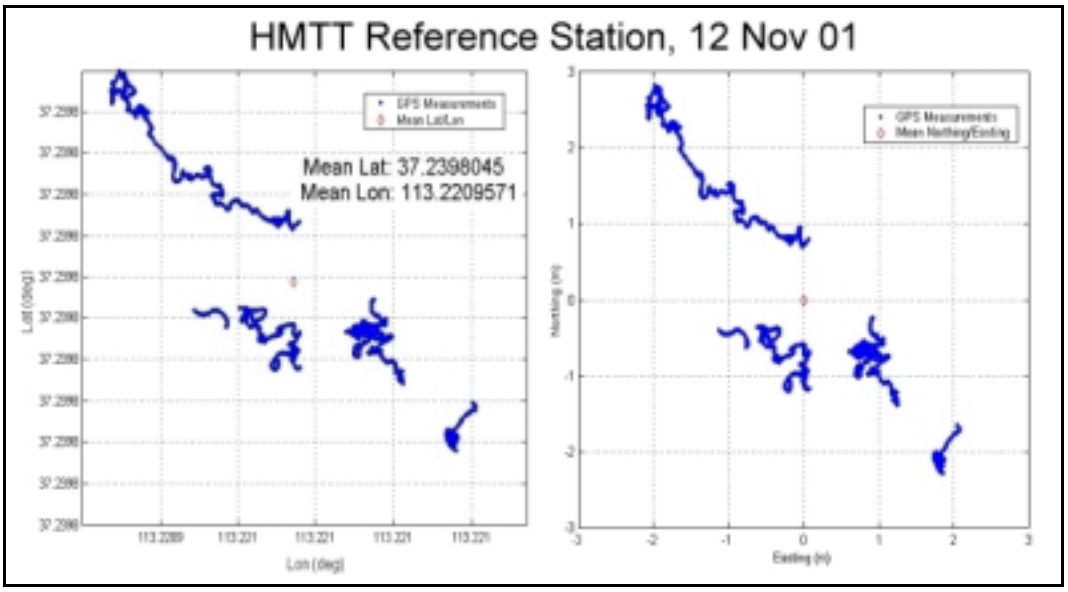

Figure 55. Reference Station Position Calculation

The calculated position has four distinct discontinuities due to the number of satellites in view changing during the data collection. These discontinuities correspond to the number of satellites in view changing as shown in the bottom plot in Figure 56. The first three plots in Figure 56 are the latitude, longitude, and altitude over time plotted in the local level frame. Discontinuities are evident in each plot when the number of satellites in view changes. The largest PDOP values also correspond to the times when the number of satellites is the lowest. Based on the measurements collected, the calculated reference station antenna position should be accurate to within 3 meters of the true position in the horizontal direction and 10 meters in the vertical direction. This level of accuracy is sufficient for this type of application. Recall that the primary goal in this research is to

determine the manikin's position relative to the F-15 sled. The exact position of the manikin is not as important as the relative change in position as it travels down the track and is ejected from the cockpit.

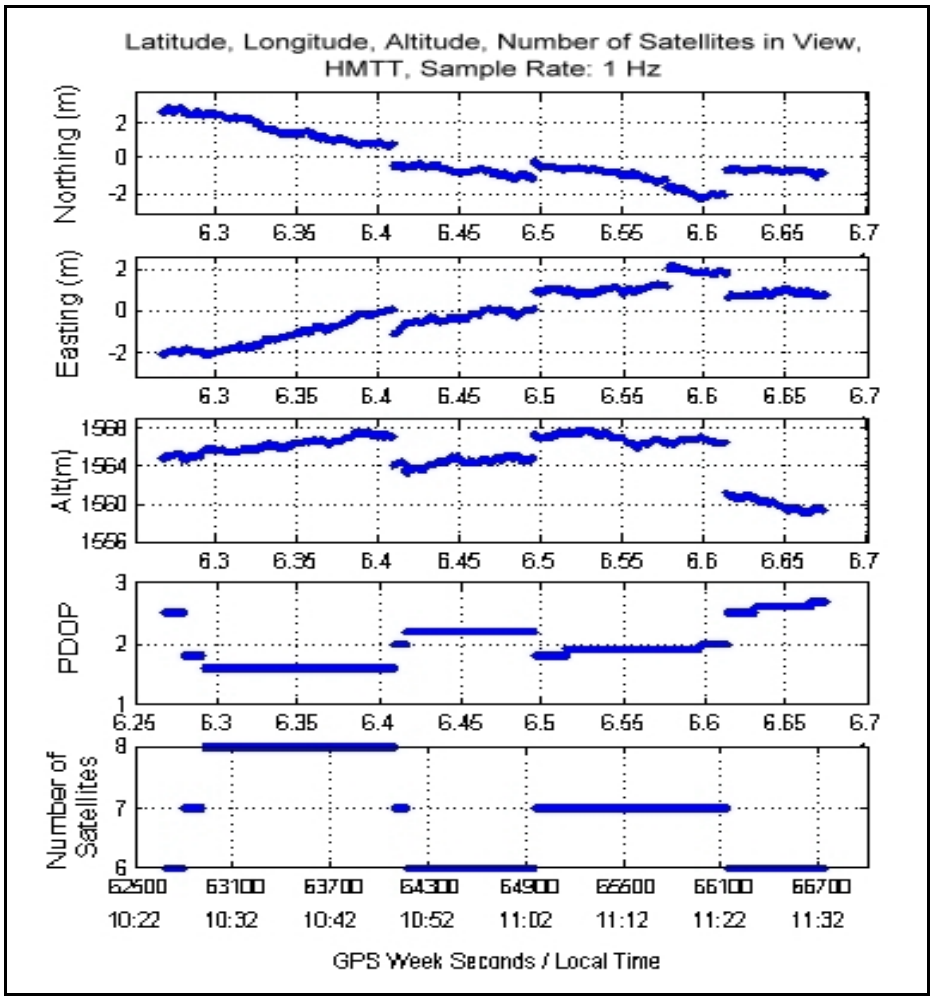

Figure 56. Reference Station Collection, 12 Nov 01

F-16 Test HMTT 721, 31 October 2001

HMTT Test 721 Overview. The first sled test was conducted at HMTT on 31 October 2001. Table 10 lists the general test details.

Table10. Relevant Data, HMTT Ejection Test Number 721

Date	31-Oct-01
ACES II SU Configuration	Retrofit
Test Time (Local)	13:31
Met Conditions	Scattered Clouds
Temp	57°F
Humidity	30%
Wind	South 3-5
Seat/Man C.G. (X)	13.42 in
Seat/Man C.G. (Z)	16.78 in
Seat Weight	179 lb
Manikin Weight	277 lb
Seat/Man Weight	456 lb
MDRC	1.45
Manikin	JPATS Case 6
Target Velocity	630 KEAS
Actual Velocity	625.6 KEAS
Sled Start Station	5308
Sled Stop Station	11560
DIVEPACS Sample Rate	20 Hz

The equipment was configured as described in Chapter 3, (DIVEPACS Configuration for Rocket Sled Ejection Testing). The DIVEPACS was placed in the aircrew survival vest's large left pocket. Life Support personnel placed the antenna inside the helmet's shell at approximately 30 degrees towards the helmet's rear. The antenna could not be positioned to point exactly at zenith due to concerns that it might interfere with the proper fit of the aircrew helmet. The antenna cable was run underneath the survival vest and sewn to the flightsuit collar to protect it from the windblast.

Approximately one hour and 30 minutes prior to rocket initiation the power was applied to the Ashtech Z-Surveyor reference station GPS Receiver. The reference station tracked 8 satellites during the ejection sequence. Approximately 10 minutes prior to rocket motor ignition the power was applied to the DIVEPACS through the 500-foot

remote arming cable. At the time of the sled's first motion the DIVEPACS was tracking six satellites. With the antenna located pointing toward the helmet's rear, it is possible that the ejection seat's headrest blocked the low elevation satellites behind the manikin. In addition, the low elevation satellites in front of the manikin may have been below the tilted antenna plane.

The DIVEPACS remained attached to the manikin until seat first motion. The ejection system was initiated at the track 9100-foot marker. The sled velocity at the time of ejection system initiation was 625.6 KEAS. Figure 57 is a picture taken from the left high-speed camera mounted on the F-15 sled.

Figure 57. Manikin Entering Airstreams, HMTT, 31 Oct 01

By the time seat rail separation had occurred, the windblast had sheared all the pockets off the survival vest, including the pocket containing the DIVEPACS. The pockets were attached to the survival vest using plastic fasteners and could not handle the force from the windblast. In the photo sequence shown in Figure 57, the DIVEPACS can be seen separating from the survival vest and antenna and flying over the manikin's left shoulder.

Both the manikin and DIVEPACS were damaged during the test. The manikin's left leg was sheared off at he hip and both arms were broken. Figure 58 and Figure 59 shows the manikin and DIVEPACS as they were found after the test.

Figure 58. Manikin After Test, HMTT, 31 Oct 01

Figure 59. DIVEPACS After Test, HMTT, 31 Oct 01

The DIVEPACS came to rest 40 feet to the track's left at the 9200-foot marker. The DIVEPACS sustained minor damage including a small crack in case bottom left corner. Six of the 25 I/O wires had been torn loose from the data logger and the G12 circuit board. The antenna lead was sheared at the receiver connector. Inspection of the internal components revealed no visible physical damage to the G12 receiver, data logger, or internal battery. After repairing the I/O cables the unit was turned off and the internal battery charged so the data could be downloaded from the data logger.

HMTT Test 721 Data Analysis. The DIVEPACS did **not** continuously track the sled position and velocity up to the point when it separated from the manikin. The sled profile as determined by the sensors located on the sled slipper is shown in Figure 60. The sled velocity was 625.6 KEAS at the time of seat first motion. The six rocket stage initiations are labeled in Figure 60.

Analysis of the high-speed film from the cameras mounted on the F-15 sled shows the manikin head slamming against the ejection seat headrest as each rocket stage is fired. At the end of each stage the manikins head slumps forward in the cockpit. It is possible that the additional movement of the manikin's head increased the dynamics on the antenna and caused the number of tracked satellites to drop below the number required to form a position solution. The DIVEPACS recorded sled velocity is shown in Figure 61.

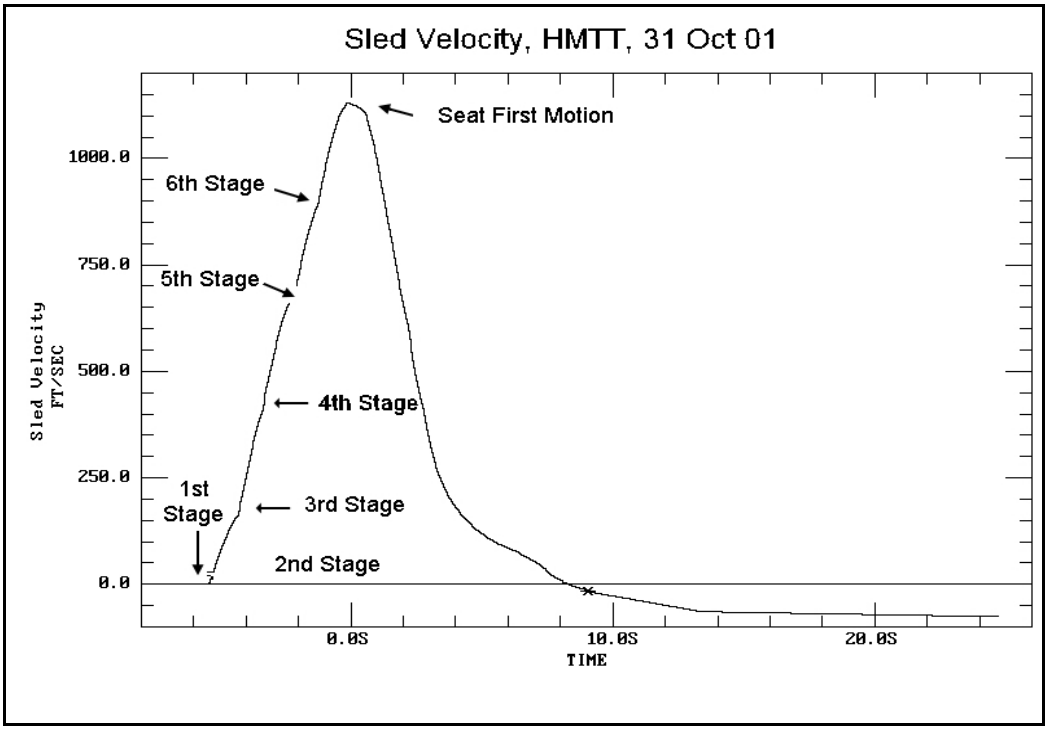

Figure 60. Sled Mounted Sensors Recorded Sled Velocity, HMTT, 31 Oct 01

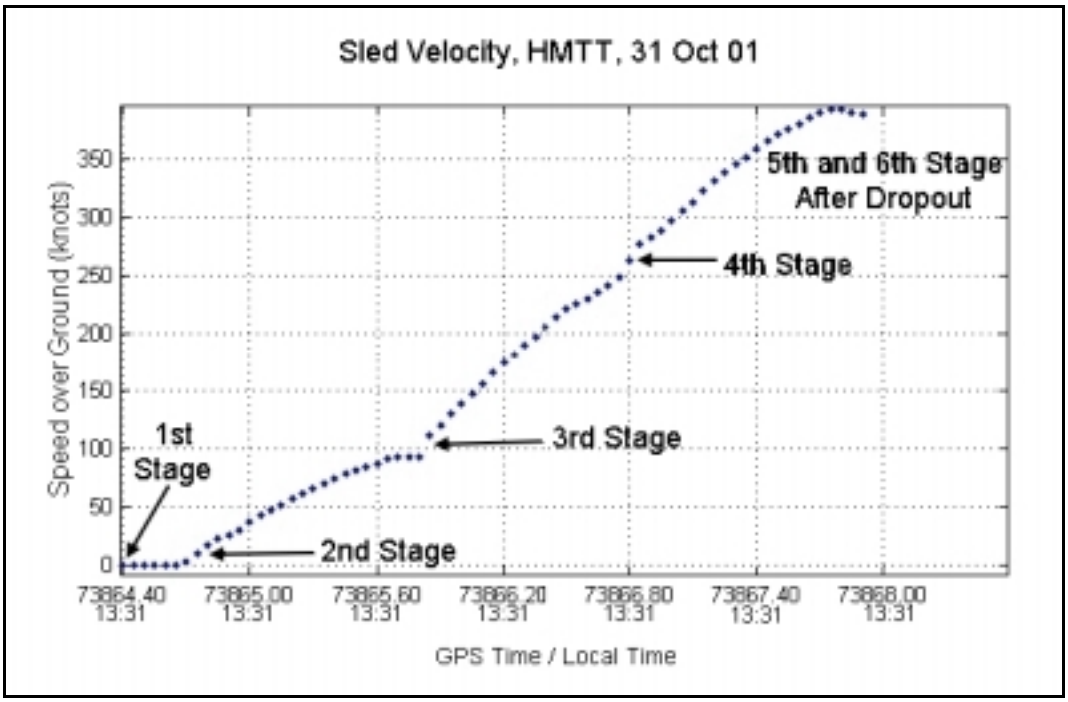

Figure 61. DIVEPACS Recorded Sled Velocity, HMTT, 31 Oct 01

The DIVEPACS was able to estimate the sled velocity and position accurately through the first four rocket motor stages. A correlation between the rocket motors stages firing and a reduction in the number of satellites tracked is shown in Figure 62. The 5th rocket stage firing caused the number of satellites to drop below 4, the number required to form a 3-D position solution. The DIVEPACS did not reacquire a position solution before it separated from the manikin at seat first motion.

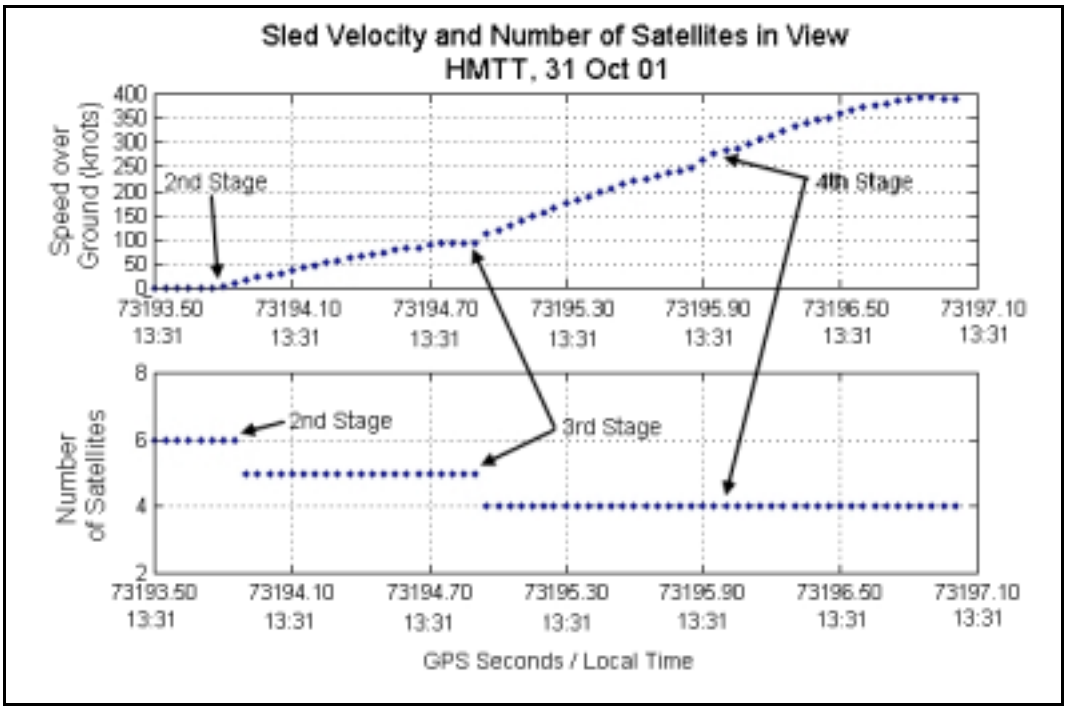

Figure 62. Sled Velocity and Number of Satellites in View, HMTT, 31 Oct 01

Figure 63 shows the sled's trajectory. A clear discontinuity is recorded when the 3rd rocket motor stage fired, dropping the number of tracked satellites from 5 to 4.

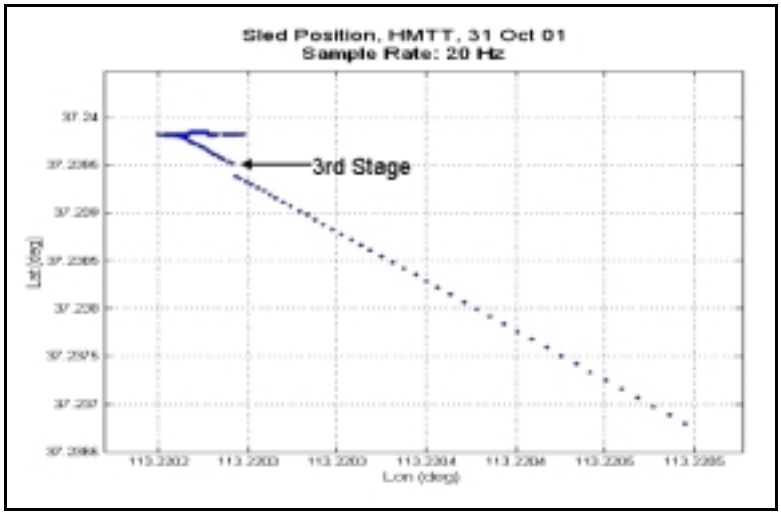

Figure 63. Sled Position, HMTT, 31 Oct 01

Figure 64 shows the manikin's vertical velocity. The track is not perfectly flat; it has a slight arc with the peak around the 9300-foot mark to allow flooding of the track's second half at a gradually increasing depth. The Red-Genie pusher sled has a water scoop that collects the water and slows the F-15 sled after the ejection seat has cleared cockpit. The DIVEPACS recorded the gradual rise in the first half of the track.

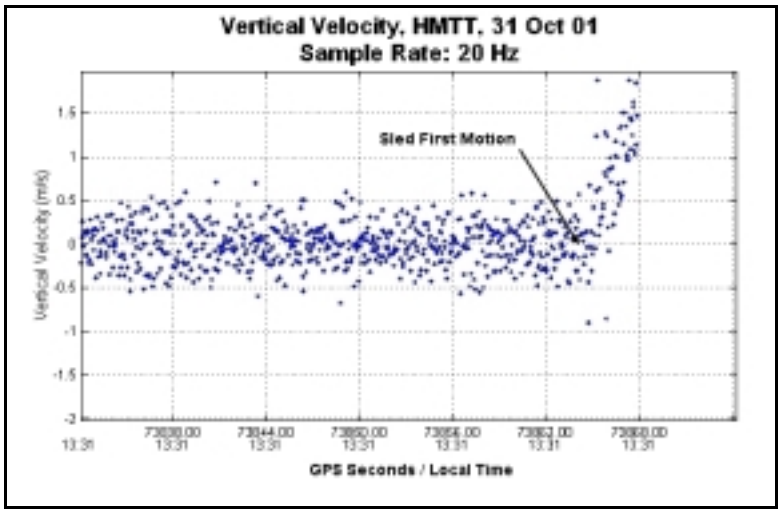

Figure 64. Vertical Velocity, HMTT, 31 Oct 01

Figure 65 shows the approximate location for each GPS satellite visible at the beginning of the test. The plot shows the 8 satellites in view by the reference station. Unfortunately, the NMEA POS message was the only message collected during the first test, so the exact 6 satellites used in the position calculation can not be determined. The NMEA POS message format is included in Appendix B, (GPS Receiver Message Formats Used in Data Collections.) The satellite geometry was favorable during the time of the ejection. However, it is possible that, with most of the satellites located behind the

sled, the antenna may have been partially obstructed by the ejection seat headrest as the manikin's head was slammed back at the each rockets stage initiation.

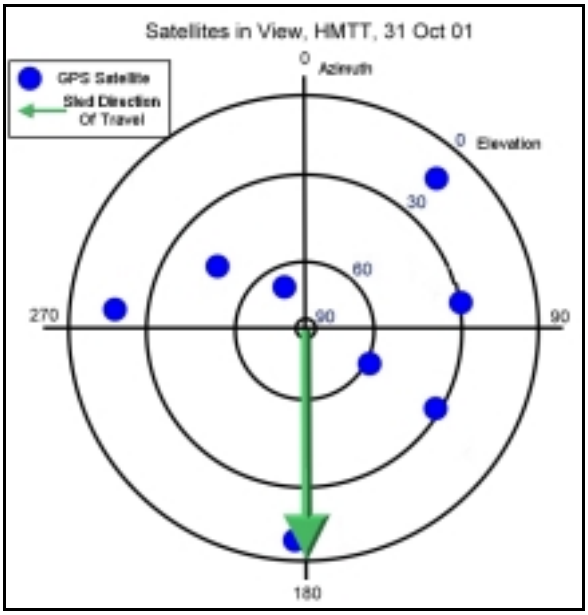

Figure 65. Satellites In View with Overlay of Sled Path

HMTT Test 721 Summary. The first ejection trial provided some valuable experience and insights into the equipment's limitations. The G12 did not perform as well as was anticipated. The 20 Hz sample rate adequately captured the position and velocity, but the receiver did not remained locked onto the satellites throughout the full acceleration to 630 KEAS. With the antenna located under the helmet's fiberglass shell, the drop in signal strength may have affected the G12's performance. Moving the antenna forward in the helmet may have improved the systems ability to handle the helmet's rocking motion as each rocket motor stage fired. These problems were investigated in the second sled trial.

F-16 Test HMTT 722, 14 November 2001

The second sled test was conducted at HMTT on 14 November 2001. The specs for the test are shown in Table 11.

Table11. Relevant Data, HMTT Ejection Test Number 722

Date	14-Nov-01
ACES II SU Configuration	Retrofit
Test Time (Local)	12:35
Met Conditions	Clear
Temp	54°F
Humidity	22%
Wind	SW 4
Seat/Man C.G. (X)	13.41 in
Seat/Man C.G. (Z)	16.50 in
Seat Weight	183 lb
Manikin Weight	276 lb
Seat/Man Weight	459 lb
MDRC	1.62
Manikin	JPATS Case 6
Target Velocity	630 KEAS
Actual Velocity	626.3 KEAS
Sled Start Station	5308
Sled Stop Station	11400
DIVEPACS Sample Rate	20 Hz

The equipment was configured as described in Chapter 3 (DIVEPACS Configuration for Rocket Sled Ejection Testing). The DIVEPACS was placed in the aircrew survival vest's large right pocket. Life Support personnel fabricated a special pocket to hold the DIVEPACS and sewed it to the survival vest. They also moved the antenna inside the helmet's shell, as shown in Figure 66.

Figure 66. Antenna Location, HMTT

The new antenna location was as far forward in the helmet liner as possible without interfering with the helmet's proper fit. The antenna cable was placed underneath the survival vest and sewn to the flightsuit collar to protect it from windblast.

Approximately one hour and 30 minutes prior to rocket initiation the power was applied to the Ashtech Z-Surveyor reference station GPS Receiver. Approximately 12 minutes prior to rocket initiation the power was applied to the DIVEPACS through the 500-foot remote arming cable. At the time of sled first motion the DIVEPACS was tracking 7 satellites.

The DIVEPACS remained attached to the manikin until seat first motion. The ejection system was initiated at the track's 9100-foot marker. The sled velocity at ejection system initiation was 626.3 KEAS. By seat rail separation the windblast had again sheared off all the survival vest pockets, including the pocket containing the DIVEPACS.

The manikin sustained minimal damage during this test. The ejection seat however, was completely destroyed after landing on the track and being hit by the Box Boy pusher sled. The DIVEPACS sustained much more damage than during the first test on 31 October. Figure 58 and Figure 59 shows the manikin and DIVEPACS as they were found after the test.

Figure 67. Manikin After Test, HMTT, 14 Nov 01

Figure 68. DIVEPACS After Test, HMTT, 14 Nov 01

The DIVEPACS came to rest 20 feet to the track's left at the 9250-foot marker. The DIVEPACS sustained serious damage, including large cracks in the case. In one corner small chunks of the case were broken loose near the center seam. Based on the damage to the case, it is possible that it hit a rock or part of the track. Almost all the I/O wires were torn loose from the data logger and G12 circuit board. The antenna lead sheared at the receiver connector. An inspection into the internal components revealed damage to the G12 J301-30 pin male connector apparently caused by the rechargeable batteries pushing forward into the circuit cards. After repairing the I/O cables and internal connections the internal battery was charged so the data could be downloaded from the data logger. Testing revealed no permanent damage to either the G12 receiver or data logger.

HMTT Test 722 Data Analysis. The DIVEPACS did **not** continuously track the sled position and velocity up to the point when it separated from the manikin. The sled velocity was 625.6 KEAS at the time of seat first motion. The high-speed film from the cameras mounted on the F-15 sled did not record the initial rocket motor initiation. However, the recorded sequence did show the manikin's head in a stable position against the ejection seat's headrest. The DIVEPACS recorded sled velocity is shown in Figure 69.

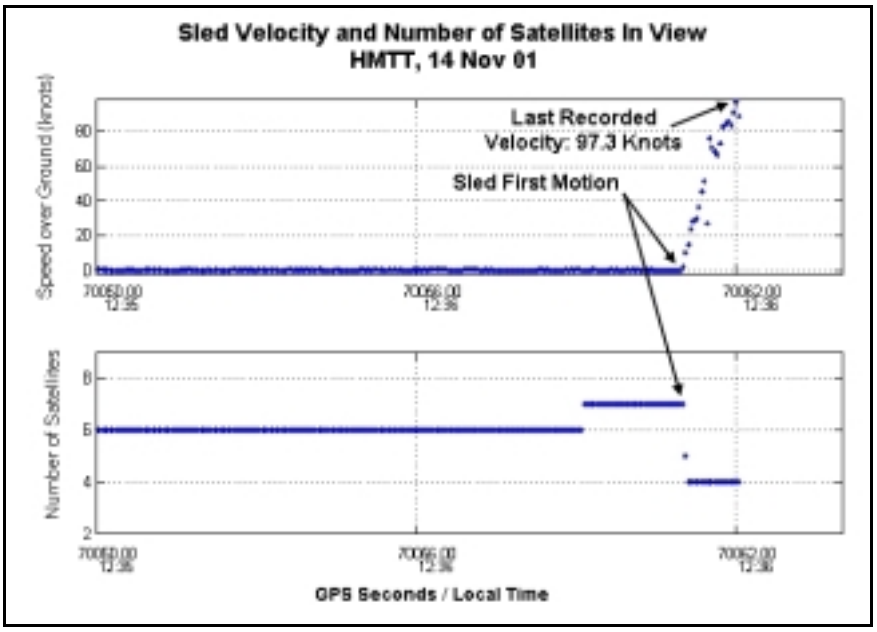

Figure 69. Sled Velocity and Number of Satellites in View, HMTT, 14 Nov 01

The DIVEPACS was only able to estimate the sled velocity and position through the first two rocket motor stages. The second plot in Figure 69 shows that the number of satellites tracked dropped immediately from 7 to 4 as the first rocket stage ignited. The last recorded speed was 97.3 knots. The DIVEPACS did not reacquire a position solution before it separated from the manikin at seat first motion.

The sled trajectory is shown in Figure 70. The DIVEPACS did not accurately determine the manikin trajectory with only four satellites in view. The same problem is shown in Figure 71 with the vertical velocity. The DIVEPACS did not accurately measure the change in vertical velocity as the sled traveled down the track.

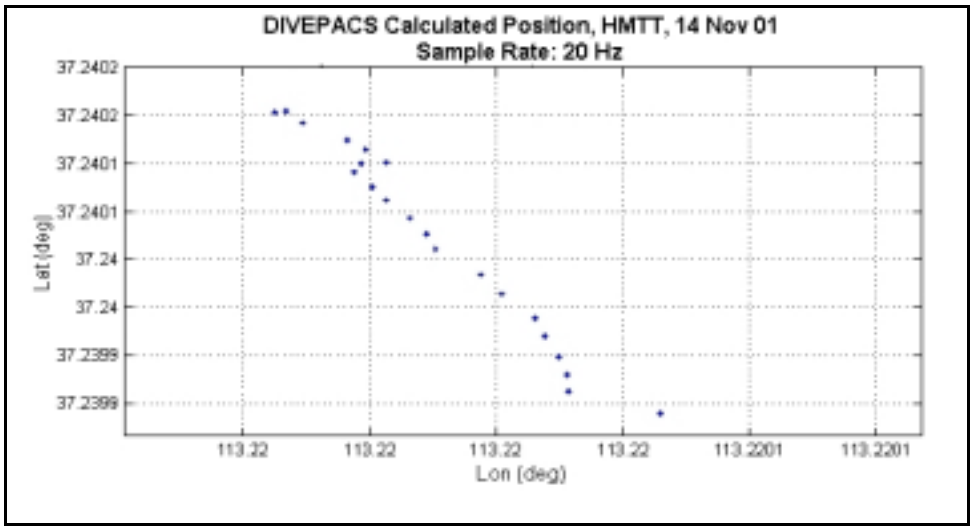

Figure 70. Sled Position, HMTT, 14 Nov 01

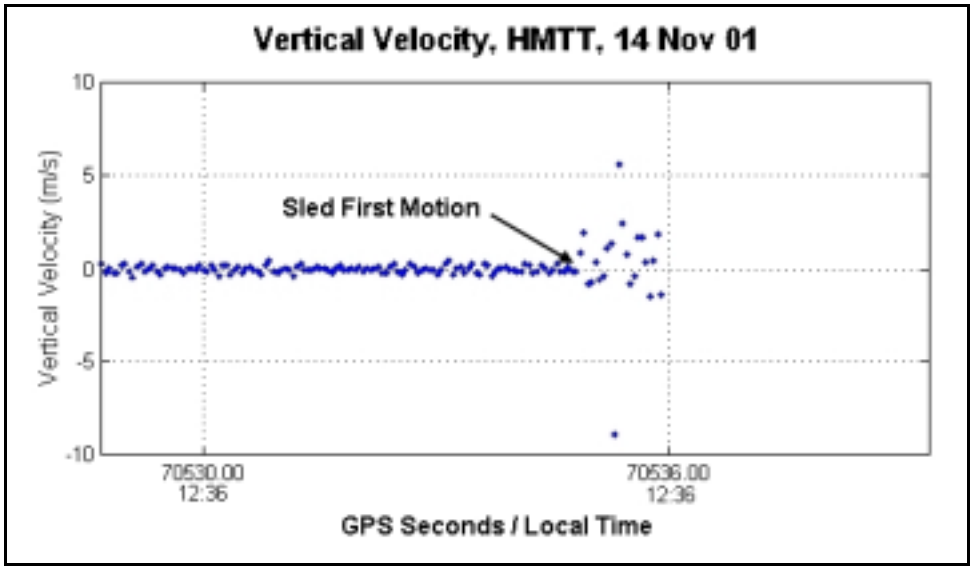

Figure 71. Vertical Velocity, HMTT, 14 Nov 01

Figure 72 is a plot of the approximate location of GPS satellites visible at the beginning of the test. The plot shows the 9 satellites in view by the reference station. In this test both the NMEA POS and the RAW CT1 were collected. The NMEA POS and RAW CT1 message formats are is included in Appendix B, (GPS Receiver Message

Formats Used in Data Collections). The satellite geometry was favorable during the ejection. The PDOP value was 1.9 just prior to rocket motor initiation.

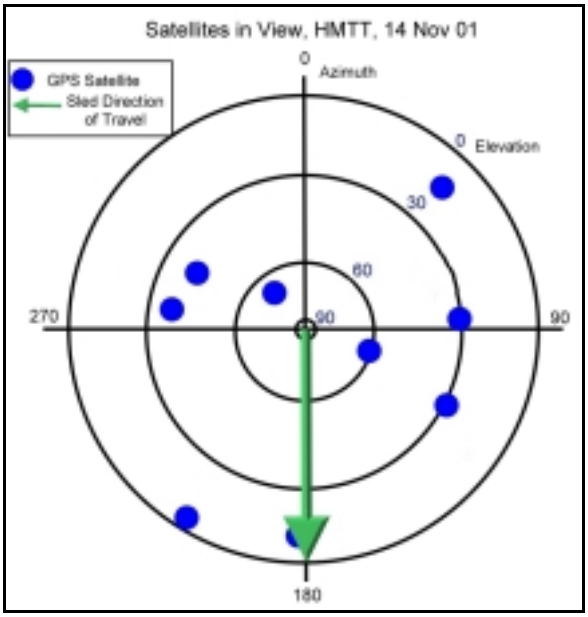

Figure 72. Satellites In View with Overlay of Sled Path

HMTT Test 722 Summary. The G12 did not perform as well as anticipated. The receiver lost lock almost immediately after the first stage rocket motor ignited. The increase in the warm-up period for the DIVEPACS prior to rocket motor ignition did not improve the performance as anticipated. The number of satellites at ignition increased from 6 to 7 compared to the first test; however, in this test the number dropped immediately after the first stage was ignited. Moving the antenna forward in the helmet did not improve the system's ability to handle the helmet's rocking motion. The G12 reference manual suggests a 20 – 30 dB gain antenna. The Antenna technologies antenna used was rated for 26 dB of gain. It is possible that placing the antenna under the fiberglass shell dropped the signal strength enough that the receiver's ability to handle the

dynamics is being degraded. One of the recommendations discussed in the next chapter is the addition of an inline signal amplifier. In future tests a special pocket made from a significantly stronger material should be fabricated and sewn to the to the survival vest. The reason for the poor performance is most likely due to the antenna. A different antenna was used for this test because the antenna from the first test was damaged and could not be repaired on site. It is possible that the second antenna, which was the same make and model as the first, did not provide the same amount of gain as the antenna in the first test. It is also possible that, although no physical damage was evident, the G12 receiver may have sustained some permanent damage in the first test when it hit the ground after separating from the manikin at 630 KEAS.

Summary

The results presented here represent the first stage of the research with the DIVEPACS. This chapter summarized the results and analysis from all three phases of the research. The DIVEPACS performed well in the initial bench testing. The stand-alone and differential accuracy was consistent with the manufacture specifications. The GPS simulations and freefall testing proved to be the most successful area in this research. In numerous freefall trials, the DIVEPACS reliably tracked multiple turns and rolls. The ejection sled trial results at Hurricane Mesa, while disappointing, showed some promising results. In both rocket sled trials, the DIVEPACS was torn from the survival vest as the manikin entered the airstreams at seat first motion. The DIVEPACS performed well in the first ejection trial despite loosing lock just prior to the seat fist

motion. The DIVEPACS however, did not perform well in the second test. The immediate loss of lock on the satellites made it impossible to produce any useful data.

These early results demonstrate that the DIVEPACS is a useful trajectory collection tool under limited platform dynamics. However, as it is currently configured, the DIVEPACS is not suited for the high dynamics encountered during the rocket sled ejection trials and improvements are required. The ejection trials did demonstrate that the DIVEPACS could survive and operate in a harsh environment.

V. Conclusions and Recommendations

Overview

The thesis described the theory, research methodology, and the test results and analysis from a GPS-based system designed to monitor the position and velocity of all major ejection-test components. This thesis provided an introduction to the history of ejection seat test and evaluation and the GPS theory necessary to guide the reader through the results and analysis from the DIVEPACS performance testing. It introduced the different design features in modern GPS receivers and how they affect a receiver's performance in a highly dynamics environment. This last section summarizes the results and provides recommendations for future testing and evaluation. To the readers interested in a shorter summary, Appendix E is the preliminary paper on this research published in the International Technical Meeting of The Satellite Division of The Institute of Navigation (ION), September 2001 proceedings.

Conclusions

The results presented in this thesis demonstrate that the DIVEPACS can accurately determine the position and velocity over a wide range of platform dynamics. The accuracy in the static collections provided a baseline for the receiver's 2DRMS accuracy. The receiver consistently produced less than two-meter 2DRMS accuracy in the horizontal, and less than 10 meters 2DRMS accuracy in the vertical direction. The simulation results showed that the DIVEPACS is capable of tracking flight profiles with

dynamics as large as 400 m/s velocity changes over a 5 second period with a limited satellite constellation. The largest successfully tracked acceleration was a simulated 5-second interval to a final velocity of 400 m/s. 400 m/s is over 775 KEAS, which was well above the test velocities encountered at Hurricane Mesa Test Track, and those expected in actual ejections.

The second performance test phase was conducted at Skydive Green County dropzone. The freefall testing proved to be the most successful area in the research. The DIVEPACS's final configuration is small enough to fit into a survival vest's large pocket without interfering with the ejection seat harness or parachute harness. The additional weight doesn't cause any significant change in freefall stability or descent rate. In numerous freefall trials, the DIVEPACS reliably tracked multiple turns and rolls. The freefall tests demonstrated that the DIVEPACS could accurately record the position and velocity during the type of turns and rolls the manikin typically undergoes during ejections.

The last phase was the rocket sled ejection trials at HMTT. The sled velocity in both tests at Hurricane Mesa exceeded 620 KEAS. At this velocity, almost any equipment placed externally on the manikin sustains a significant amount of damage. The maximum velocity in the majority of escape system tests is below 450 KEAS. At these lower speeds the DIVEPACS may prove to be a very valuable tool. The DIVEPACS may have performed well at 630 KEAS if tested at a longer track where the acceleration rate could be lowered. It is a reasonable assumption based on the results from the three test phases that it would handle the dynamics if ejected from an aircraft flying straight-and-level at 630 KEAS.

An extensive number of simulations demonstrated that the G12 is capable of handling straight-line accelerations in the laboratory far exceeding what was experienced at Hurricane Mesa. Minor modifications to the DIVEPACS, such as an inline signal amplifier, or a different antenna with a higher gain, may be all that is needed to improve the performance in rocket sled ejection trials.

Recommendations

Additional testing is necessary to determine the DIVEPACS's performance fully in a highly dynamic environment. The straight-line acceleration simulation results are very encouraging. The real-world performance should be improved by adding an in-line signal amplifier between the antenna and G12 receiver. The in-line amplifier may provide enough signal gain to boost the performance in the field to match the results found with the GPS simulator more closely. The antennas used for the freefall tests and the ejection trials provided 26 dB of gain. The inline signal amplifiers provide as much as 30 dB of gain. The amplifiers (a typical model is shown in Figure 73) are about the size of a two-inch long pencil and cost less than $300.

Figure 73. Inline GPS Signal Amplifier

The receiver 5-volt antenna lead powers the amplifier. This option should be explored before replacing the G12 receiver with the G12 High Dynamics Missile Applications (G12 HDMA) model. The G12 HDMA may be the best solution if the future experiments identify that the tracking errors are due to oscillator vibration induced noise.

The one area where the DIVEPACS may prove to be the most useful is monitoring ejections from flight vehicles. Unfortunately, weather delays made it impossible to evaluate the DIVEPACS's performance in an ejection from a flight test vehicle. Based on the results from the testing, it is a reasonable assumption that it would handle the dynamics of an ejection from an aircraft flying straight-and-level at the beginning of the ejection sequence.

Another application that should be investigated is monitoring tests conducted at locations that do not have theodolite cameras. A limitation associated with theodolite cameras is that they must be placed at carefully surveyed positions to provide any measure of accuracy. The DIVEPACS can be quickly attached to almost any platform and incorporated in a test plan without the restrictions on surveying the flight path or camera location. The flight plans can be more flexible because changes to the flight path are not limited by camera locations. Once the receiver is configured, the DIVEPACS can continue to operate without any operator assistance until the internal memory capacity or batteries are exhausted.

In addition to the increased flexibility, the DIVEPACS can augment the theodolite systems position and velocity accuracy. Since the theodolite cameras typically record an event from the side, the altitude measurements are more accurate than the horizontal

measurements. This is the opposite case for the DIVEPACS, for which the altitude measurement errors are always larger than the horizontal measurement errors. These two systems could be combined to increase the overall accuracy in the position and velocity measurements.

The results presented in this thesis demonstrate that the DIVEPACS can provide accurate position and velocity over a wide range of platform dynamics. The DIVEPACS performed well in the initial bench testing. The ejection sled trial's results at Hurricane Mesa, while disappointing, showed some promising results. Modifications to the manikin's survival vest are necessary to protect the equipment so the full ejection profile can be recorded. Additional testing is needed to determine the DIVEPACS's full capabilities.

Contributions

The DIVEPACS can collect position and velocity data that may not be obtained by other methods. Its real strength is its low cost and ease of integration into an existing test program. This system can be quickly integrated into a test plan to provide accurate position and velocity data without the extra expense and delay of setting up a large number of theodolite cameras. The small size and weight make it easy to attach to almost any platform. This system would be very useful for testing the performance of next generation escape system parachutes, air delivery payloads, or parachute-retarded ordnance.

Appendix A. Data Collected by the JPATS Manikin Sensors

This appendix is included to show the type of data that can be collected during an ejection test by the Joint Primary Aircraft Training System (JPATS) manikin sensors. Table 12 lists the channel information from the 31 Oct 01 test conducted at HMHTT and is typical of the type of data the collected during ejection seat testing and validation.

Table 12. JPATS Manikin Sensor Channels

Test Program: F16 Structural Integrity	
Test Designation: HMTT 722	
Test Date: 14 Nov 2001	
Test Velocity: 600 KEAS	
Manikin: LARD 1	**DAS: 95-012**
Data/Filter Rate: 10,000 Hz/2,000 Hz	
Trigger: Keyboard, T - 15 Seconds	
T-M Pack: none	**Main Battery Pack:98-12-01**
Relay: 97-13	**Backup Battery: 98-22**

Cables	
DASPWR-A	
DASTRIG	
DASCOMM	
EVENT	
4 PIGTAILS	
Seat box special	

Channel	Description	Channel	Description
1	Reserved	9	Seat/Man Separation
2	Reserved	10	Seat Release from Crewman
3	System Init	11	Drogue Deploys
4	Seat First Motion	12	
5	Seat/Rail Separation	13	
6	STAPAC Ignites	14	
7	Parachute Deploys	15	
8		16	

Channel	Ch Sym	Channel Description	Sensor	S/N	Units	Excitation	Sensitivity	Resistance	Range
1	NFX	Head/Neck Force X	Denton 1716	718	lbs.	10 V	.0007932	175	+/- 2000
2	NFY	Head/Neck Force Y	Denton 1716	718	lbs.	10 V	.0008159	175	+/- 2000
3	NFZ	Head/Neck Force Z	Denton 1716	718	lbs.	10 V	.0004427	350	+/- 3000
4	NMX	Head/Neck Moment X	Denton 1716	718	in-lbs.	10 V	.0006695	175	+/- 2500
5	NMY	Head/Neck Moment Y	Denton 1716	718	in-lbs.	10 V	.0006731	175	+/- 2500
6	NMZ	Head/Neck Moment Z	Denton 1716	718	in-lbs.	10 V	.0009102	350	+/- 2500
7	HLAX	Head Acceleration X	Entran EGV3-F-250	97C97C27TB06	G	10 V	.09035	225	+/- 100
8	HLAY	Head Acceleration Y (-Y)	Entran EGV3-F-250	97C97C27TB06	G	10 V	-.09389	225	+/- 100
9	HLAZ	Head Acceleration Z	Entran EGV3-F-250	97C97C27TB06	G	10 V	.09078	225	+/- 100
10	CLAX	Chest Acceleration X (-X)	Entran EGV3-F-250	97C97C28TB03	G	10 V	-.09389	225	+/- 100
11	CLAY	Chest Acceleration Y	Entran EGV3-F-250	97C97C28TB03	G	10 V	.09205	225	+/- 100
12	CLAZ	Chest Acceleration Z	Entran EGV3-F-250	97C97C28TB03	G	10 V	.09191	225	+/- 100
13	LLAX	Lumbar Acceleration X	Entran EGV3-F-250	97F97F10TP06	G	10 V	.08852	225	+/- 100
14	LLAY	Lumbar Acceleration Y (-Y)	Entran EGV3-F-250	97F97F10TP06	G	10 V	-.08739	225	+/- 100

Channel	Ch Sym	Channel Description	Sensor	S/N	Units	Excitation	Sensitivity	Resistance	Range
15	LLAZ	Lumbar Acceleration Z	Entran EGV3-F-250	97F97F10TP06	G	10 V	.09035	225	+/- 100
16	LFX	Lumbar Force X	Denton 1914	296	lbs.	10 V	.0006609	175	+/- 3500
17	LFY	Lumbar Force Y	Denton 1914	296	lbs.	10 V	.0006635	175	+/- 3500
18	LFZ	Lumbar Force Z	Denton 1914	296	lbs.	10 V	.0002448	350	+/- 3500
19	LMX	Lumbar Moment X	Denton 1914	296	in-lbs.	10 V	.0005109	175	+/- 3500
20	LMY	Lumbar Moment Y	Denton 1914	296	in-lbs.	10 V	.0005140	175	+/- 3500
21						10V		175	+/- 500
22	CARX	Chest Angular Rate X (-X)	ATA ARS-01	237 / V01	rad/sec	5 V	-13.4544	No	+/- 35
23	CARY	Chest Angular Rate Y (-Y)	ATA ARS-01	243 / V03	rad/sec	5 V	-14.4786	No	+/- 35
24	CARZ	Chest Angular Rate Z (-Z)	ATA ARS-01	244 / V22	rad/sec	5 V	-13.7160	No	+/- 35
25	SARY	Seat Angular Rate Y	ATA ARS-01	246 / 009	rad/sec	5 V	14.2034	No	+/- 35
26	SARZ	Seat Angular Rate Z	ATA ARS-01	532 / 012	rad/sec	5 V	11.1336	No	+/- 35
27	PSPLAX	Pri Seat Pan Linear Acceleration X (-X)	Entran EGV3-F-250	96J96J15TB01	G	10 V	-.08201	225	+/- 250
28	PSPLAZ	Pri Seat Pan Linear Acceleration Z (Y)	Entran EGV3-F-250	96J96J15TB01	G	10 V	.07862	225	+/- 250
29	PSPLAY	Pri Seat Pan Linear Acceleration Y (-Z)	Entran EGV3-F-250	96J96J15TB01	G	10 V	-.07890	225	+/- 250
30	SARX	Seat Angular Rate X	ATA ARS-01	239 / 008	rad/sec	5 V	14.044	No	+/- 35
31	RBSG	Right Block	250UN GF=2.105	N/A	eU	10 V	0.0005287	350.32	+/- 6000
32	RWSG	Right Web	250UN GF=2.105	N/A	eU	10 V	0.0005294	350.48	+/- 6000
33	RFSG	Right Fwd (Top)	062UW GF=2.135	N/A	eU	10 V	0.0005358	350.47	+/- 6000
34	RMSG	Right Mid	062UW GF=2.135	N/A	eU	10 V	0.0005371	350.40	+/- 6000
35	RASG	Right Aft (Bottom)	250UN GF=2.105	N/A	eU	10 V	0.0005292	350.42	+/- 6000
36	LBSG	Left Block	250UN GF=2.105	N/A	eU	10 V	0.0005294	350.38	+/- 6000
37	LWSG	Left Web	250UN GF=2.105	N/A	eU	10 V	0.0005299	350.53	+/- 6000
38	LFSG	Left Fwd (Top)	062UW GF=2.135	N/A	eU	10 V	0.0005368	350.59	+/- 6000
39	LMSG	Left Mid	062UW GF=2.135	N/A	eU	10 V	0.0005373	350.58	+/- 6000
40	LASG	Left Aft (Bottom)	250UN GF=2.105	N/A	eU	10 V	0.0005291	350.44	+/- 6000

Appendix B. GPS Receiver Message Formats Used in Data Collections

The G12 GPS receiver can output data in several formats including NMEA, Ashtech's proprietary NMEA-style, and raw messages. This appendix lists the different GPS data message types of recorded during the three different research phases.

B-File generated ASCII data file

The B-file is written by the Ashtech Z-Surveyor and stored on the receiver PCMCIA card. The software program "Ashtech Download", version 2.00, and "gps_convert.exe" were used to convert the data stored in a binary format to the "AFIT ASCII" format shown in Table 13. The ASCII data file displays the measurements for each satellite and time epoch on a separate line.

Table 13. AFIT ASCII Data Format

Column	Column Data Type	Sample Data
Column 1	Measurement time (Receiver clock time) (GPS week seconds)	148660.000
Column 2	PRN	1
Column 3	L1 C/A-code pseudorange measurement (m)	20416332.683
Column 4	L1 P-code pseudorange measurement (m)	20416331.854
Column 5	L1 carrier-phase measurement (L1 cycles)	18241.671
Column 6	L1 Doppler measurement (Hz)	1325.035
Column 7	C/No for L1 C/A-code pseudorange (dB Hz)	13
Column 8	C/No for L1 P-code pseudorange (dB Hz)	14
Column 9	L2 C/A-code pseudorange measurement (m)	20416341.071
Column 10	L2 P-code pseudorange measurement (m)	8671.683
Column 11	L2 Doppler measurement (Hz)	1032.495
Column 12	C/No for L2 P-code pseudorange (dB Hz)	14

RINEX

The Receiver Independent Exchange Format (RINEX) is a set of standard definitions that permits the interchangeable use of GPS collected data from different GPS receiver makes and models. A full RINEX format description can be found at the http://www.unavco.ucar.edu website. The B-files collected by the Ashtech Z-surveyor were converted to RINEX format before uploading into OPUS.

NMEA

Standard NMEA messages are output as a string of ASCII characters delimited by commas. The messages are output from the receiver serial port to a PC for processing or recording. There are over 20 different NMEA messages that provide data such as user position, velocity, and the number of satellites in view. The three NMEA messages used for the majority of the thesis research were the GGA, GSV, and POS message. The tables below described the format for each of these messages.

GGA Message. GGA is the NMEA 3-D GPS Position Message. This message contains data on the receiver position and velocity.

Table 14. NMEA GGA Message Format

Sample Message: *$GPGGA,170152.80 ,3940.778340,N,08351.655652, W,1,11,0.9,600.808,M,-33.77,M,,*6D*	
Field	**Description**
170152.80	UTC Time (hhmmss.s)
3940.778340	Latitude
N	Latitude sector
08351.655652	Longitude
W	Longitude sector
1	Position fix type
11	Number of satellites used in position computation
0.9	HDOP
600.808	Altitude above mean sea level (m)
M	Altitude unit of measure
33.77	Geoidal separation value
M	Geoidal separation unit of measure (m)
	Age of Differential corrections (s)
	Differential base station ID number
*UE00*3A*	Checksum

GSV Message. GSV is the NMEA Satellites in View Message. This message contains data on the satellite PRN, location, and signal strength.

Table 15. NMEA GSV Message Format

Sample Message: *$GPGSV,2,1,08,01,56,323,52.2,22,56,100,53.3,20, 71,219,53.0,29,17,099,44.5*70*	
Field	Description
2	Total number of GSV messages to be output
1	Message number
08	Total number of satellites in view
01	Satellite PRN number
56	Elevation (deg)
323	Azimuth (deg)
52.2	Signal to noise ration (dbHz)
22	Satellite PRN number
56	Elevation (deg)
100	Azimuth (deg)
53.3	Signal to noise ration (dbHz)
20	Satellite PRN number
71	Elevation (deg)
219	Azimuth (deg)
53.0	Signal to noise ration (dbHz)
29	Satellite PRN number
17	Elevation (deg)
099	Azimuth (deg)
44.5	Signal to noise ration (dbHz)
*UE00*3A*	Checksum

POS Message. POS is the NMEA Position Message. This message contains data on the receiver position and velocity.

Table 16: NMEA POS Message Format

Sample Message *$PASHR,POS,0,06,172437.00, 3714.00389682,N,11313.256039,,01564.848,R,000.0,00.0,000.0,0 2.501.7,01.9,01.4,UE00*3A*

Field	Description
0	Position fix type
06	Number of satellites used in position computation
172437.00	Current UTC Time hhmmss
3714.389682	Latitude
N	Latitude sector
11313.256039	Longitude
W	Longitude sector
01564.848	Altitude above mean sea level (m)
R	Reserved
000.0	True track/true course over ground (deg)
000.0	Vertical velocity (m/s)
02.5	PDOP
01.7	HDOP
01.9	VDOP
01.4	TDOP
1.2	Firmware version
*UE00*3A*	Checksum

Ashtech Proprietary

Ashtech proprietary messages are similar to the NMEA format. The Ashtech messages are a string of ASCII characters delimited by commas. The Ashtech message may exceed the maximum of 80 characters allowed in a NMEA formatted message.

RAW DATA

Raw data messages contain information such as pseudorange measurements, position, velocity, ephemeris, and satellite almanac data. The G12 outputs raw data messages in the CT1 format shown below. Raw messages provide the pseudorange and PRN data necessary for differential corrections.

Table 17. RAW CT1 Message Format

Sample Message: *$PASHR,CT1,Binary Data String + Checksum*		
Binary Type	**Bytes**	**Content**
(adj_rcvtime)	4	Time data was received
sv_num	1	The number of satellites in the message (1 – 6)
Remainder	1	The number of satellites remaining for the current epoch
(chn1)	1	Channel (1 – 12)
(prn1)	1	Satellite PRN number
(smooth_rng1)	8	Smoothed pseudorange measurement
(chn2)	1	Channel (1 – 12)
(prn2)	1	Satellite PRN number
(smooth_rng2)	8	Smoothed pseudorange measurement
(chn3)	1	Channel (1 – 12)
(prn3)	1	Satellite PRN number
(smooth_rng3)	8	Smoothed pseudorange measurement
(chn4)	1	Channel (1 – 12)

Binary Type	Bytes	Content
(prn4)	1	Satellite PRN number
(smooth_rng4)	8	Smoothed pseudorange measurement
(chn5)	1	Channel (1 – 12)
(prn5)	1	Satellite PRN number
(smooth_rng5)	8	Smoothed pseudorange measurement
(chn6)	1	Channel (1 – 12)
(prn6)	1	Satellite PRN number
(smooth_rng6)	8	Smoothed pseudorange measurement
checksum	2	Checksum

Appendix C. DIVEPACS Wiring Diagrams

This appendix is included to record all the custom cables required to interface the G12 receiver, data logger, and rocket sled. A detailed drawing of the protective case is included for completeness.

Case Dimensions

This case is designed to house and protect the G12 receiver, data logger, and battery pack. Veridian, the contractor responsible for configuring the JPATS manikin, manufactured the case.

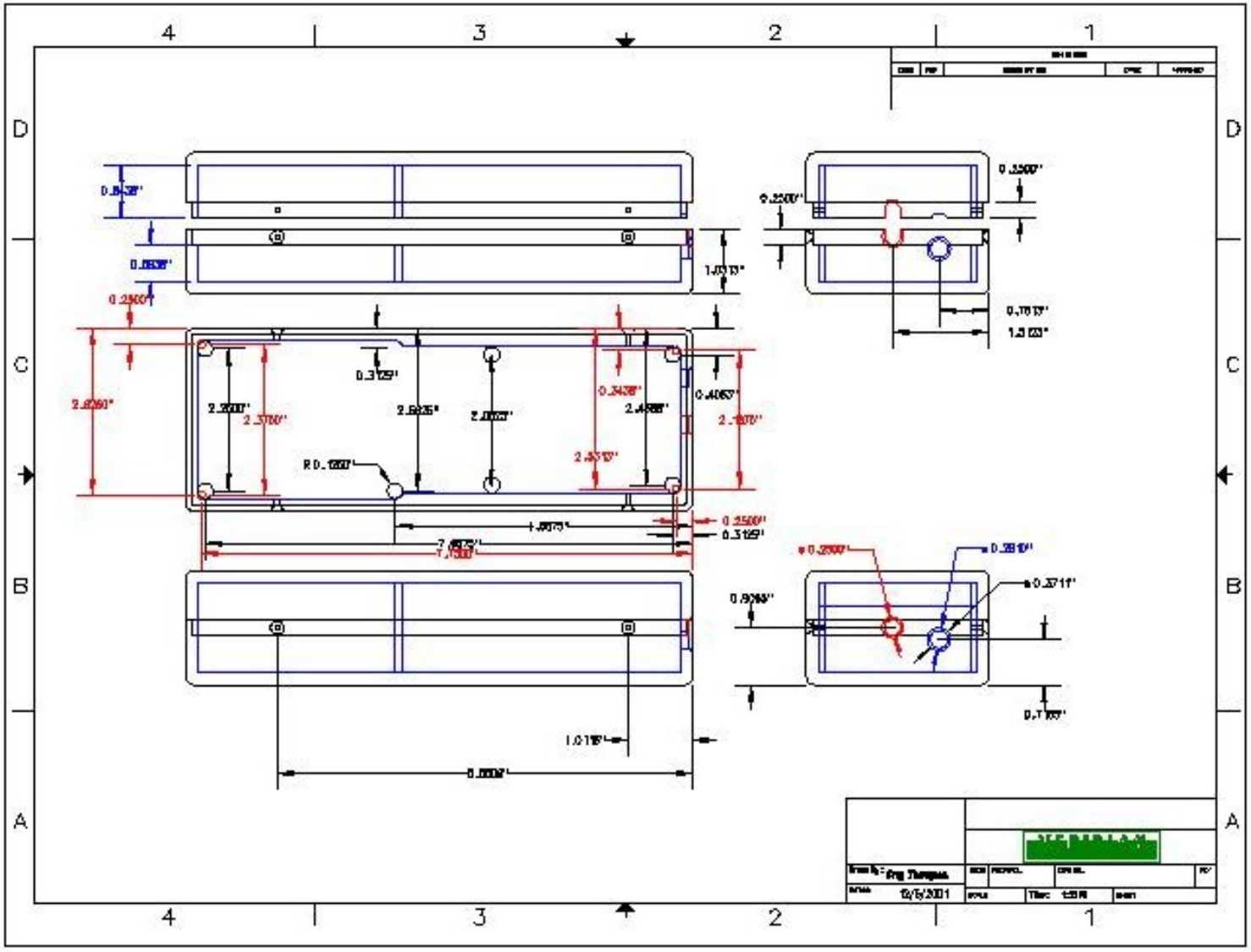

Figure 74. Case Dimensions

Magellan G12 DB25 Cable

The Magellan G12 DB25 Cable is used to turn the receiver on/off and also to connect it to the GPS receiver through the serial port.

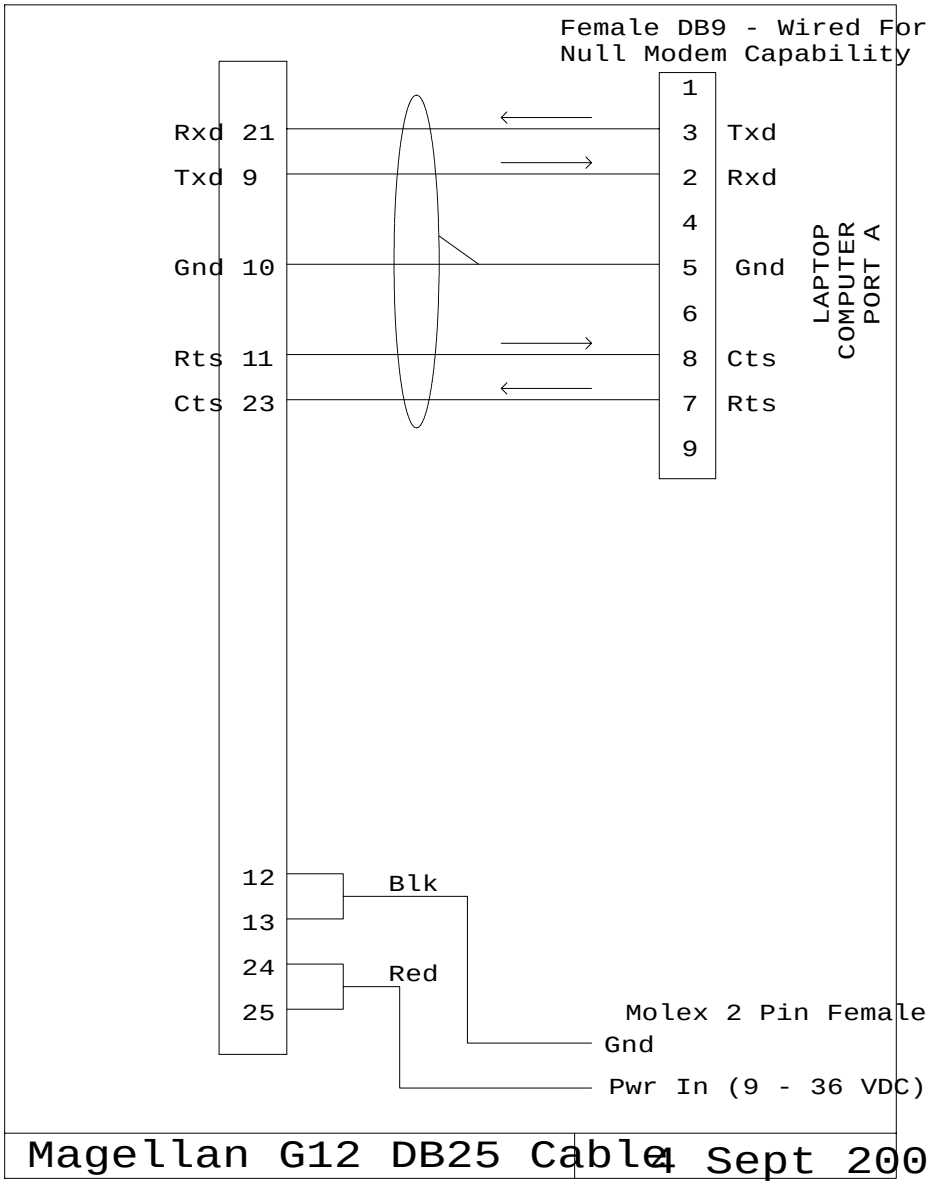

Figure 75. Magellan G12 DB25 Cable

GPS to Data Logger

This GPS to Data Logger cable is used to connect the stand-alone data logger to the G12 sensor. This cable was utilized during the Phase II freefall testing.

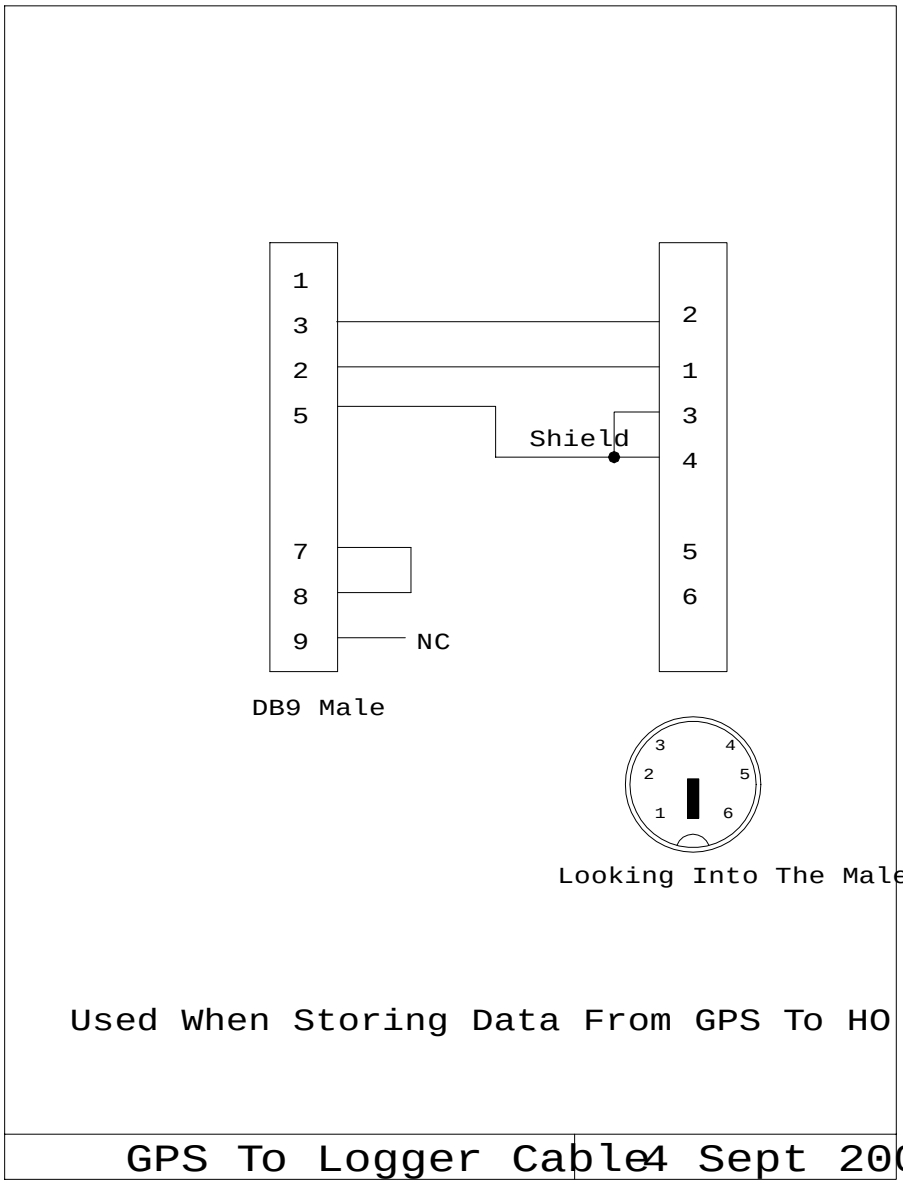

Figure 76. GPS to Logger Cable

Ejection Seat Interface at Test Time

This Ejection Seat Interface at Test Time cable is used during static data collection, and freefall testing. This cable allows data to pass from the G12 to the data logger. It provides the capability to turn the unit on/off remotely and also monitor the G12 and data logger red and green status LEDs. During rocket sled testing the connectors pull apart as the manikin and seat rise out of the sled cockpit.

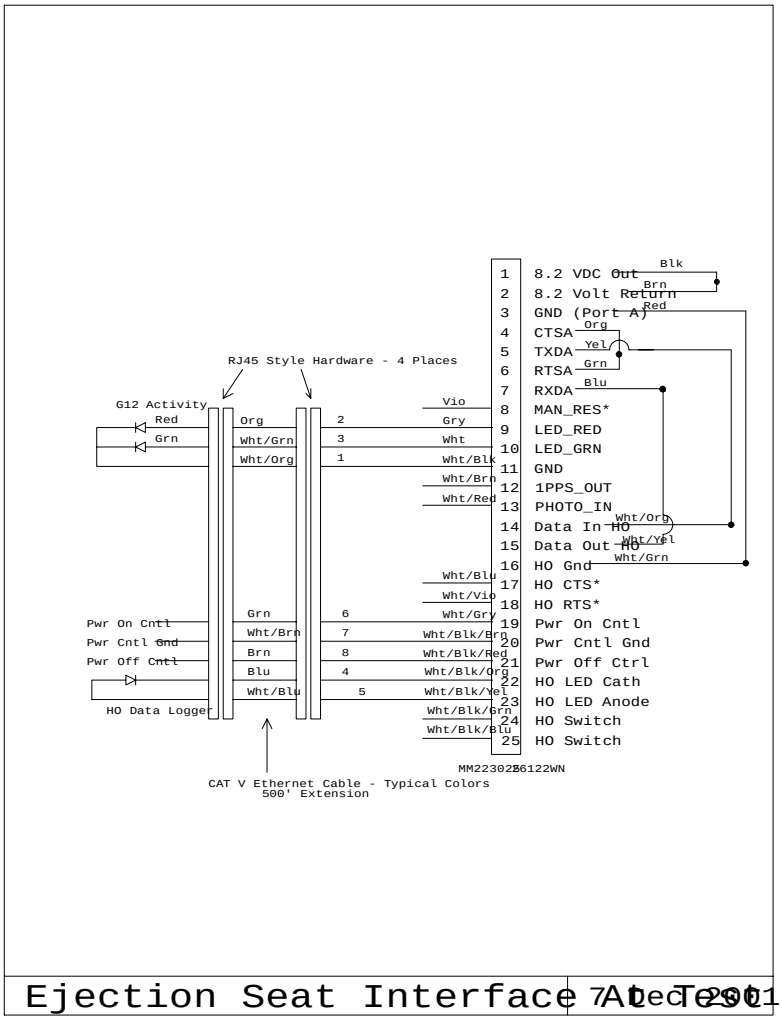

Figure 77. Ejection Seat Interface at Test Time

GPS Ejection Module Internal

Figure 78 is the wiring diagram for the internal connections between the power supply, data logger, and G12 receiver.

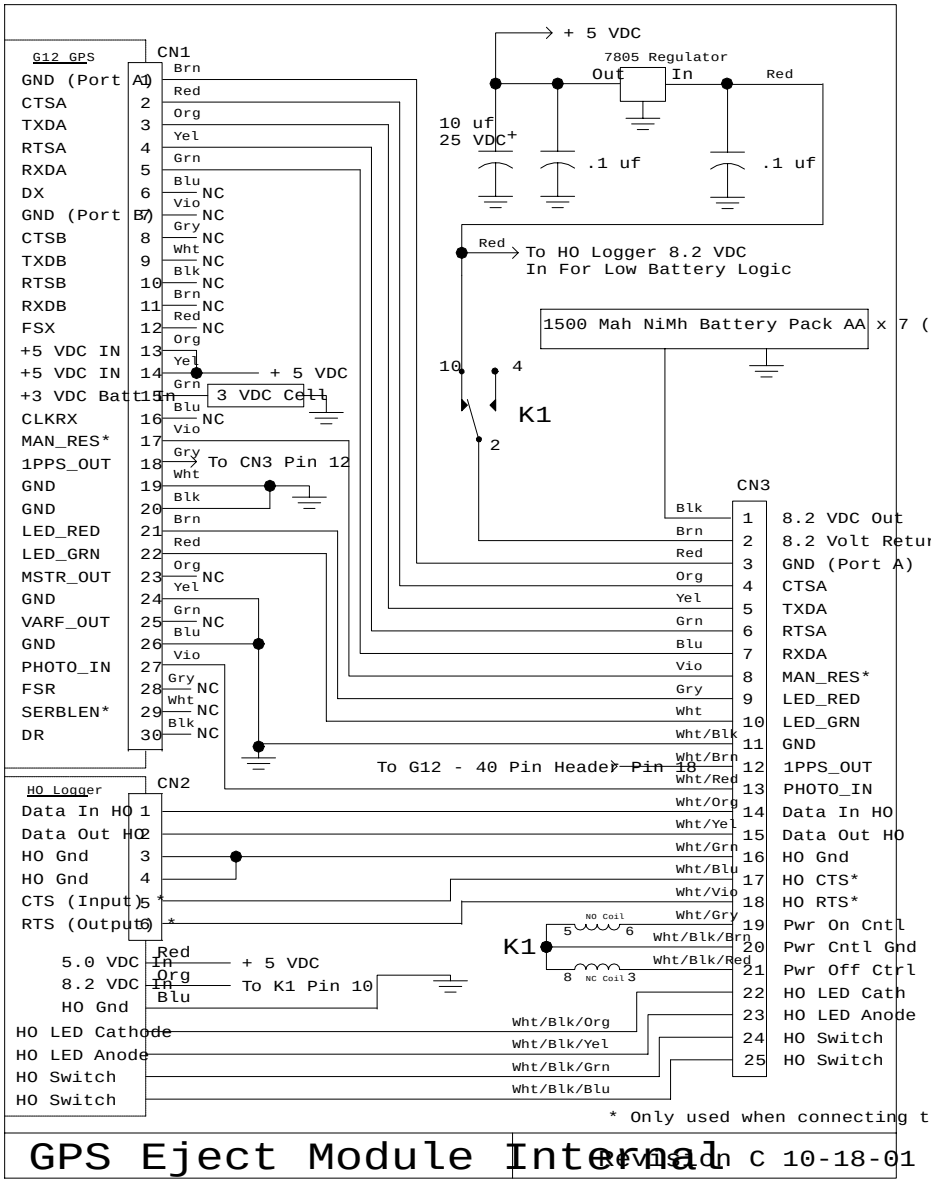

Figure 78. GPS Ejection Module Internal

GPS H.O. Data Cable

The GPS H.O. Data cable connects a stand-alone data logger to the serial port of a PC.

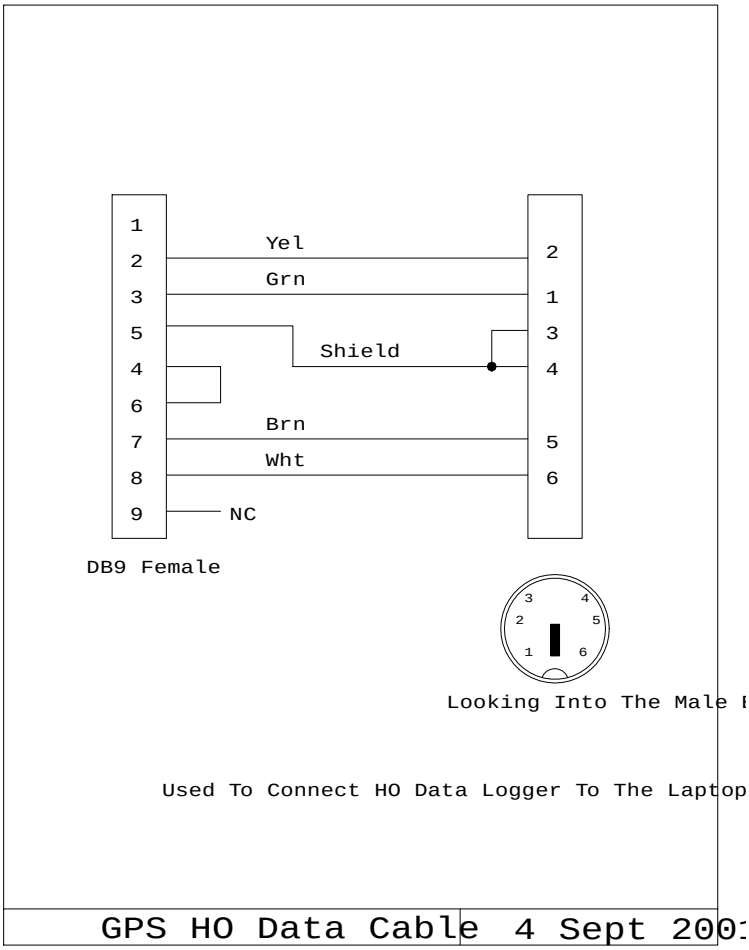

Figure 79. GPS HO Data Cable

GPS to H.O. Data Logger

The GPS to H.O. Data Logger cable connects the G12 GPS receiver's serial port to the H.O. Data data logger.

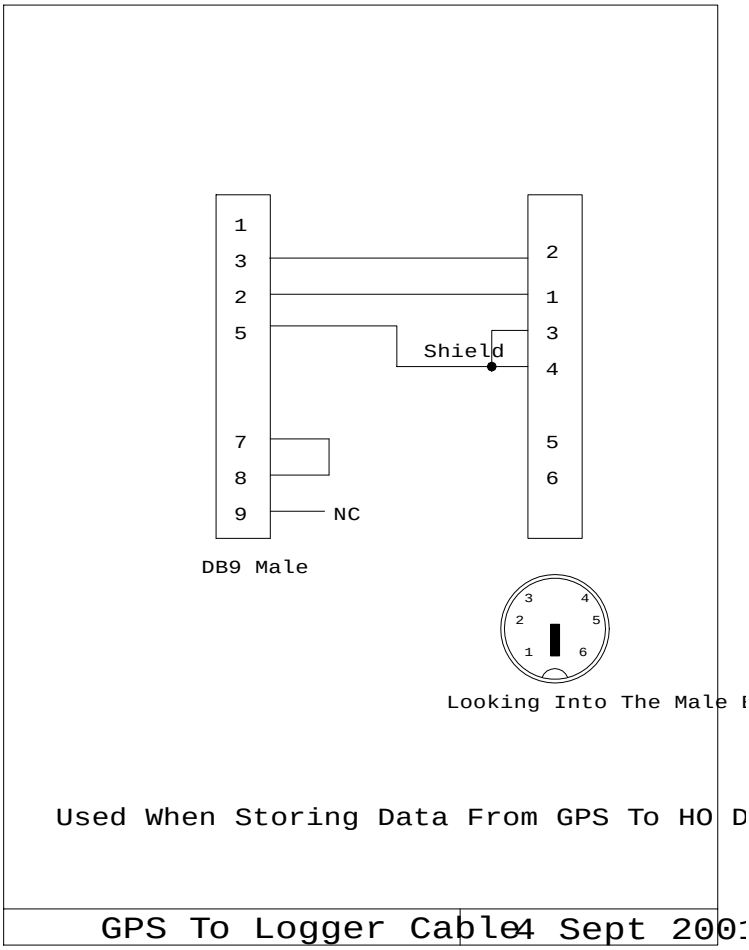

Figure 80. GPS To Data Logger Cable

Appendix D. GPS Equipment Hardware Descriptions

This appendix lists the equipment specification sheets provided by the equipment manufactures for each hardware item used in the research.

DIVEPACS GPS Receiver

Ashtech manufactured the G12 GPS receiver used during the research. The specifications are listed in Table 18. This information was obtained on the Ashtech products website.

Table 18. G12 Sensor Specifications

General	12-channel, continuous tracking, L1 C/A code and carrier phase tracking
DGPS Software	Differential remote and base station options
Real-Time DGPS Position Accuracy[1]	Static or Dynamic[2] Horizontal CEP 40cm Horizontal 95% 90cm Vertical 95% 1.6m
Velocity	1,000 nmh[3]
Altitude	60,000 ft
Acceleration	20g's (G12 Sensor Remote)
Acquisition	Hot start: 15 sec typical, w/current almanac, position, time, & ephermeris Warm start: 45 sec typical, w/current almanac, position, & time Cold start: 2 min typical, no almanac, position, or time
Reacquisition Time	< 2 sec
Position Update Rate (standard)	up to 10 Hz, G12 Sensor Remote (up to 20 Hz optional[4]) up to 2 Hz, G12 Sensor Base Station (up to 20 Hz optional[4])
Raw Data Update Rate (standard)	code & carrier, 2 Hz (up to 20 Hz optional)

Other	Includes Strobe Correlator™ multipath mitigation, Receiver Autonomous Integrity Monitoring (RAIM), Event marker, geoid and magnetic variation models, position latency output, programmable measurement strobe
Input Voltage	9-36vDC
Power Consumption	1.8W (receiver) 0.3W (antenna)
Connector	DB25 (pin compatible with GG24 Sensor and Z12 Sensor)
Serial Comm	2 RS-232 serial ports, up to 115,000 bps External LED drivers
Input Messages	Ashtech OEM command set RTCM 104 v2.1 (Remote Message types 1, 2, 3, 6, 9, 16). All G-12 Sensor
Output Messages	NMEA-0183 v2.01 and Ashtech OEM command set RTCM 104 v2.1 (Base Station Message types 1, 2, 3, 6, 9, 16). G-12 Sensor Base Station version only.
Time Mark Output	1 PPS (5V TTL) 340 ns (autonomous accuracy) 45 ns (DGPS accuracy)
Operating Temp	-30°C to +60°C
Storage Temp	-40°C to +85°C
Humidity	95% non-condensing

[1]Autonomous GPS accuracy subject to degradation to 100m 2DRMS under the USDoD imposed Selective Availability Program.

[2]Based on tests using an Ashtech G12 base station Ashtech Geodetic antenna, G12 Remote with Ashtech Marine IV antenna, short baseline.

[3]Higher altitude and velocities up to 9km/s are available under validated export license.

[4]When 20 Hz positions are generated, the maximum number of satellites used is 8, the receiver still tracks up to 12 satellites and raw data is still available for up to 12 satellites. When positions are generated at 10 Hz, or lower, the receiver tracks and uses up to 12 satellites.

DIVEPACS GPS Receiver Configuration Settings

There are a number of options for configuring the G12 GPS receiver. Table 19 lists the receiver settings used in each research phase. The page numbers refer to the

corresponding section of the Ashtech G12 GPS OEM Board and Sensor Reference Manual, Part Number: 630068, Revision C. Commands not listed were set to the default value, (as defined in the reference manual).

Table 19. G12 Receiver Commands

Setting	Overview	Page Number
$PASHS,CRR,E	Code Correlator Mode	55
$PASHS,LPS,10,3,1	Set the tracking loop parameters for high dynamics	72
$PASH S,UTS,ON	Enable clock steering	108
$PASH S,CTS,A,OFF	Turn off handshaking for port A	57
$PASH S,POP,20	Position and raw data update rate	82
$PASHS,RCI,0.05	Set the output interval for raw messages	127
$PASHS,SPD,A,9	Set baud rate of Port A to 115,200 bps	96

DIVEPACS Antenna Specifications

Antenna Technologies Inc manufactured the antennas used during the research. The antenna specifications and mounting information are shown in Figure 81.

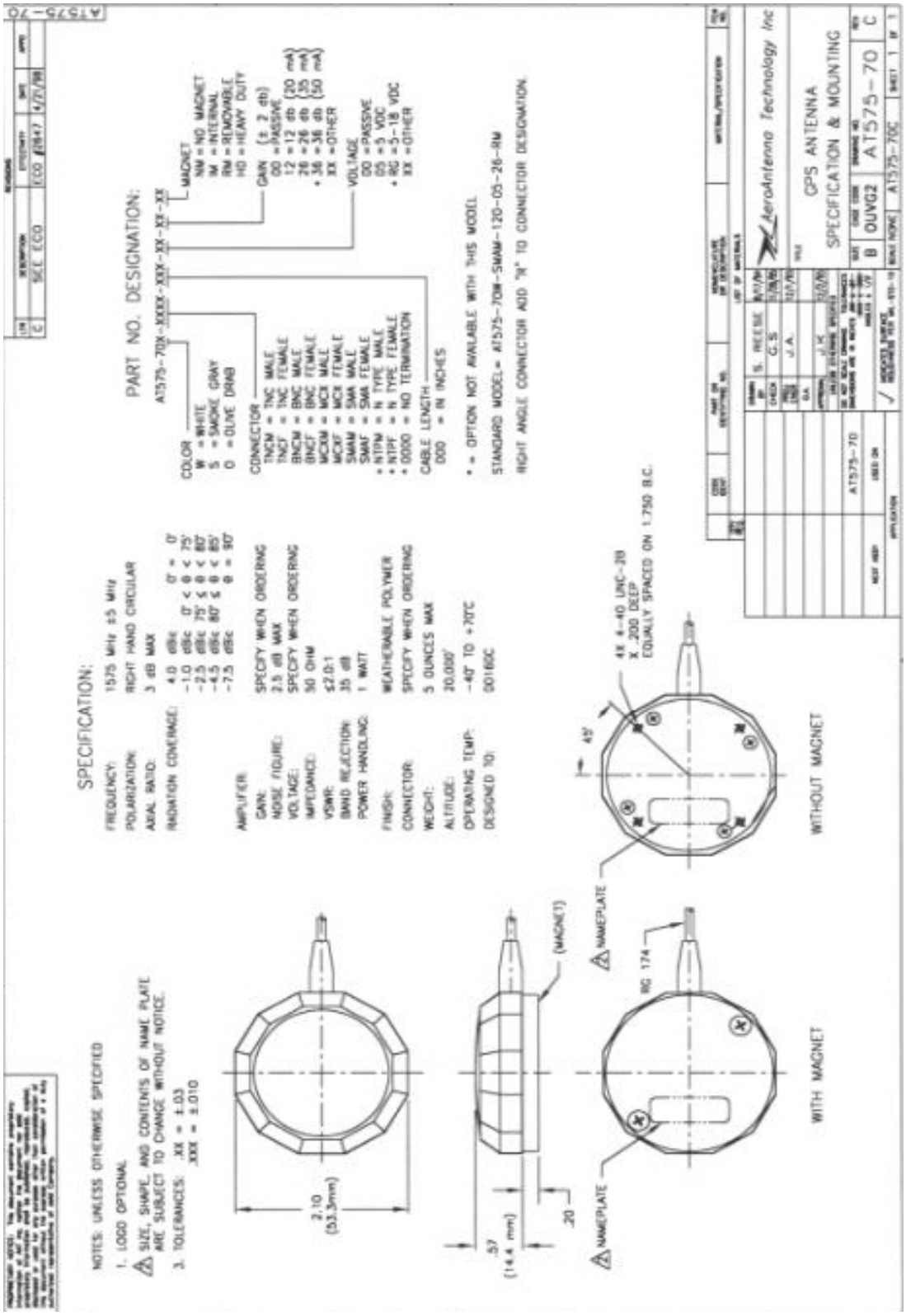

Figure 81. GPS Antenna Specification and Mounting

Marine III Antenna - L1/L2 GPS

ASH 700700.C

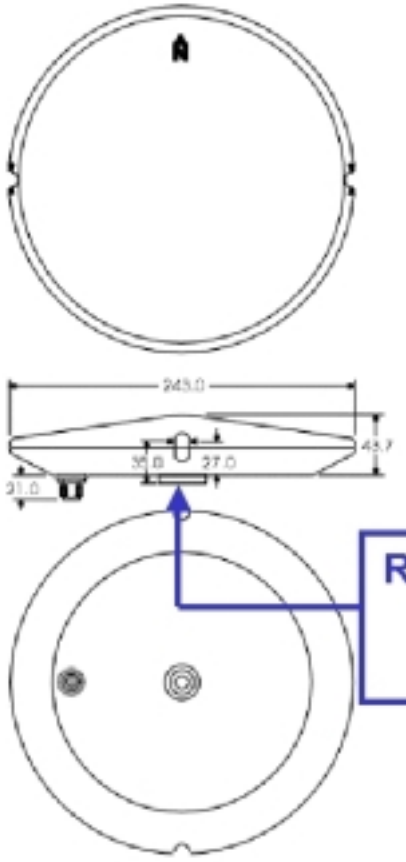

Electrical Characteristics	
Frequency	L1 1575.42 ± 10.23 MHz
	L2 1227.60 ± 10.23 MHz
Polarization	RHCP
Antenna Gain	5.2 dBiC
DC Power	5 - 15V, 45 mA, Typical
LNA Gain L1	39dB ± 3dB
LNA Gain L2	39dB ± 3dB
Output	50 ohm, type N
Humidity	100%
Temperature	-40°C to +65°C
Weight	0.96 Kg

NOTE: All dimensions in millimeters.

Figure 82. Ashtech Marine Antenna III L1 / L2

Appendix E. Institute of Navigation Paper

Appendix E contains the paper published in the ION 2001 GPS conference proceedings held in Salt Lake City, Utah. This paper was written in the early stages of the research and was based on the information available prior to the Phase III rocket sled trials at Hurricane Mesa.

Using the GPS To Collect Trajectory Data for Ejection Seat Design, Validation, and Testing

By
1Lt Reece Tredway, Lt Col Mikel Miller, and Maj John Raquet
Air Force Institute of Technology School of Engineering
2950 P Street Bldg. 640
WPAFB, OH 45433
Tel: (937) 656-4576
www.afit.edu

BIOGRAPHY

1Lt Brian Reece Tredway is a Masters student at the Air Forces Institute of Technology (AFIT). He received his BS in Electrical Engineering from Arizona State University in 1997. His interests include the GPS and GPS/INS integration.

Lt Col Mikel Miller is an Assistant Professor of Electrical Engineering at the Air Force Institute of Technology where he is responsible for teaching and research related to integrated GPS and inertial navigation systems. He has been involved with GPS testing and development since 1989.

Maj John Raquet is an Assistant Professor of Electrical Engineering at the Air Force Institute of Technology. He is responsible for teaching and research related to GPS. He has been actively involved in GPS testing and development since 1991.

ABSTRACT

The dynamic characteristics of an aircraft ejection seat are of crucial concern when evaluating aircraft ejection systems and their ability to safely separate aircrew members from disabled aircraft. Every ejection seat model undergoes real-time dynamic tests to determine potential injury to aircrew members during ejection. Ejection seat tests are conducted at the High-Speed Test Track near Holloman AFB, New Mexico. The test facility consists of a 50,000-foot long track and provides the required telemetry and high-speed photography to monitor and validate the aircraft escape system performance. Test and evaluation of the ejection seat requires very accurate determination of the position and velocity profiles during each test run to determine the relative positions between the aircraft, ejection seat, manikin, and the ground. Current test and evaluation systems rely on expensive camera systems to determine the position and velocity profiles [2].

This paper presents design and initial test results from a new GPS-based system capable of monitoring all major ejection-test components. Small, low-power, lightweight GPS receivers, capable of handling high accelerations, are mounted on the manikin and/or ejection seat to obtain the position and velocity during the ejection sequence. The goal of the research is to augment the current video systems with a differential GPS-based measurement system. The differential GPS-based system should meet or exceed the accuracy of the high-speed film and video systems.

INTRODUCTION

Since their inception ejection seats have been tested at ejection seat proving grounds. The different test facilities consist of long sled tracks with the required telemetry and high speed photography equipment to monitor and validate each aircraft escape system performance.
This paper briefly describes the ejection seat testing program and presents the preliminary design and performance results from a new differential GPS based system capable of measuring the position, velocity, and rotations of all the major ejection system components during ejection sled tests as well as actual in-air ejection tests.

Current Ejection Seat Testing

Located at Holloman AFB, N.M., the 846th Test Squadron maintains and operates one the Air Force's largest ejection seat proving grounds.

Figure 1 shows a simulated F-16 forward fuselage mounted to the Air Force Multi Axis Seat Ejection (MASE) rocket sled. The MASE is only one type of rocket sled used in ejection seat testing. The MASE rocket sled is unique in that the fuselage sits high enough above the track so that it can be pitched down, up, rolled, yawed, or any combination of the above. This allows the ejection seat designers to test the ejection seat's performance as it enters the air stream at different orientations, simulating real world scenarios.

Figure 1: MASE rocket sled

The sled's speed depends on the ejection seat model and type of test. The average test speed is 600 knots equivalent air speed (KEAS) [2].

The Advanced Dynamic Anthropomorphic Manikin (ADAM) is used to simulate an aircrew member during the ejection tests. Figure 2 shows the ADAM manikin. The ADAM stands 74.3 inches, with a weight of 217 pounds.

Figure 2: ADAM

Over forty sensors located throughout the manikin convert mechanical movement into electrical signals. In addition to the sensors located at each joint, accelerometers and compression sensors monitor important parameters such as neck loads and spinal compression.

The manikin is designed to resemble the human body with the same range of motion and associated degrees of freedom. To simulate a female aircrew member, a smaller manikin called LOIS is used. The Lightest Occupant In Service (LOIS) manikin is 60 inches tall and weights 105 pounds. LOIS is functionally identical to the ADAM in the type and location of sensors and data collection equipment.
Regardless of which manikin is used, it is outfitted with the same standard issue flightsuit, aircrew survival vest, and helmet as the pilot it simulates.

To avoid the possibility of telemetry data dropout, the data collected by the manikin sensors is stored inside the manikin in a data logger for post processing. The data logger and it's battery are located in the manikin chest cavity. Each data logger can collect and store up to 64 analog channels at a sample rate of up to 20,000 Hz. The larger ADAM can hold two 64 channel data loggers, while the smaller LOIS can house only one 64 channel data logger.

During the ejection trials the position of the major system components are tracked by a combination of film and video cameras. The primary tracking camera is the video Tracking Information System (TIS). In addition to the TIS, 16 and 70 mm film cameras provide general surveillance of the rocket sled, ejection seat, and manikin. A typical ejection test uses approximately 15 cameras to monitor the ejection sequence [6]. The TIS and film cameras can be fixed or panned by hand depending on the type of surveillance required.

Figure 3 shows a typical ejection profile plotted with data from the TIS video system. The position accuracy of the TIS is 40 – 60 cm. All final data were processed utilizing two smoothing passes and a 9-point fourth-order smoothing algorithm [6].

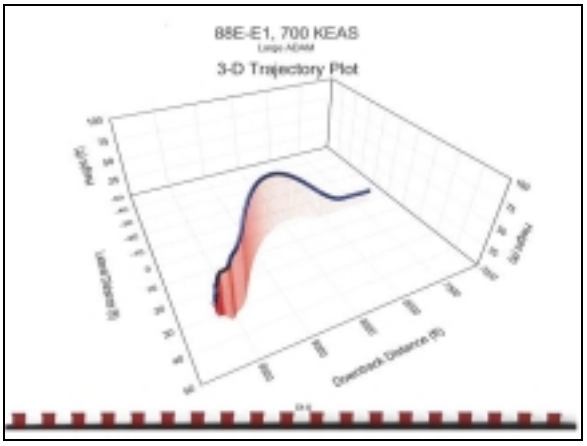

Figure 3: 3-D Manikin Trajectory Plot

As shown in Figure 3, the and ejection seat left the fuselage at a downtrack distance of approximately 7500 ft and rose to a height of approximately 100 ft, where the manikin separated from the ejection seat and then landed about 30 feet to the left of the test track.

In addition to the TIS video system and the 16 and 70 mm film cameras, the test track has the capability to monitor the seat ejection from the cockpit using high speed film cameras mounted on the MASE sled. The high speed film cameras are not used in most of the ejection tests due to the additional cost of the film and lengthy processing time.

RESEARCH GOALS

The goal of this research is to augment the current video system with a new system called the Differential GPS (DGPS), Independent Velocity, Position, and Attitude Collection System (DIVPACS). The DIVPACS should meet or exceed the sub-meter accuracy of the current video systems. It supplies its own power, data logger, and control interface, making it totally independent of the monitored platform. DIVPACS collects the position and velocity data for the ejection system designers in a format similar to the existing TIS outputs.

SYSTEM CONFIGURATION

The DIVPACS is designed to fit into the pockets of a standard aircrew survival vest. Figure 4 shows the DIVPACS as it is configured for Phase II freefall testing as described in the next section.

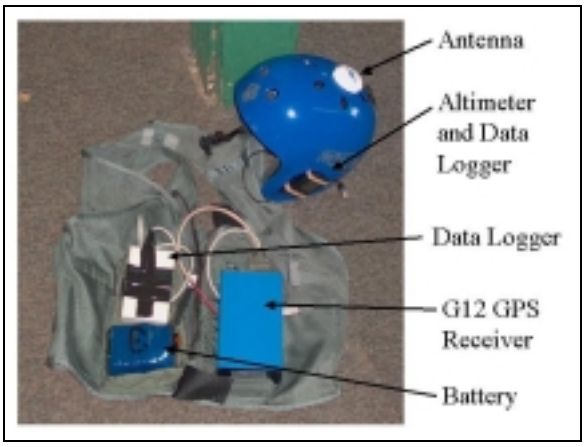

Figure 4: DIVPACS configured for freefall testing

The components are shown on the aircrew survival vest that is worn by the manikin. This configuration keeps the components located close to the center of mass of the manikin. It is important that any bulky items placed on the manikin are positioned symmetrically around the manikin center so that the equipment doesn't cause the manikin to become unstable in flight and tumble when it enters the airstreams. The helmet shown in Figure 4 is not the type worn by the manikins during actual ejection trials, but is a standard skydiving helmet. The helmet and barometric altimeter were used for initial testing only during skydiving tests conducted at the Skydive Green County dropzone. The results are presented later in the paper.

GPS Receiver and Antenna

In a typical ejection sequence the ejection components experience accelerations as high as 20g [2]. In order to handle the high dynamics, the DIVPACS incorporated the Ashtech® G12 GPS Receiver. The G12 is an original equipment manufactured (OEM), 12-channel, single frequency (L1), coarse acquisition (C/A) code and carrier receiver. The receiver offers consistent and reliable

tracking with peak acceleration rates greater than 23 g's, over 450 g/s of jerk, and vibration levels of $0.1G^2$/Hz [3]. The re-acquisition time is 2 seconds, and the hot start time to first fix is 11 seconds. The G12 can output NEMA messages, Ashtech proprietary messages, and raw measurements.

One of the design constraints on the system is that it be small enough to fit into the pockets of the survival vest shown in Figure 4. The size of the G12 is 108mm x 58.4mm. It weights 2.8 ounces and has a power consumption of 2.1 Watts including the power applied to the antenna. A typical aircrew helmet and ejection harness is shown in Figure 5.

Figure 5: Aircrew member in ejection seat

The antenna is external from the receiver and is located on top of the helmet shown in Figure 4. The ADAM will wear a standard Air Force issue aircrew helmet with the antenna located inside the plastic shell toward the front of the helmet.

Tracking Information System (TIS)

The Holloman AFB test track uses a TIS video system that processes data at 60 frames per second [2]. It provides the system designers the ability to examine an ejection sequence frame by frame to determine if the ejection seat and manikin remained stable during the entire ejection sequence.

The DIVPACS G12 is limited to a 20Hz sampling rate, but based on the test data from previous ejections a 20 Hz sample rate should be adequate to determine the manikin's position and velocity [2]. Also note that when the G12 sample rate is set to either 10 or 20 Hz, only 8 satellites are used to calculate a position solution.

Data Logger

All the data collected from the DIVPACS GPS receiver is stored in an H.O. Data Compu-Log RS-12DD data logger for post processing. The data logger is designed to collect and store the output from any RS-232 source at a rate of up to 115,000 bps. A separate 9v battery powers the data logger. The data is placed into non-volatile memory so it is protected in the event of power loss. Due to the high dynamics, the original container and I/O connections will be replaced with a ruggedized container and connectors prior to the start of actual ejection tests.

MODELING AND SIMULATION

All the software necessary to calculate the manikin's position and velocity are written using MATLAB®. Once the test is complete, the data collected in the data logger and the data from the DGPS reference station located at the test site is downloaded to a desktop PC or laptop for post processing.

Differential GPS (DGPS)

DGPS is a technique used to improve the accuracy of GPS. The increased accuracy over standalone GPS comes from the addition of an independent GPS receiver operating at an accurately determined reference station. The differences between the known reference station location and the calculated position are continuously determined, and those differences are used to remove common errors between the reference station and the mobile GPS receiver. Reference stations are currently in place at each of the ejection seat proving grounds.

Carrier Phase DGPS

In order to accurately track the manikin's position and velocity, it is necessary to have the most accurate position solution possible. For the ejection tests located at the ejection seat proving grounds it is possible to keep the distance between the mobile and reference receiver under 5km, and in most cases under 1km. A reference station located at the site provides the differential corrections. With baselines of 10km or less it is possible to resolve the integer ambiguities precisely [5]. The problem is simplified by the requirement for post processing of the data.

The research plan calls for starting with carrier phase smoothed code techniques which should provide a 50 cm level accuracy, then applying search techniques for the exact integer, or the ambiguities can be treated as non-integer states in a floating ambiguity solution as part of the navigation state vector. This may not be possible if the ionosphere, troposphere, and clock errors cannot first be reduced to the centimeter level [5]. The biggest challenge to using carrier phase DGPS is the possibility of cycle slips during a high speed, high dynamic ejection sequence. We will attempt to use the Ashtech commercial carrier phase DGPS software.

GPS-Based Attitude Determination

Aircraft attitude can be determined by Inertial Navigation Systems [4]. Inertial Navigation systems rely on spinning gyros or ring laser gyros for attitude determination. In general aviation applications, a vertical gyro is used for pitch and roll determination and a separate gyro are used for heading determination. GPS-based attitude determination uses the relative position of multiple antennas. If mm-level antenna position accuracy is obtained, attitude accuracies of 0.2° rms are attainable with baselines as short as 1 meter [1]. A typical configuration has one master antenna and two slave antennas.

PERFORMANCE TESTING METHODOLOGY

The main focus of the initial system testing was to ensure that the DIVPACS could operate reliably during testing at an ejection seat proving grounds, either at Holloman AFB, or Hurricane Mesa Utah. The initial efforts focused on collecting data in a number of different system configurations for post processing. Due to the expense of the sled testing, it is expected that only two or three actual sled runs will be accomplished. A majority of the testing will be in the freefall skydiving configuration.

This section describes the system testing methodology. The next section describes the results of each phase of the testing.

Phase I Testing

The first phase was the initial bench testing of the hardware. The first challenge was to assemble the separate components into cases that could provide the necessary protection during the ejection sequence. In a typical

ejection the manikin accelerates at over 15 g's. The special cases and connectors also protect the equipment since there exists the possibility that the manikin could fall directly on the equipment as it lands under the parachute. The original battery and I/O cables were replaced with plastic connectors designed specifically to withstand the ejection forces. The circuit boards were removed from the factory containers and placed into metal containers. The cases and data logger are designed so that if the manikin should land directly on the equipment they will retain the data even if the I/O cables are damaged and the battery disconnected.

Phase II Testing

The second phase of testing was to configure the DIVPACS for freefall. The focus was to ensure the equipment was stable during freefall and able to reliably track enough satellites to determine a position and velocity, even if the manikin was tumbling in flight. Freefall was the natural choice for testing equipment designed to monitor ejection profiles. The manikin rotations can be closely duplicated in freefall to test the GPS receiver's ability to remain locked onto the satellites as the antenna's pointing direction changes.

Figure 6 shows the DIVPACS as it was configured for freefall testing. The difference between the freefall configuration and the ejection configuration is the modification of the survival vest pockets to fit around the parachute harness. The other difference is the use of the lightweight skydiving helmet. Neither of these changes the operation of the GPS receiver and data logger.

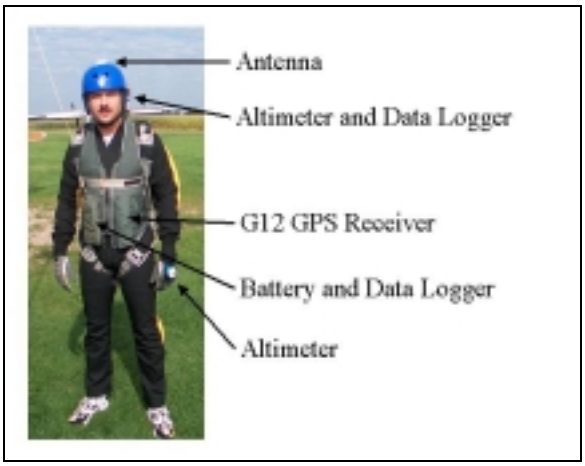

Figure 6: DIVPACS configured for freefall testing

Although the maximum velocity during freefall is approximately 140 mph, compared to the 600+ mph ejection velocity, the environment is similar to the ejection testing. In both cases the equipment must be located close to the center of mass of the body with the weight evenly distributed. The accelerations from the parachute opening are two or three g's compared to the 15 to 20 g accelerations experienced during ejection. Once the parachute is deployed the freefall and ejection environment are identical.

The DIVPACS GPS receiver, data logger, and battery are packed into the two large pockets of the aircrew survival vest. The GPS antenna is placed on top the helmet. The antenna is placed slightly toward the rear of the helmet, because the most stable freefall position is with the front of the body toward the ground with the head tilted back toward the horizon. This position keeps the back of the head oriented toward the sky. During the ejection the manikin is in a more upright seated position. For the ejection testing the antenna will be placed further forward on the helmet.

Phase III Testing

The last phase of testing is to configure the DIVPACS for an ejection from a seat mounted into a MASE rocket sled. Each ejection proving grounds has a differential station on site, but for these tests a separate G12 receiver and antenna will be set up as a reference station. The reason for configuring a separate reference station is so the differential software can be validated.

Only two or three actual phase III trials are expected due to the cost of the testing. The tests are scheduled for October or November of 2001.

Scope of Research

The goal of this research is to develop a system to accurately measure the position and velocity of an ejection component, seat or manikin, with accuracy that meets or exceeds the accuracy of the current video system.

The research equipment budget covers two Ashtech G12 receivers, two data loggers, and multiple antennas. One Ashtech Z-Surveyor receiver is also available for use as a DGPS reference station. During this research the benefits of different antenna locations and single/multiple receiver configuration will be investigated.

The expense of the tests allows scheduling of only one or two trials only on the MASE rocket sled. If it becomes impossible to use the DIVPACS on an a MASE sled run because of scheduling conflicts or equipment failures, then the data collected during the freefall tests will be the primary basis for the analysis.

RESULTS

The first freefall tests were conducted on September 2, 2001. The goals of the preliminary testing were to determine if the equipment could be configured to fit into the pockets of the survival equipment and not interfere with the parachute harness or cause freefall instability; produce a position solution in non-differential mode during stable freefall, and determine if the system would track during high dynamics such as tumbling.

The DIVPACS was installed into the aircrew survival vest and tested in the freefall configuration, as shown in Figure 6. Figure 7 shows the flight profile for the first test. The DIVPACS was unable to lock onto enough satellites in the aircraft to form a position solution. In future tests the operator will relocate closer to the aircraft door, which is made of a large Plexiglas sheet. Tracking inside the aircraft is a problem unique to the freefall testing and not a requirement for the final system.

The average freefall period is 55 seconds before the parachute is deployed. This is ample time for the G12 GPS receiver to acquire enough satellites to form a position solution. Fifty-five seconds is also enough time for the operator to complete multiple turns and rotations to test the effects of different antenna configurations on the receiver's ability to remain locked on enough satellites to form a double difference position solution.

The position solution was calculated by the GPS receiver and reported using the NEMA 3-D GGA position message. In future tests the raw measurements from the receiver will be used to form position solutions. The sample rate was 5 Hz. The flight profile is consistent with a normal freefall skydive. The sharp changes in the flight direction after canopy deployment shown in Figure 7

are spiral turns flown to reduce the altitude before returning to the drop zone.

The helmet mounted barometric altimeter recorded an exit altitude from the aircraft of 13,650 feet. The position accuracy for the barometric altimeter is approximately 50 feet. The GPS locked on to enough satellites to calculate the first position solution at 13,648 feet. The actual altitude at aircraft exit was probably a little higher than the barometer altimeter measured. The total freefall time between exit and position solution was less than 1 second.

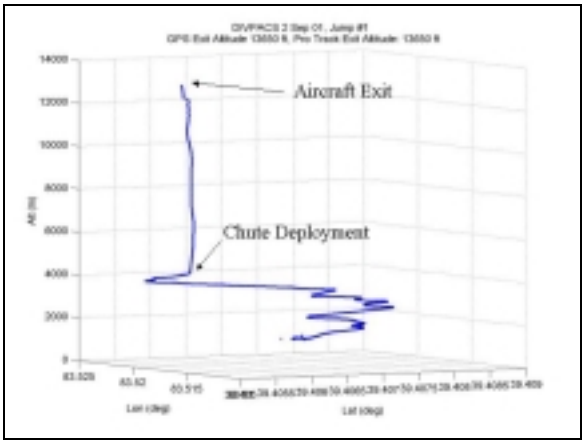

Figure 7: Phase II results in freefall configuration

This is consistent with the manufactures specifications for the G12 receiver. The receiver had been tracking before entering the aircraft so the almanac and ephemeris were less than 1 hour old.

The discontinuity shown in Figure 7 at the beginning of freefall may be due to additional satellites coming into view. The operator attempted to remain in a stable freefall position during this test. The only time the antenna was not pointed as close to zenith as possible was during the initial aircraft exit. It is possible that the initial discontinuity is due to the antenna sweeping from the horizon to a zenith direction. At this time there is insufficient data to determine the exact cause of the initial discontinuity or the change in the number of tracked satellites during the test.

Figure 8 shows a plot of the number of satellites tracked and the corresponding altitude during the test. The receiver never tracked less than 4 satellites during freefall, canopy deployment, or the flight time under canopy back to the drop zone. The number of satellites tracked did drop by one when the chute deployed. The drop in satellites may be due to the operator's head jerking down when the canopy opened. The reason for the change in the number of satellites tracked after landing is due to the operator looking down to adjust and remove the equipment. The reasons for the change in the number of tracked satellites will be investigated further in upcoming freefall tests.

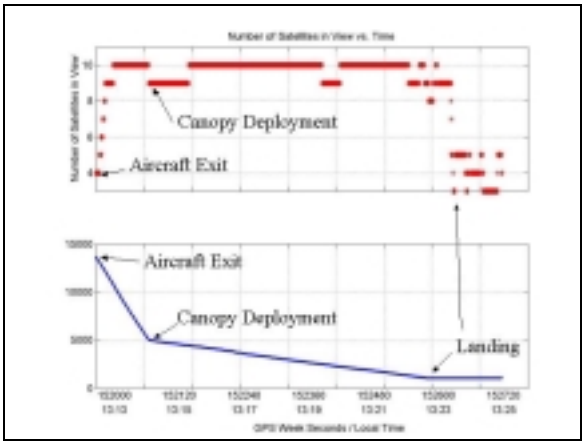

Figure 8: Number of Satellites in View

The additional weight of the components increased the average freefall speed, as recorded by the helmet-mounted altimeter, from 124 mph to 132 mph. The personnel responsible for validating ejection seat performance evaluated the DIVPACS configuration and reported that the total weight of the DIVPACS is comparable to the weight of the survival equipment carried in the aircrew survival vest. No difference to freefall stability was noticed with the

additional equipment mounted in the survival vest.

In future tests the antenna will be relocated form the top of the skydiving helmet to the inside of a standard issue aircrew helmet. Preliminary results show that antenna suffers only minor attenuation from the helmet's plastic shell. The reason for relocating the antenna to the inside of the helmet is to reduce the neck loading effects on the manikin when the antenna is exposed to the wind stream on top of the helmet.

CONCLUSIONS

In this paper the principals and problems of position and velocity determination in a highly dynamic ejection environment were described. The DIVPACS system is a very different approach to measuring the position and velocity of the different ejection system components. In all the tests the G12 receiver in a stand-alone configuration calculated the position solution. The next tests will focus on using the raw measurements to form a differential solution.

ACKNOWLEDGEMENT

The authors would like to thank the Air Force Research Lab, Human Effectiveness division, especially Mr. John Plaga for his contributions during the hardware acquisition and configuration. In addition the authors would like to thank the 846th Test Squadron, Holloman AFB. Their generous financial support made it possible to attend the 2001 ION Conference.

DISCLAIMER

The views expressed in this article are those of the authors and do not reflect the official policy or position of the United States Air Force, the Department of Defense, or the U.S. Government.

REFERENCES

[1] Hayward, Rodger C., Demoz Gebre-Egziabher, and David J. Powell, "GPS-Based Attitude For Aircraft," Proceedings of the International Conference on Integrated Navigation. Systems Department of Aeronautics and Astronautics, Stanford University, Stanford, CA.

[2] Air Force Research Lab, Crew Escape Technologies. "Design, Validation and Testing of the Russian K-36 Derivative Ejection Seat," Report K-36F – 3.5A

[3] Haax, Lin, Abousalem Mohamed, and James Murphy. "The Ashtech G12-HDMA: A Low Cost, High Performance GPS Space Receiver," Proceedings of ION National Technical Meeting 2000, Salt Lake City, UT, 19-22 September 2000.

[4] Titterton, D.H. and J. L. Weston. *Strapdown Inertial Navigation Technology*. Peter Peregrinus Ltd, on Behalf of the Institution of Electrical Engineers, London, United Kingdom

[5] Cannon, M. Elizabeth. “High Accuracy GPS Positioning Techniques and Applications II,” Navtech Seminars and GPS Supply. 10 Sep 2001.

[6] Plaga, John. "TIS Optical Data Comments." Electronic Message. 19 September 2001.

Bibliography

[1] Hayward, Rodger C., Demoz Gebre-Egziabher, and David J. Powell, "GPS-Based Attitude For Aircraft," Proceedings of the International Conference on Integrated Navigation. Systems Department of Aeronautics and Astronautics, Stanford University, Stanford, CA.

[2] Air Force Research Lab, Crew Escape Technologies. "Design, Validation and Testing of the Russian K-36 Derivative Ejection Seat," Report K-36F – 3.5A.

[3] Haax, Lin, Abousalem Mohamed, and James Murphy. "The Ashtech G12-HDMA: A Low Cost, High Performance GPS Space Receiver," Proceedings of ION National Technical Meeting 2000, Salt Lake City, UT, 19-22 September 2000.

[4] Titterton, D.H. and J. L. Weston. Strapdown Inertial Navigation Technology. Peter Peregrinus Ltd, on Behalf of the Institution of Electrical Engineers, London, United Kingdom.

[5] Cannon, M. Elizabeth. "High Accuracy GPS Positioning Techniques and Applications II," Navtech Seminars and GPS Supply. 10 Sep 2001.

[6] Plaga, John. "TIS Optical Data Comments." Electronic Message. 19 September 2001.

[7] Bryson, David F. F-16 Aces II Structural Upgrade Sled Test Program of The Modified F-16 Ejection Seat, 21 September 2001. Contract No. F41624-98-D-1002. Phoenix, AZ: Universal Propulsion Co., Inc. (Document No. 9566).

[8] Misra, Pratap and Per Enge. Global Positioning System; Signals, Measurements, and Performance. Lincoln, Massachusetts: Ganga-Jamuna Press, 2001.

[9] U.S. Coast Guard Navigation Center, "GPS Status Message." n. pag. http://www.navcen.uscg.mil. 12 December 2001.

[10] The Aerospace Corporation, "GPS Segments." n. pag. http://www.aero.org/overview. 7 November 2001.

[11] Spilker, J.J. (1994). "GPS Navigation Data," in Global Positioning System: Theory and Applications I. Ed B. Parkinson, J. Spilker, P. Axelrad and P. Enge. Washington DC: AIAA, 1996.

[12] Dana, Peter H. "The Geographer's Craft Project." Department of Geography, The University of Colorado at Boulder. 1 May 2000.

[13] *G12™ GPS OEM Board and Sensor Reference Manual*. Part Number 630068, Revision C. Santa Clara: Magellan Corporation Ashtech Precision Products, September 2000.

[14] Gerber, Eduard A. "State of the Art – Quartz Crystal Units and Oscillators," in Time and Frequency: Theory and Fundamentals. Ed. Byron E. Blair. Washington D.C.: U.S. Government Printing Office, 1974.

[15] Ward, Phillip. "Satellite Signal Acquisition and Tracking," in *Understanding GPS: Principals and Applications*. Ed. Elliott D. Kaplan. Norwood, MA: Artech House, INC, 1996.

[16] "Advanced Real Time Data Acquisition Systems." Excerpt from unpublished article. pag. http//www.emecorp.com. 29 July 2001.

[17] The TOPCON Corporation, "GPS Electronics Innovations and Features." n. pag. http://www.topconlaser.com/gps/tech/GPSInnovations.html#HDSV. 10 January 2002.

[18] National Geodetic Survey, http://www.ngs.noaa.gov. 15 February 2002.

[19] "Ejection Seats." Excerpt from unpublished article. n. pag. http://www.martin-baker.co.uk/eject_naces.html. 15 February 2002.

[20] Coyne, Kevin. "The Ejection Site." Excerpt from unpublished article. n. pag. http://www.ejectionsite.com/emakers.htm. 15 February 2002.

Vita

Captain Brian Reece Tredway entered the United States Air Force in August of 1982. Upon graduation from enlisted basic training he applied for Explosive Ordnance Disposal (EOD). His enlisted assignments as an EOD Technician included Indian Head Navel Ordnance Station Maryland, Redstone Arsenal Alabama, McChord AFB Washington, Spangdahlem AB Germany, Soesterberg AB Netherlands, Saudi Arabia, and finally Luke AFB, Arizona.

In 1994 he was accepted for the Airman's Education and Commissioning Program. He received his Bachelor of Science degree in Electrical Engineering from Arizona State University in 1997. He was commissioned through the Air Force Officer Training School where he was recognized as a Distinguished Graduate.

His first commissioned assignment was at Wright-Patterson AFB, Ohio in January 1998. In August 2000, he entered the Graduate School of Engineering and Management, Air Force Institute of Technology. His interests include the GPS and GPS/INS integration. After graduation he was assigned to Air Force Research Lab at Eglin AFB, Florida.

REPORT DOCUMENTATION PAGE

Form Approved
OMB No. 074-0188

1. REPORT DATE *(DD-MM-YYYY)*	2. REPORT TYPE	3. DATES COVERED *(From – To)*
11-03-2002	**Master's Thesis**	Aug 2001 – Mar 2002

4. TITLE AND SUBTITLE

USING THE GPS TO COLLECT TRAJECTORY DATA FOR EJECTION SEAT DESIGN, VALIDATION, AND TESTING

5a. CONTRACT NUMBER

5b. GRANT NUMBER

5c. PROGRAM ELEMENT NUMBER

6. AUTHOR(S)

Tredway, Brian Reece, Captain, USAF

5d. PROJECT NUMBER

5e. TASK NUMBER

5f. WORK UNIT NUMBER

7. PERFORMING ORGANIZATION NAMES(S) AND ADDRESS(S)

Air Force Institute of Technology
Graduate School of Engineering and Management (AFIT/EN)
2950 P Street, Building 640
WPAFB OH 45433-7765

8. PERFORMING ORGANIZATION REPORT NUMBER

AFIT/GE/ENG/02M-27

9. SPONSORING/MONITORING AGENCY NAME(S) AND ADDRESS(ES)

AFRL/HEPA
Attn: Mr. John Plaga
Q Street, Building 824 DSN: 785-1155
WPAFB OH 45433-7765 e-mail: John.Plaga@wpafb.af.mil

10. SPONSOR/MONITOR'S ACRONYM(S)

11. SPONSOR/MONITOR'S REPORT NUMBER(S)

12. DISTRIBUTION/AVAILABILITY STATEMENT

APPROVED FOR PUBLIC RELEASE; DISTRIBUTION UNLIMITED.

13. SUPPLEMENTARY NOTES

14. ABSTRACT

The dynamic characteristics of an aircraft ejection seat are a crucial concern when evaluating aircraft ejection systems and their ability to separate aircrew members safely from disabled aircraft. Every ejection seat model undergoes real-time dynamic tests to determine potential injury to aircrew members during ejection. Ejection seat tests are conducted at high-speed test tracks. The test track facilities provide the required telemetry and high-speed photography to monitor and validate the aircraft escape system performance. Ejection seat test and evaluation requires very accurate position and velocity determination during each test run to determine the relative positions between the aircraft, ejection seat, manikin, and the ground. Current test and evaluation systems rely on expensive video camera systems to determine the position and velocity profiles.
This research presents the design and test results from a new GPS-based system capable of monitoring all major ejection-test components. Small, low-power, lightweight GPS receivers, capable of handling high accelerations, are mounted on the manikin and/or ejection seat to obtain the position and velocity during the ejection sequence. The research goal is to augment the camera system with a differential GPS-based measurement system capable of providing accuracy that meets or exceeds the current video systems accuracy.

15. SUBJECT TERMS

Global Positioning System, GPS, Differential GPS, DGPS, Ejection Seats, Navigation, Theodolite

16. SECURITY CLASSIFICATION OF:			17. LIMITATION OF ABSTRACT	18. NUMBER OF PAGES	19a. NAME OF RESPONSIBLE PERSON
a. REPORT	b. ABSTRACT	c. THIS PAGE			Mikel M. Miller, Lt Col, USAF (ENG)
U	U	U	UL	170	19b. TELEPHONE NUMBER *(Include area code)* (937) 255-6565, ext 4278; e-mail: M.Miller@afit.edu